INVESTIGATIONS OF THIAZOLO[5,4-D]THIAZOLES AND PERYLENEQUINONES AND THEIR FUNCTION AS ORGANIC PHOTOREDOX CATALYSTS

by

Thomas S. Perrell

A thesis submitted to the faculty of
The University of North Carolina at Charlotte
in partial fulfillment of the requirements
for the degree of Master of Science in
Chemistry

Charlotte

2024

Approved by:

_____
Dr. Michael G. Walter

_____
Dr. Jordan Poler

_____
Dr. Jessica White

_____
Dr. Tino Hofmann

ABSTRACT

THOMAS SNIDER PERRELL. Investigations of Thiazolo[5,4-d]thiazoles and Perylenequinones and Their Function as Organic Photoredox Catalysts. (Under the direction of DR. MICHAEL G. WALTER)

Within the broader field of photochemistry, photoredox catalysis has emerged as a field of significant and growing relevance in the modern world. While there are many versatile and potent photoredox catalysts, these species are typically toxic and expensive transition metal catalysts. As such, there is a growing desire to develop and study a new generation of photoredox catalysts that are lower cost, sustainable, and organic or naturally derived.

In this work, we demonstrate that thiazolo[5,4-d]thiazoles (TTzs) and fugally derived perylenequinone (PQ) dyes can act as viable, next-generation photoredox catalysts. Across the two series of dyes, nine new photoredox catalysts were characterized by their photophysical properties and have been shown to drive an imine alkylation reaction at high yields (54-90%) with a low concentration of catalyst loading (0.1-0.2 mol%). Analysis of the photophysical properties of both dye series have reveal trends which govern catalytic performance, and demonstrate which traits are ideal in the development of new photocatalysts.

Additionally, while photoredox catalysis is a broadly studied subject matter, the influence of wavelength on product yield, or mechanistic effects is often overlooked. Both the TTz and PQ dye series share the distinct characteristics of having two reversible reductions with distinct spectral characteristics. The initial hypothesis was that using multiple wavelengths of light to achieve excitation of both the non-reduced and a reduced state of the catalyst could result in the enhancement of product formation. The effect of wavelength on catalyst performance was observed to have divergent effects for the two series of dyes. When illuminated by both high energy (405 nm) and low energy (595 nm) light when using TTzs dyes, product formation was

found to be unaffected or negatively affected in such conditions. Conversely, PQ dyes demonstrated a noticeable increase (2-20% yield improvement) when exposed to multiple wavelengths of light. The results of this work demonstrate not only the existence of new types of photoredox catalysts, but further highlights the importance of studying the effect of wavelength on the performance of photoredox catalysts.

ACKNOWLEDGEMENTS

Attempting to express the gratitude and thanks I feel towards everyone who helped me accomplish this task in a single page feels almost as difficult as writing the rest of this thesis. Instead, I will spend this time acknowledging those who played the largest role in elevating me to this point in my life.

I would firstly and most importantly like to thank my parents for instilling in me such a strong sense of curiosity and a lifelong love of learning from a young age. Since I first learned to speak, I've been asking questions – and that hasn't changed a bit today. Thanks to my parents, when I don't know the answer to something, I don't feel bad for not knowing, but I instead look for an opportunity to learn more. My parents, and their willingness to put up with my endless barrage of questions when I was a kid, are no doubt the reason why I am here today.

Pursuing higher education is a difficult task, but I've been lucky to go through it with my girlfriend Haley who has supported me throughout the entire process as well. I'm so fortunate to share my time and experiences with someone who has been able to sympathize with my struggles and celebrate my triumphs! Also, I am always grateful that I have someone to rant to about my research, even if it mostly sounds like gibberish to her.

Lastly, I have many amazing educators and teachers that I have encountered over the years that I also must thank for allowing me to reach these heights. There's no way I could list all of them here, but I truly have been fortunate to have some incredible teachers. Of these educators, the most recent, and significant has been Dr. Walter whose guidance enabled me to complete my research. While I still never feel entirely sure what I'm doing, Dr. Walter always makes me feel like I'm going in the right direction in the end.

To everyone listed on this page, and in my heart – **Thank You.**

TABLE OF CONTENTS

LIST OF TABLES

LIST OF FIGURES

CHAPTER 1: INTRODUCTION

1.1 Photochemistry Background and Motivations

On the whole, photochemistry is an investigation into how light affects chemistry in a wide variety of processes. These occur by way of light-matter interactions, such as absorbance, fluorescence, emission, as well as many other examples.[1] Since the 1980's there has been a renewal of interest in photochemistry, specifically concerning the use of it to drive chemical synthesis.[2] The most well-known instance of utilizing photochemistry is the use of solar panels to harness the Earth's largest natural energy source – the Sun. Utilizing the Sun's natural energy has become a broad scientific goal for the betterment of society.[3-5] While photochemistry is often conducted inside dark laboratory settings with artificial light sources, there is a long-standing hope that the power of the Sun can be harnessed to drive many essential chemical transformations.[5] By developing these such methods, society will benefit on the whole from reduced costs, higher efficiency, and more sustainable chemical synthesis. While there are many such avenues towards this future, the focus of this work is on a particular aspect of this field, photoredox catalysis.

1.2 Photoredox Catalysis

Photoredox catalysis is the act of driving redox chemistry with a light activated catalyst in order to achieve chemical transformations. Photoredox catalysis is one of the most significant examples of utilizing photochemistry in organic synthesis.[6] Despite a promising future for the applications of this field, photoredox catalysis is plagued by a few key issues preventing widespread adoption and commercialization. One of the biggest of these is the lack of suitable catalysts which are effective, sustainable, and affordable across a broad range of synthetic

applications.[7,8] While many powerful photoredox catalysts exist, they often have a secondary issue that prevents widespread adoption. For a great deal of time, photocatalysts made of ruthenium and iridium complexes have dominated studies into photocatalysis due to their long excited state lifetimes and powerful redox energies, which make them incredibly efficient photoredox catalysts.[9,10] These materials, are unfortunately incredibly expensive and difficult to obtain at scales necessary for industrial and commercial applications. Additionally, these materials are not environmentally sustainable and have deleterious effects on the environment.[11] These factors have led to a desire to create more sustainable, lower cost, highly efficient organic photocatalysts. There is optimism that a new generation of such catalysts could drive previously discovered and perhaps new synthetic routes for a variety of organic transformations.[12,13]

This work is primary focused on the characterization of photocatalysts in the context of a specific imine alkylation reaction. This type of reaction is of great societal interest, especially concerning pharmaceutical applications, due to the formation of drug-precursors.[14] These types of reactions are have only recently been shown to be capable of being driving photocatalytically, especially under mild conditons.[15-17]

Catalysts capable of broad light absorption, especially in lower energy wavelengths, is also a roadblock in the widespread adoption of this type of chemistry. Many standard photocatalysts, iridium and ruthenium complexes included, require intense irradiation with UV or near-UV light to drive photoredox chemistry.[9] In practice, this means that widespread use of these catalysts in industrial settings require complex redox-flow reactors to bombard the solution with a specific wavelength of light to generate product yield.[18] While this is does not totally prevent their use in these settings, it gets us no closer to harnessing the Sun's energy to drive

chemical synthesis. Broad, lower energy absorbers would be more useful when working towards the eventual goal of using sunlight to drive chemical reactions.[19,20]

When developing suitable photoredox catalysts, in addition to considering the above factors, one must also consider the ideal photophysical properties for these materials. Studies have determined that long excited state lifetimes coupled with powerful ground state and excited state redox potentials are ideal for the performance of photoredox catalysts.[21] It is generally believed that a fluorophore with an excited state lifetime of less than 1 ns is incapable of driving photoredox catalysis.[2] The development of an ideal photocatalyst is a complex ordeal and requires careful consideration for each of the above factors.

1.3 Thesis Summary

It is our sincere hope that this body of work will contribute to the slow yet steady march of progress towards sustainable photocatalysis. Herein, we examine two series of photocatalysts, thiazolo[5,4-d]thiazoles (TTzs), and natural, fungal derived perylenequinone-like (PQ) dyes capable of driving an imine alkylation reaction. These two catalysts have many similarities and differences across their photophysical properties that contribute to their performance as photocatalysts. The first chapter of this work will introduce the TTz series and dive deeply into their photophysical properties and their ability to drive chemical synthesis. The second chapter will fully examine the PQ dyes and ruminate on their novel ability to generate higher amounts of product when exposed to multiple wavelengths of light.

CHAPTER 2: TTZ PHOTOREDOX CATALYSIS

2.1 What is a TTz?

Recently, the Walter group has been heavily investigating the properties of several derivatives of a unique heterocyclic material, thiazolo[5,4-d]thiazoles (TTzs). Functionalization of these heterocycles with organic substituents creates materials with many useful characteristics. Dipyridinium TTzs have previously been shown to exhibit photophysical properties similar to viologens. These compounds typically demonstrate high fluorescence quantum yield, short excited state lifetimes just above the diffusion limit, and reversible electrochromism with two electrochemical reductions.[22] Additionally, TTzs have demonstrated electrofluorochromism and photochromic properties.[23] This is seen in thin gel films where the various redox states of TTzs exhibit different colors upon electrochemical reduction.[24] A visual representation of this process is seen in Figure 2.1. The reversible reductions, combined with high quantum yields are key components when considering the use of TTzs as potential photocatalysts.

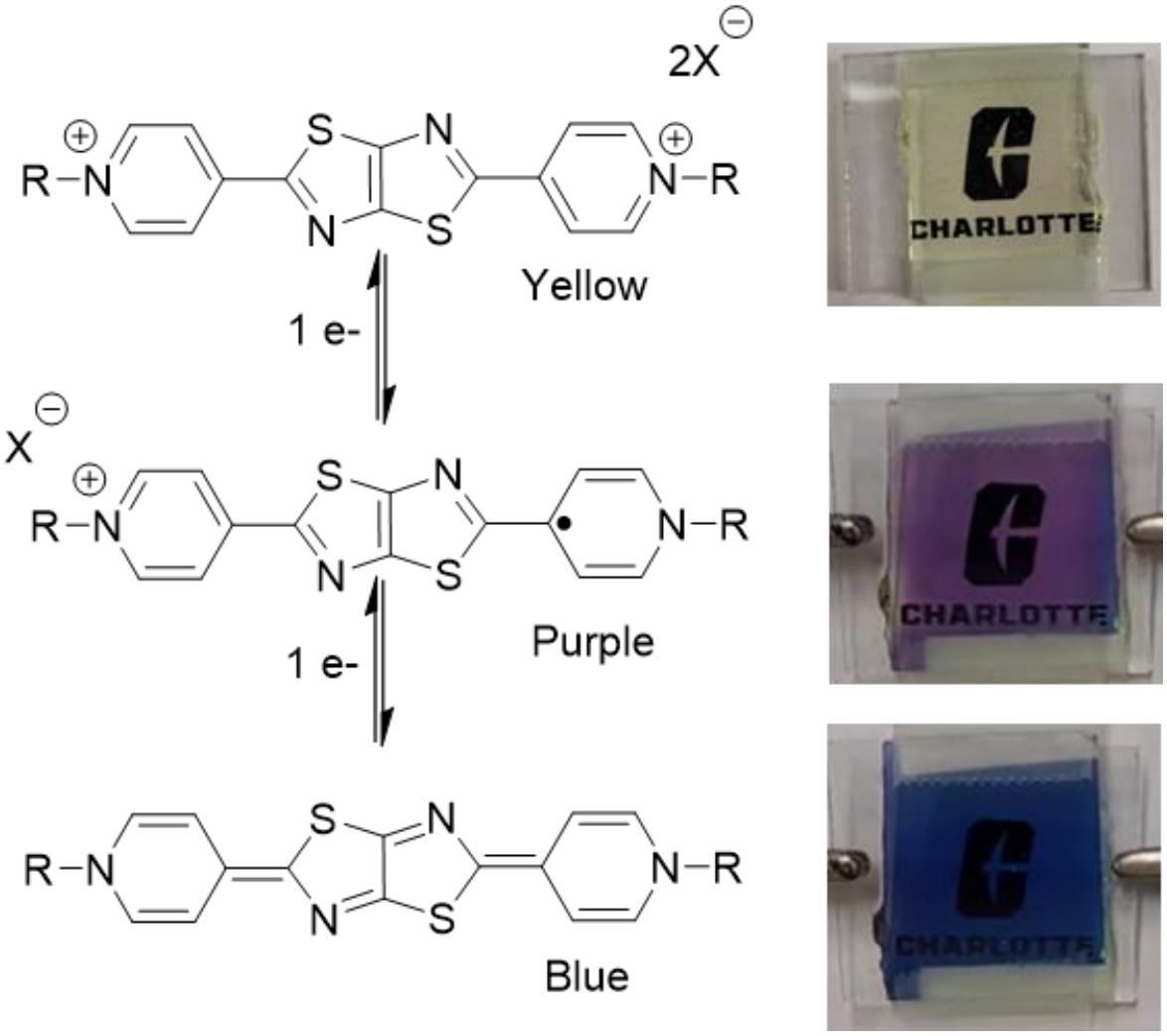

Figure 2.1: Electrochemical reduction of TTz derivatives with corresponding structure and visual appearance in thin gel films sandwiched between conductive glass electrodes.

2.1.1 TTz Catalyst Synthesis

Initial investigations were conducted using a series of 4 dipyridinium TTz derivatives. Each of these derivatives can be easily synthesized, using the general scheme shown in Figure 2. The initial synthesis of $(Py)_2TTz$ is a one-step condensation reaction between 4-pyridinecarboxylic acid, and dithiooxamide. Following this, $(Py)_2TTz$ can be functionalized into the four derivatives shown in Figure 2.2 with a single synthetic step accompanied by an ion-

exchange upon completion. Each derivative demonstrates a remarkable decrease in cost and ease of access relative to leading iridium and ruthenium photoredox catalysts.

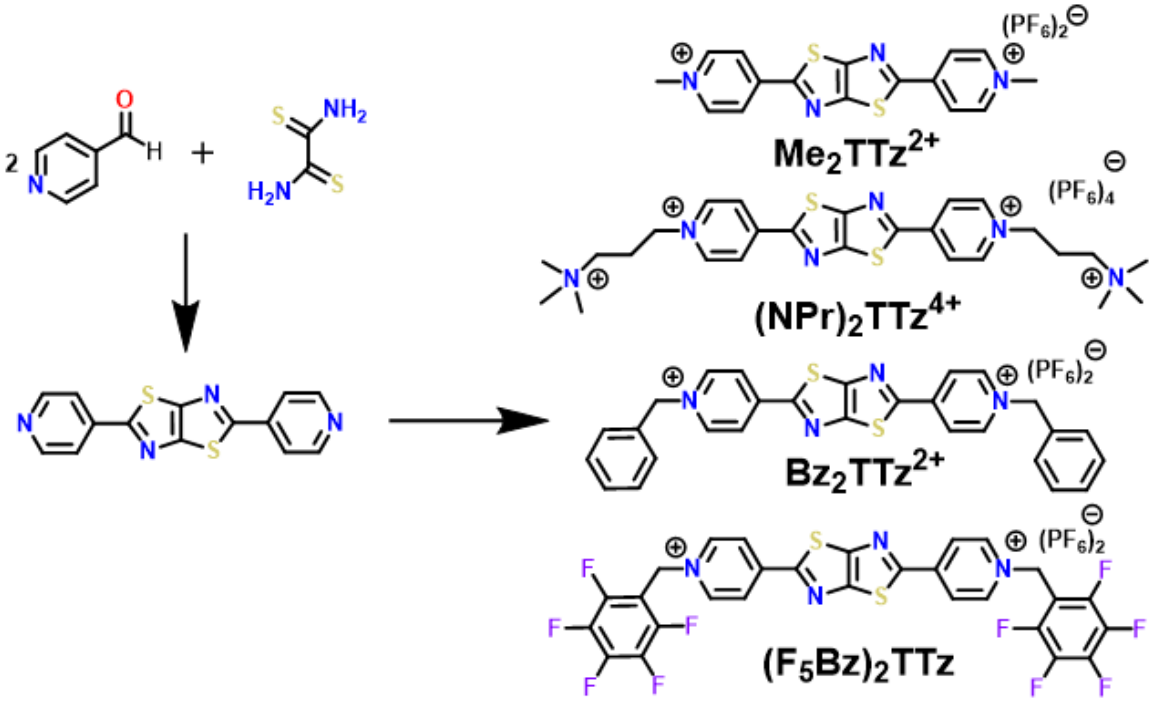

Figure 2.2: Structures and generic synthesis scheme of the Dipyridinium TTz photocatalyst series.

2.1.2 TTz Photophysical Properties

Each TTz derivative was characterized by their photophysical properties in order to better understand the factors that could contribute to functioning as a photoredox catalyst. Ensuring that the materials are irradiated with light that corresponds to their absorption is key to utilizing them as photoredox catalysts. Additionally, the quantum yield and fluorescence lifetimes of materials are key variables that add to the overall understanding of a photoredox catalyst's performance. These properties are reported in Table 2.1.

Table 2.1: Photophysical properties of TTz catalyst derivatives.

TTz Dye	λ_{max} Abs (nm)	λ_{max} Emi (nm)	Φ_F	E^*_{ox}[a] V (vs SCE)	E_{red}[b] V (vs SCE)	τ_F (ns)
[(MePy)$_2$TTz] (PF$_6$)$_2$	421	465	0.99	2.36	-0.52	1.81
[(BzPy)$_2$TTz] (PF$_6$)$_2$	409	467	0.94	2.50	-0.46	1.80
[(NPrPy)$_2$TTz] (PF$_6$)$_4$[c]	391	459	0.96	2.70	-0.47	1.92
[(F$_5$BzPy)$_2$TTz] (PF$_6$)$_2$	419	472	0.58	2.56	0.40	2.05

[a] Calculated using onset of absorbance in DCM

[b] Converted to vs SCE from vs Fc^+/Fc

[c] Photophysics determined in ACN, all others in DCM

Each TTz derivative in this series exhibits a similar absorbance spectrum, with a λ_{max} Abs ranging from 391-421 nm, as well as similar λ_{max} emission ranging from 459-472 nm. The absorption and emission peaks are relatively narrow compared to other materials, such as the perylenequinone like materials discussed in chapter 2. Three of the TTzs demonstrate high fluorescence quantum yield (>0.94 Φ_F) apart from [(F$_5$BzPy)$_2$TTz] (PF$_6$)$_2$ (Φ_F = 0.58). The TTz catalyst series has short excited state lifetimes compared to iridium and ruthenium catalysts, with fluorescent lifetimes ranging from 1.80-2.05 ns, compared to lifetimes of >1000 ns.[9,25] This characteristic would typically predict poor performance as a photocatalyst, as this is only slightly

above the diffusion limit (~1 ns) for photocatalysis, however this does not seem to prevent their functioning in the studied reactions.

2.2 Initial Investigations of TTz Photocatalysts

The TTz catalyst series was used to investigate an imine alkylation reaction via trifluoroborates that was previously demonstrated using an iridium catalyst.[26] Trifluoroborates are chosen due to their use in numerous photocatalytic settings, as well as the comparative advantage over organolithium compounds due to lower costs, greater stability, and relative ease of synthysis.[27,28] Primary investigation used three R-BF_3K substrates (Cyclohexyl-, Isopropyl-, and Benzyl-) later adding two additional substrates as a proof of concept (Cyclopentyl-, and Allyl-). The general scheme for this reaction and utilized R-BF_3K substrates are shown in Figure 2.3.

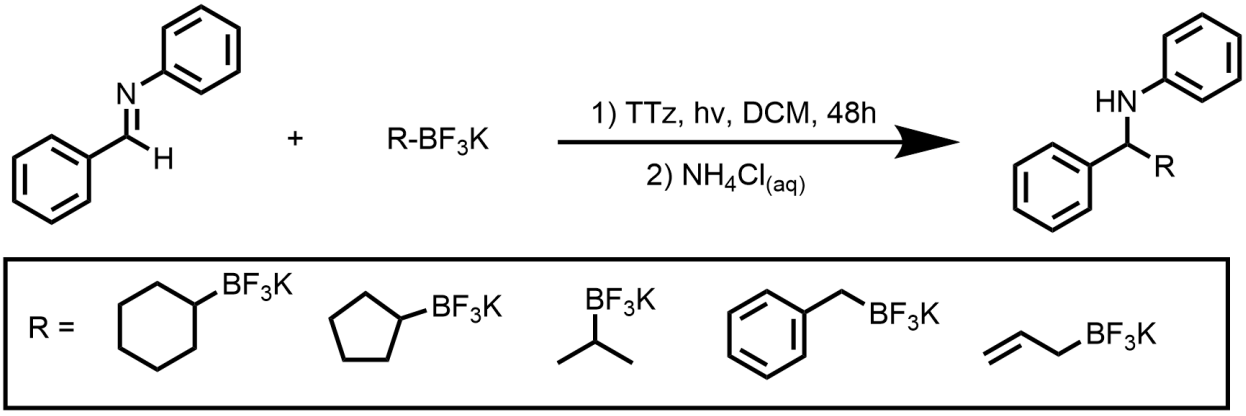

Figure 2.3: Generic scheme for photocatalytic alkylation of imine (N-benzylaniline) substrate

A series of synthetic trials revealed that each of the studied TTzs could be used as viable photocatalysts driving each reaction with high yields (63-90%). These reactions were prepared in a nitrogen glovebox with dry DCM and sealed in a vial with parafilm to ensure that anerobic conditions were maintained throughout the reaction. Oxygen was found to be highly deleterious

to product formation. Upon reaction completion, the reaction mixture is worked up in a separatory funnel where the product is quenched with aqueous NH_4Cl. The organic phase is then separated and placed onto a rotovap to remove excess solvent. An internal standard ~11mg of 1,3,5-trimethoxybenzene (TMB) is added prior to collection of ^{1}H-NMR data to determine the product yield. The yield data for each combination of materials is shown in Table 2.2.

Table 2.2: Average (3-point) ^{1}H-NMR with internal standard, determined yield and turnover number (TON) for TTz and R-BF_3K reaction.

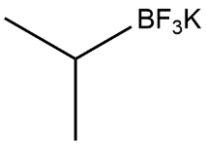

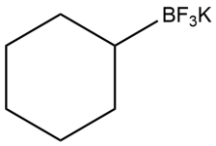

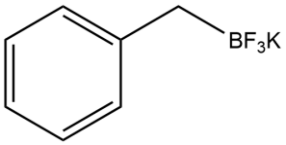

Photocatalyst	**Isopropyl-BF_3K**	**Cyclohexyl-BF_3K**	**Benzyl-BF_3K**
[(MePy)$_2$TTz](PF$_6$)$_2$	86.3 ± 1.3 (370)	90.1 ± 5.9 (415)	54.3 ± 4.5 (242)
[(BzPy)$_2$TTz](PF$_6$)$_2$	86.1 ± 1.3 (296)	78.3 ± 4.4 (312)	55.8 ± 0.1 (180)
[(NPrPy)$_2$TTz](PF$_6$)$_4$	69.8 ± 1.3 (268)	69.5 ± 1.8 (284)	56.7 ± 7.4 (233)
[(F$_5$BzPy)$_2$TTz](PF$_6$)$_2$	82.6 ± 1.3 (340)	64.3 ± 0.7 (215)	63.4 ± 6.0 (215)

To determine the mechanism and ensure that a radical chain-reaction mechanism was not involved, light-dark experimentation was performed over a period of 100 hours. The data from this experiment is shown in Figure 2.4 and demonstrates that as illumination is ceased, so too

does product formation. In a radical chain reaction system, product formation would continue in the absence of light and cause the quantum yield of reaction to exceed unity.[29]

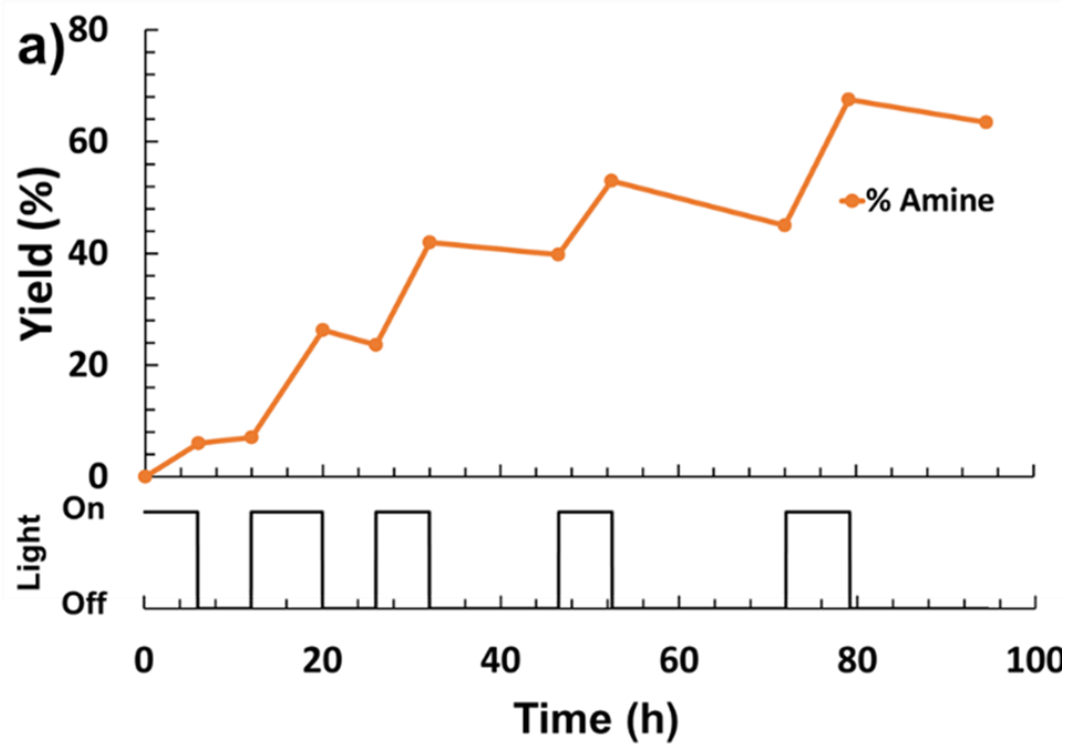

Figure 2.4: GC-MS determined amine product formation over time from light-dark experimentation.

2.3 Energetics and Catalytic Cycle

When analyzing a photoredox reaction, in-depth analysis must be conducted on the redox energy values for each redox-active species in the system. This is best represented by using a redox energy diagram, the likes of which is shown for this system in Figure 2.5.

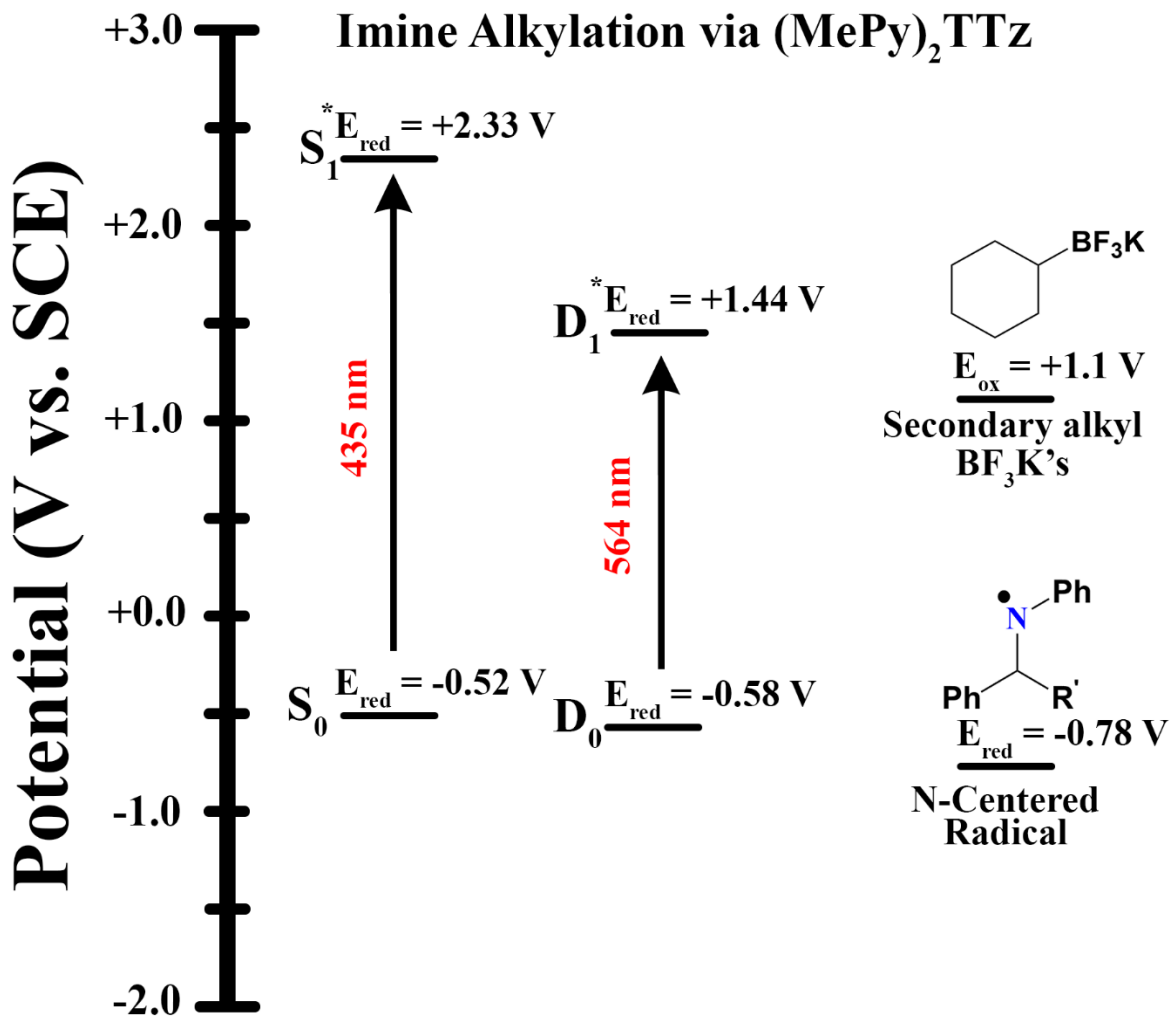

Figure 2.5: Redox Energy level diagram for $[(MePy)_2TTz](PF_6)_2$ with favorable $^*E_{ox}$ for oxidation of isopropyl-BF_3K via non-reduced and singly-reduced states

These energy values can be better understood by Eq. 2.1. which shows how E^*_{ox} (the excited state redox potential) can be calculated. Within the equation, $E_{0,0}$ is given in eV, while E_{ox} is given in volts, but due to the assumption of a single electron transfer mechanism, these values can be interchanged at a 1 eV:1 V ratio.[2]

Eq. 2.1 $E^*_{ox}\left(\frac{cat^{\bullet+}}{cat^*}\right) = E_{ox}\left(\frac{cat^{\bullet+}}{cat}\right) - E_{0,0}$

The value $^{*}E_{ox}$ indicated the oxidation potential of the photocatalyst upon excitation into an S_1 state. For $[(MePy)_2TTz](PF_6)_2$, when in the TTz^{2+*} state, this energy value is +2.33 V, which is +1.23 V greater than the oxidation potential of a secondary alkyl-BF_3K, meaning that this step is favorable. E_{red} (ground state reduction potential), for TTz^{1+} is -0.52 V. This value is obtained through cyclic voltammetry and is the compound's first reduction potential. This value is compared to the reduction potential of the N-centered radical species present in the reaction scheme (-0.78 V). Comparing these two values indicates a -0.20 V unfavourability, which would imply that this reduction either will not occur, or will occur slowly, and likely become the rate limiting step within the catalytic cycle.

Figure 2.5 also lists the $^{*}E_{ox}$ for the singly-reduced state of TTz, or $TTz^{*\bullet+}$. While the $^{*}E_{ox}$ is sufficiently high to indicate a favorability towards the oxidation of an additional R-BF_3K substrate it is difficult to determine if this actually occurs. As discussed later, while the various oxidation states of TTz are associated with differing absorption spectra, the reaction does not exhibit color changes in line with expectations, so the presence of any particular oxidation state cannot be determined. Additionally, $TTz^{*\bullet+}$ is expected to be an excited radical doublet state (D_1). D_1 states are known for typically having very short lifetimes, on the order of picoseconds, well below the diffusion limit for driving chemical reactions.[30,31] There is evidence for additional mechanisms involved in the catalytic cycle, so this possibility cannot be fully excluded.

Considering these factors, the proposed catalytic cycle for this system, which does not include the possibility of R-BF_3K oxidation via $TTz^{*\bullet+}$, is shown in Figure 2.6. The energy values for the oxidation and reduction of the reactant species are also represented in the cycle,

when considering the use of $[(MePy)_2TTz](PF_6)_2$. These values are different but still similar for the other dyes in the TTz series.

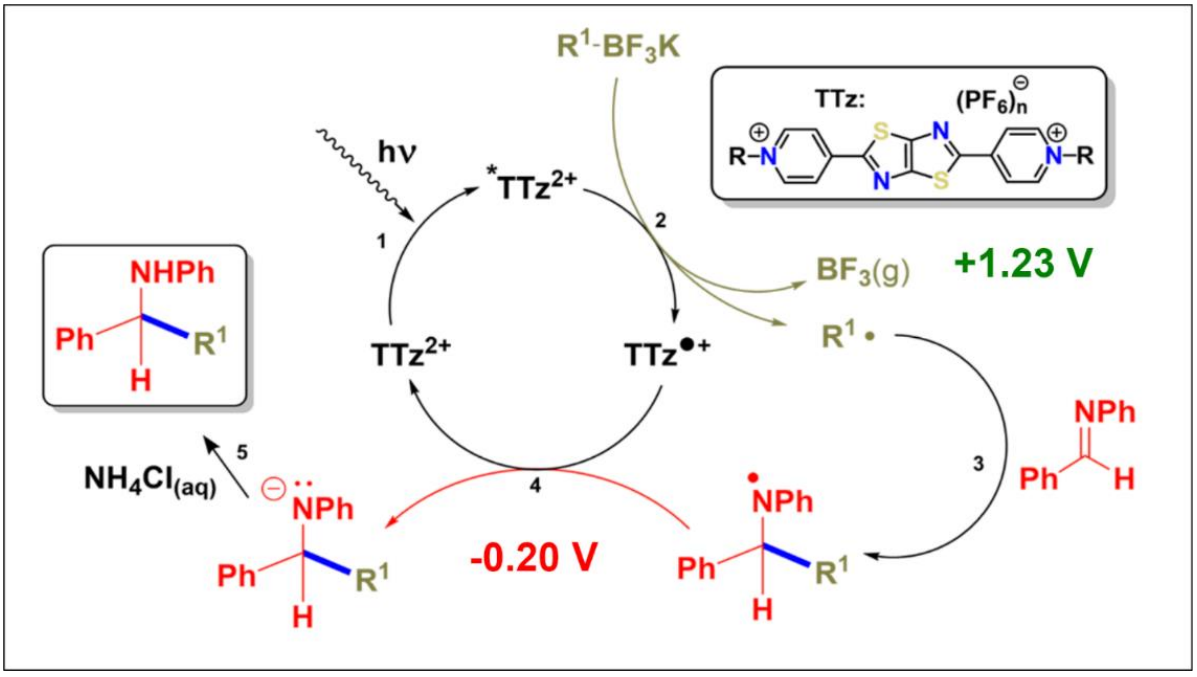

Figure 2.6: Photochemically (TTz^{2+}) driven alkyl-BF_3K coupling with an imine (N-benzylaniline).

The perceived energetic unfavourability of this system is a vexing complication and one of the primary motivators in the further investigation of this system. Additionally, the curiosity towards the role of the singly- and doubly-reduced states of the TTz catalyst and their photoactivity within the system were of great interest.

2.4 Constructing a Multi-Wavelength Photoreactor

2.4.1 A Case for a New Reactor Design

All studies discussed up to this point in the works utilized the Penn Ph.D Photoreactor M2, designed by Nobel Prize-winning chemist, David MacMillian.[32] This photoreactor was very sophisticated with a design philosophy emphasizing the standardization of photoreaction, but had

a few key design flaws that did not enable wavelength dependent experimentation. The exterior of the previously utilized Penn Ph.D Photoreactor M2 is shown in Figure 2.7.

Figure 2.7: Penn PhD Photoreactor M2**.**

The photoreactor came with a series of included LED arrays were advertised as emitted light at 395, 420, and 450 nm. Upon analysis of the emission spectra for these arrays, this was found to not be the case. Spectral analysis of each array was conducted by opening the photoreactor while the arrays were on and measuring with an Ocean Optics system. All LED arrays had broad emissions, centered at 450 nm which are shown in Figure 2.8.

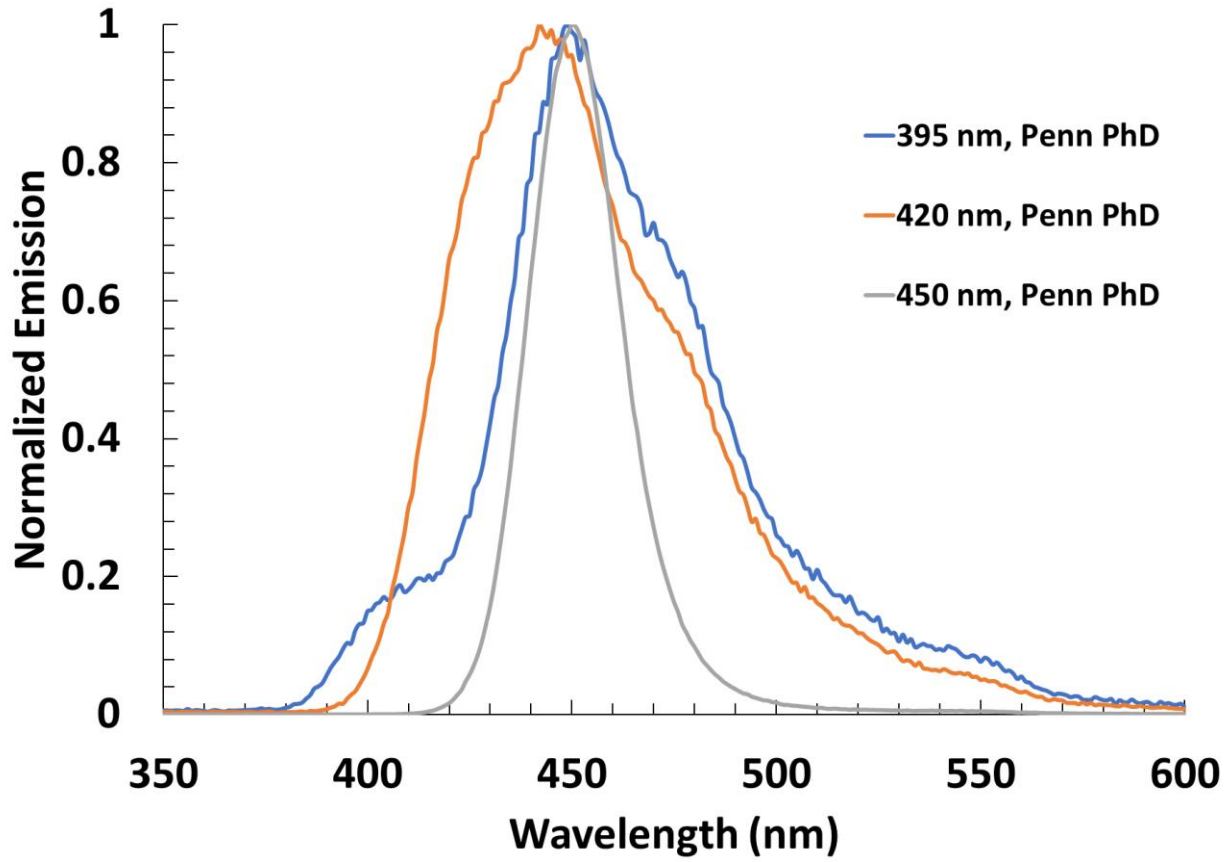

Figure 2.8: Normalized emission spectra of Penn PhD Photoreactor lamp arrays.

Our experimental design required light emitters with specific wavelength emission and ideally a modular design to enable the light configuration to be changed at will. The result of these design requirements was the *Perrell Plug-and-Play Photoreactor* (5P).

2.4.2 Photoreactor Design

The goal was to create a simplistic design that allowed for each of these design objectives to be accomplished, ideally with a low price point. The top-down layout of the 5P is shown in Figure 2.9. Following this design, a hotplate or stir plate can be affixed with the LED arrays and small a fan to enable a low cost, modular design. Additionally, this layout enables the use of 1-4

LED arrays at a time, allowing for variable intensity and up to 4 different types of emitters to be used on a single reaction vessel. Figure 2.10 contains images showing the 5P while in use.

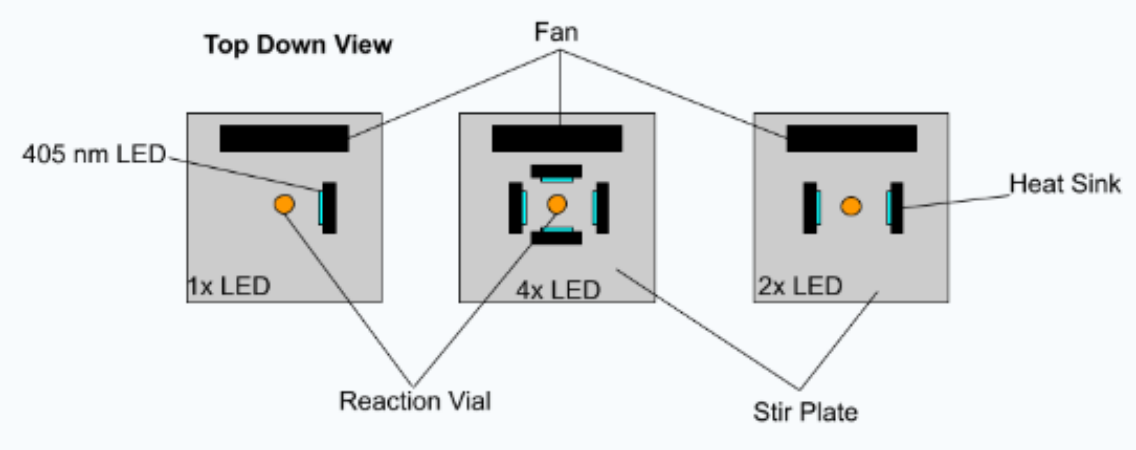

Figure 2.9: Block diagram of Prototype Perrell Plug-and-Play Photoreactor in 1, 2, and 4 array configurations.

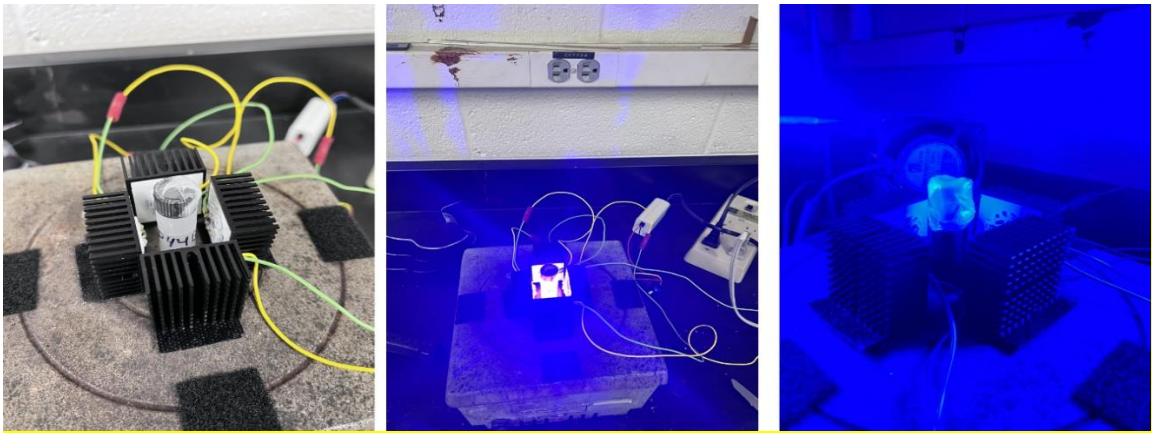

Figure 2.10: Prototype Perrell Plug-and-Play Photoreactor configured for 4x 405 nm LED arrays.

The LED arrays used in the 5P are Luxeon C Color LEDs mounted on a LuxDrive Saiph Star Metal Core in a 3-Up configuration. Each of these arrays houses three LEDs. The LED array is adhesively mounted onto a finned heatsink made of black anodized aluminum – which facilitates heat dispersion. To further dissipate heat, a fan is positioned to blow air across the

reactor set up. These arrays and the heatsinks on which they are mounted are shown in Figure 2.11.

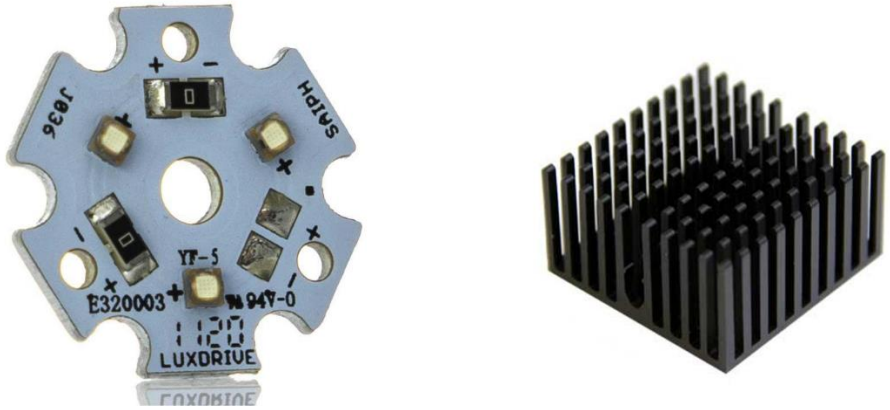

Figure 2.11: LED arrays and heatsinks Used for *5P*.

The emission ranges for the LED arrays were chosen based on potential applications towards existing research projects, but the design is theoretically compatible with any type of LED array, as long as the emission range and luminous power is characterized and accounted for. The emission ranges for all LED arrays purchased and utilized to date are shown in Figure 2.12. Note that all names for LED arrays correspond to the name they were sold under and are not indicative of the exact emission characteristics.

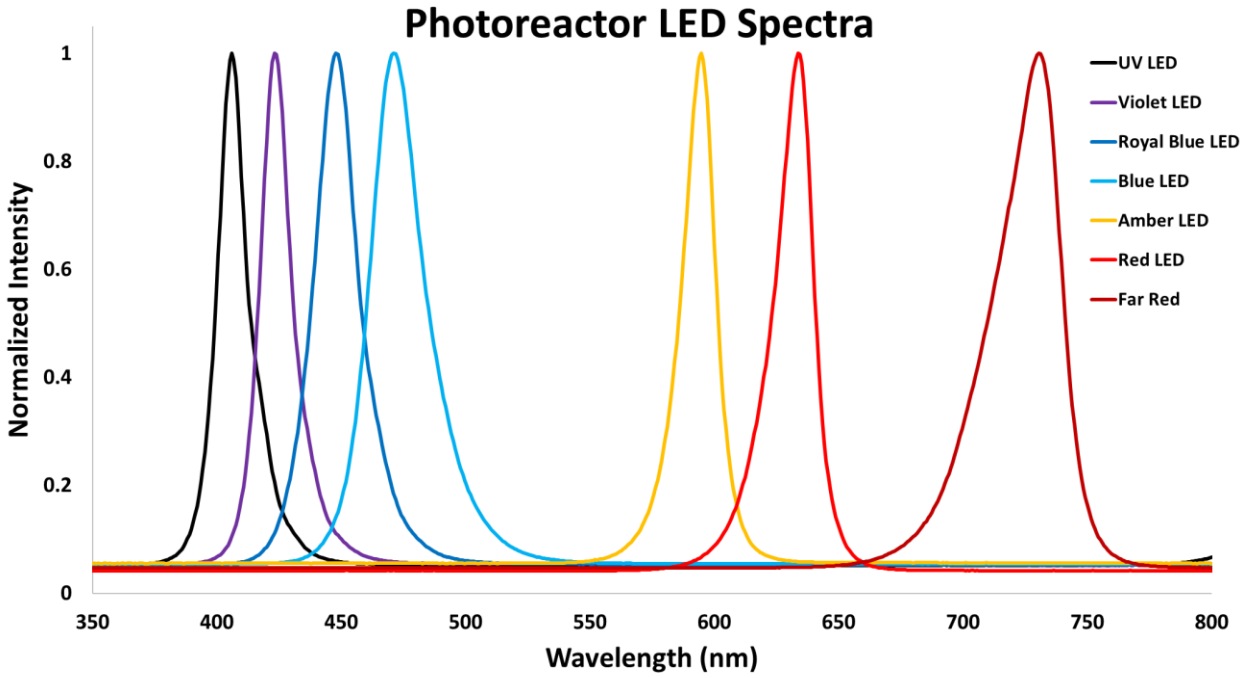

Figure 2.12: Emission of LED Arrays

The Penn Ph.D M2 Photoreactor was well characterized and reported a 1.85-Watt intensity regarding the light that reached the reaction vessel when considering all optical effects within the reactor.[32] This high level of optimization was achieved by using a reflective column that surrounded the reaction vessel – limiting the scattering of light. By comparison, the 405 nm LED arrays, which were initially used to calibrate the photoreactor, report a wattage of 980 mW at a current of 700 mA per LED. Considering this, when the reactor is utilizing 2 of the LED arrays (6 individual LED cells), there are 5.88 Watts emitted, assuming a constant 700 mA current. The actual intensity of the light hitting the reaction vessel is lower than this, due to the dissipation of light, as well as scattering.

2.4.3 Photoreactor Characterization

Considering these factors, the new reactor needed to be standardized and compared against past studies to ensure that it could produce comparable results. The first goal in the characterization of the reactor was to examine light intensity and determine the number of LED arrays that would produce results similar to the Penn PhD M2 photoreactor. The 405 nm arrays were chosen for this study as they emitted light most closely attuned to the λ_{max} absorbance of $[(MePy)_2TTz](PF_6)_2$. In addition to configuration of the number of LED arrays, the power of each LED array can be further controlled using a rheostat that is connected to either a dial or a controller software, such as LabView. While this capability was not utilized for the studies mentioned in this report, it is a useful design consideration. This system also allows for the lights to be toggled on and off at specific time intervals. By taking advantage of this, precision studies could be conducted on a photoreaction to second-scale time intervals. While further improvements can be made to the 5P, the photoreactor is fully capable of completing the relevant research goals of both this project and other Walter lab research objectives. Figure 2.13 shows the simplified reaction scheme for the reaction used to conduct this study.

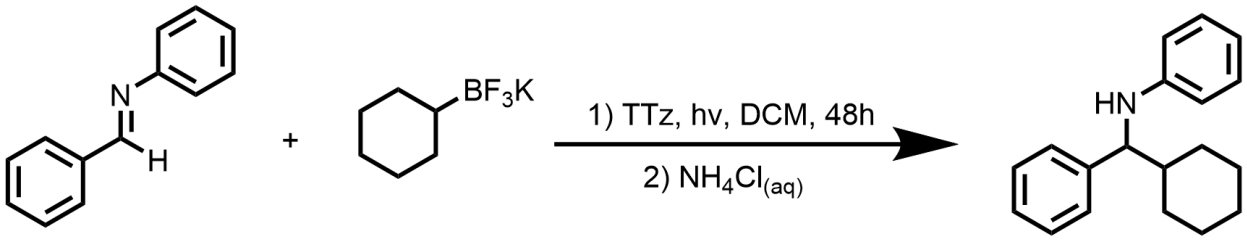

Figure 2.13: Reaction Scheme for Photoreactor Characterization

Shown in Table 2.3. are the results from this study, using the Cyclohexyl-BF_3K substrate. This combination of reagents were chosen due to producing the highest yields in previous studies (90.1%).

Table 2.3:Yields using $[(MePy)_2TTz](PF_6)_2$ and Cyclohexyl-BF_3K with Differing Numbers of LED Arrays

Reaction Parameters	48 Hour Yield (%)	72 Hour Yield (%)
Penn PhD Photoreactor	90	-
4x 405 nm LED Arrays	55	58
2x 405 nm LED Arrays	86	83
1x 405 nm LED Array	78	83

Ultimately, this study found that when using 2 of the 405 nm LED arrays, the product yield was comparable with the Penn PhD M2 Photoreactor. Additionally, this study revealed and interesting consideration with light intensity, as it was determined that using too intense of light irradiation is deleterious to product formation. While it may initially seem as if more light is always a positive predictor of product formation, due to photobleaching and degradation, this can be an issue. This is an intriguing property that warrants additional investigations and will likely vary considerable depending on the catalyst being utilized. Ultimately, the highest performance with 2 arrays was not only an important discovery for the calibration of the 5P versus the Penn PhD M2 Photoreactor, but also important for any future studies which utilize a variable intensity photoreactor.

To further confirm functionality of the 5P, each previously investigated imine alkylation was examined using the new reactor. Additionally, two new R-BF_3K substrates were utilized, a Cyclopentyl- and Allylic- substrate expanding the synthetic scope. The results of these studies are shown in Table 2.4.

Table 2.4: Yield Results of Various BF_3K Substrates

Substrate	Isopropyl-	Cyclohexyl-	Benzyl-	Cyclopentyl-	Allyl-
Iridium Catalyst + Penn PhD	60	73	70	-	70
$(MePy)_2TTz$ + Penn PhD	86	90	54	-	-
$(MePy)_2TTz$ + 5P	83	86	50	83	73

2.5 Investigating the Effect of Wavelength on TTz Photocatalysis

During the initial investigation of the reaction, kinetics tracking experiments were carried out using GC-MS and an internal standard of decane. This study revealed the existence of a ~8 hour induction period at the start of the reaction where product formation does not occur. This study also revealed a series of color changes with an unknown relationship to product formation. This data is shown in Figure 2.14.

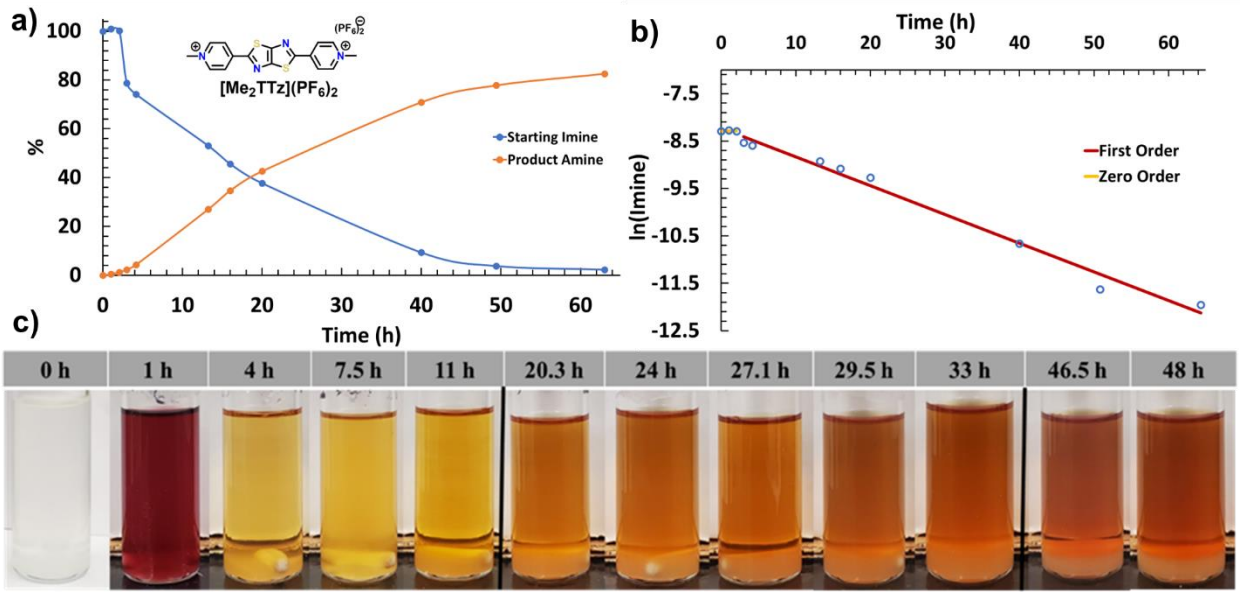

Figure 2.14: a) GCMS tracking data showing delay in product formation. b) Natural log of imine concentration as a function of time. c) Images of reaction vial color at various time points during reaction.

This induction period does not have a strong explanation, and it was speculated that there could be an additional element at play that led to this delay of product formation. Initial hypotheses centered around the idea of a photoactive singly- or doubly-reduced state. Previously, there have been studies reporting the existence of a "super-reducing" species of photocatalyst that can exist within similar systems.[33] These mechanisms involve different mechanisms such as excited doublet states with anomalously long excited state lifetimes and doubly-reduced states capable of becoming excited via a different wavelength of light to perform novel processes.[34] It is necessary to include that at the time of this study's commencement, the later of the two mechanisms had not yet been reported and this possibility was not considered in our study. Retrospectively, experimental design would have likely been different had this publication been available and us aware at project inception.

It was hypothesized that the singly- or doubly-reduced TTz could be accumulating in this initial period, at which point a critical concentration is reached where the TTz can be consistently excited into the super reducing state to enable product formation. The singly-reduced state (TTz^{1+}) of $[(MePy)_2TTz](PF_6)_2$ has a lower absorbance in the near-UV region, and a prominent absorbance peak at 600 nm, while the doubly-reduced state has a broader absorbance peak around 700 nm. These differences would theoretically lead to a simple means of identification within a reaction solution. The absorbance spectra of the various states of $[(NPrPy)_2TTz](PF_6)_4$ is shown in Figure 2.15. which is very similar across the catalyst series.

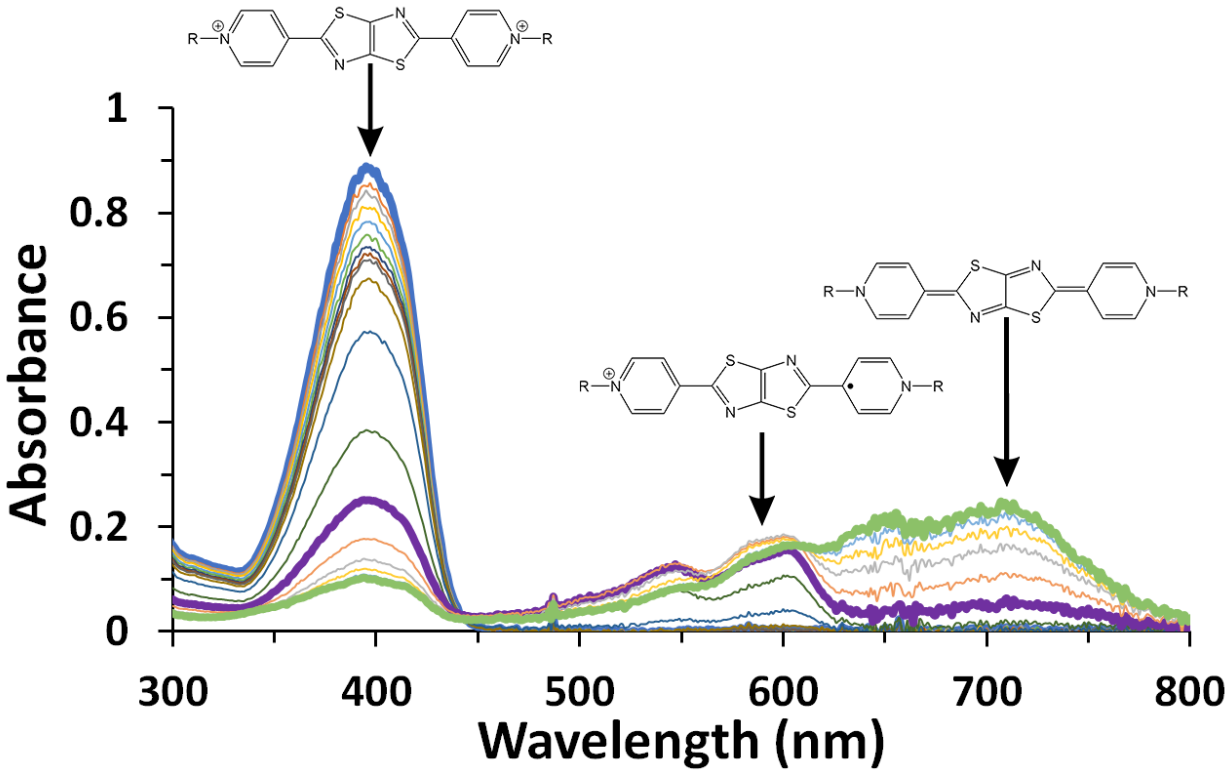

Figure 2.15: Absorbance of TTz States

If the singly- or doubly-reduced TTz species can as a super-reducing species, it should be capable of reaching this state via excitation at the lower energy 600 nm wavelength, that corresponds to the λ_{max} absorbance of TTz^{1+}. The formation of a super-reducing species during

this time would likely explain the delay preceding product formation, as well as the formation of product despite the lack of energetic favorability for the reduction of the N-centered radical species. Probing this characteristic was the primary goal in the development of the 5P. This is due to the precise and tunable wavelengths that can be used to excite with a predetermined wavelength. Shown in figure 2.16 is the redox energy diagram that represents the energy of a hypothetical super-reducing species of TTz. This energy is obtained in a similar fashion as the energy of $^{*}E_{ox}$, adding the energy of a photon at the onset of absorption for TTz^{0}.

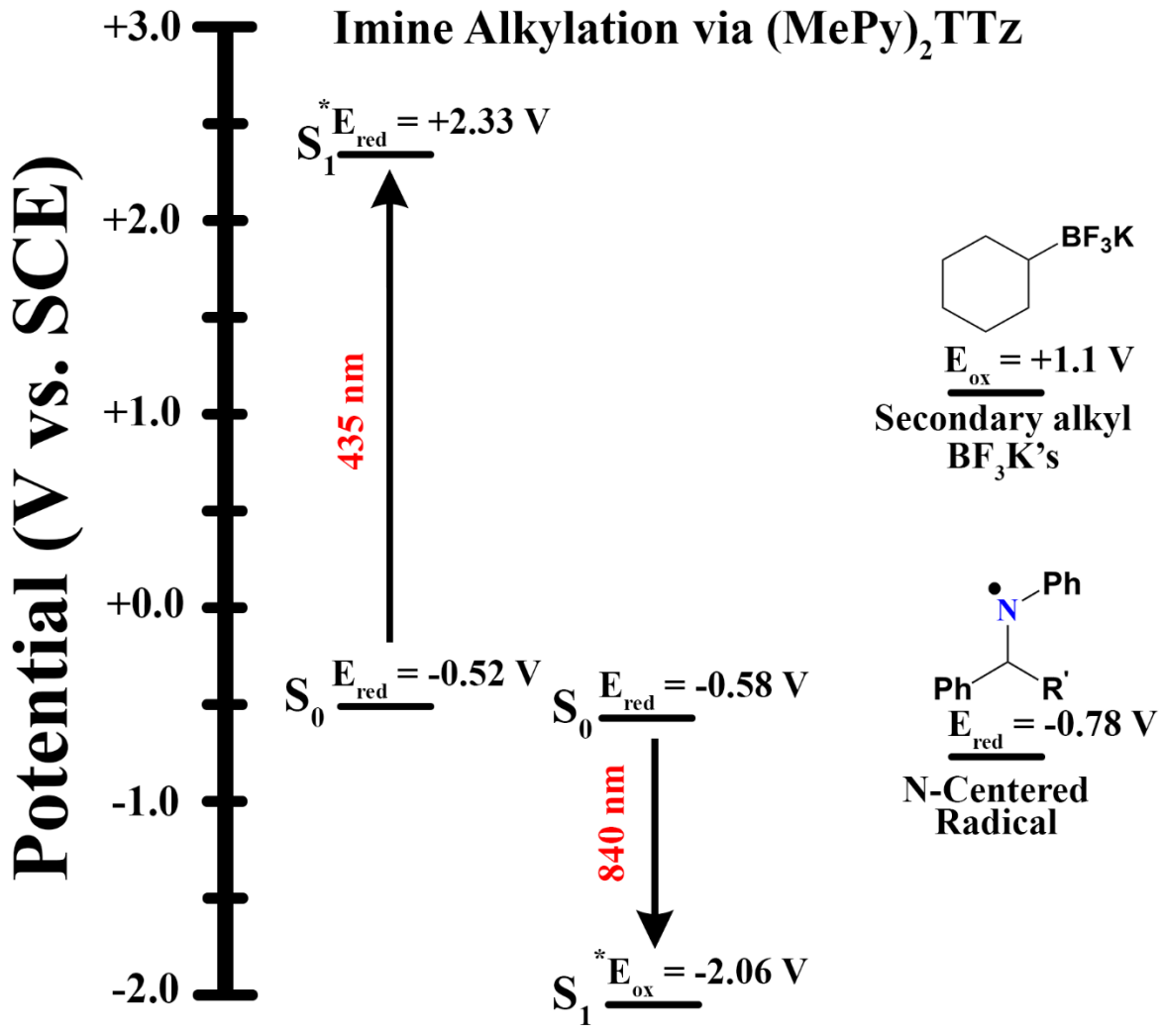

Figure 2.16: Redox energetics diagram for imine alkylation via $[(MePy)_2TTz](PF_6)_2$ including proposed super-reducing state

2.5.1 Variable Single Wavelength Experiments

A series of experiments were conducted using the new photoreactor along with $(MePy)_2$ TTz and Cyclohexyl-BF_3K. This combination was chosen due to ease of availability, and the fact that this was the combination of catalyst and substrate giving the highest yield in prior studies. Reactions completed with various wavelengths of light revealed that the reaction yield was depressed as the light was shifted towards lower energy wavelengths, which was consistent with previous expectations. Table 2.5 shows the yields at each wavelength of light.

Table 2.5: Yields using $(MePy)_2$TTz and cyclohexyl-BF_3K with variable light wavelengths.

Light Configuration	NMR Yield (%)
2x 405 nm LEDs	86
2x 425 nm LEDs	49
2x 450 nm LEDs	37
2x 470 nm LEDs	15
2x 5000K LEDs	6

2.5.2 Dual Wavelength Experiments

A limited number of dual-wavelength experiments were conducted following single-wavelength wavelength dependency trials. Retrospectively, especially considering developments discussed in chapter 3, a wider array of experiments would have been conducted to better understand the mechanisms at play.

This series of experiments indicate that the use of 530 and 595 nm LED arrays, in addition to 405 nm arrays does not increase product formation for this imine alkylation reaction. In fact, the use of a secondary wavelength of light seems to counterintuitively decrease the amount of product formation. The results of the dual wavelength experiments, as well as control experiments for the use of the corresponding single wavelengths are shown in Table 2.6.

Table 2.6: Yields from Dual-Wavelength and Single Wavelength Control Trials using $(MePy)_2TTz$ and cyclohexyl-BF_3K

Light Configuration	NMR Yield (%)
2x 405 nm LEDs	86
2x 530 nm LEDs	3
2x 405 nm + 2x 530 nm LEDs	66
2x 595 nm LEDs	0
2x 405 nm + 2x 595 nm LEDs	51

During the initial acquisition of this data, the lower yields when coupling the 405 nm arrays with 530 and 595 nm arrays were thought to be due to experimental error, contamination, or some other anomaly. It is now believed that this data is indicative of a general trend, and that illumination of lower energy wavelengths (<500 nm) leads to a lower amount of product formation. Considering the further decrease in product yield that is observed with 595 nm relative to 530 nm (15% absolute decrease), illumination of a reduced state of TTz likely decreases yield by way of greater catalyst degradation, or the formation of a non-redox active species.

A graphical illustration of this trend, accompanied by the spectra of each redox state of TTz is shown in Figure 2.17.

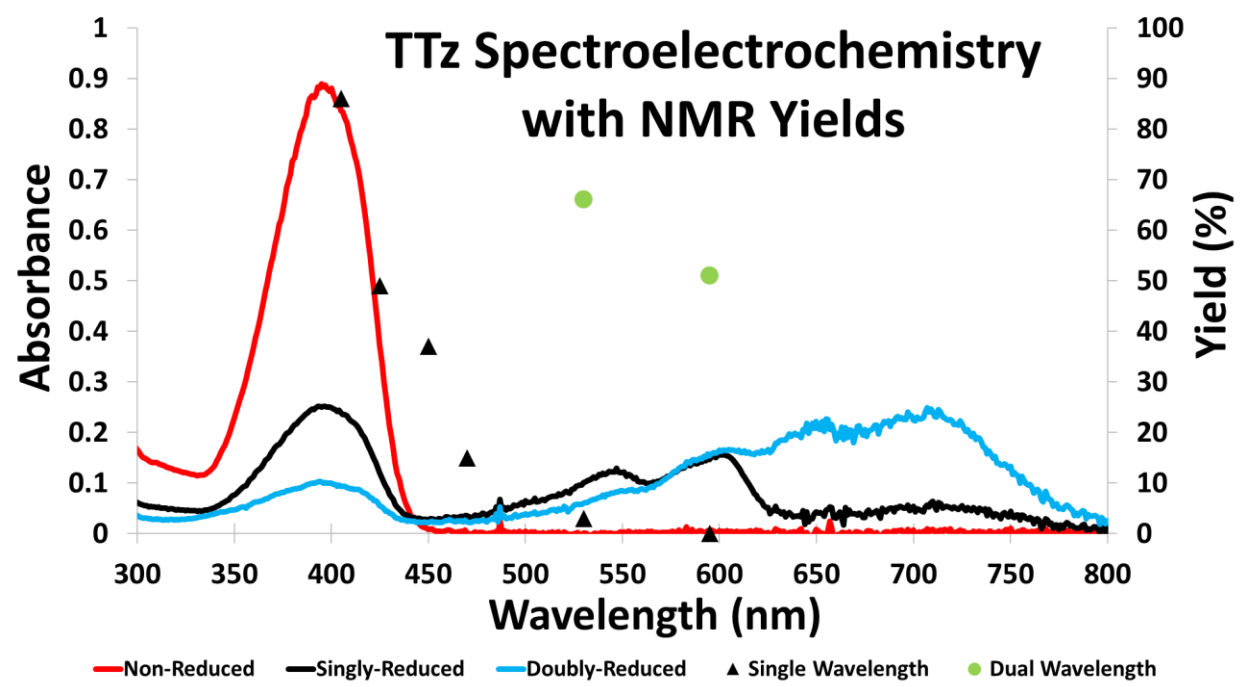

Figure 2.17.: Graphical Overlay of TTz absorbance by redox state and NMR yield at each wavelength

2.6 Stern-Volmer Analysis

Stern-Volmer analysis was conducted to better understand the effects of R-BF_3K substrate choice on Step 2 of the catalytic cycle. Upon absorption of a photon, the TTz will enter into a singlet excited state (TTz^{*2+}) can exit this state through fluorescence or a non-radiative method. One such non-radiative method is the oxidation of the carbon-boron bond through diffusion as shown in Step 2 of the catalytic cycle. The catalytic cycle is shown again in Figure 2.18 for additional reference.

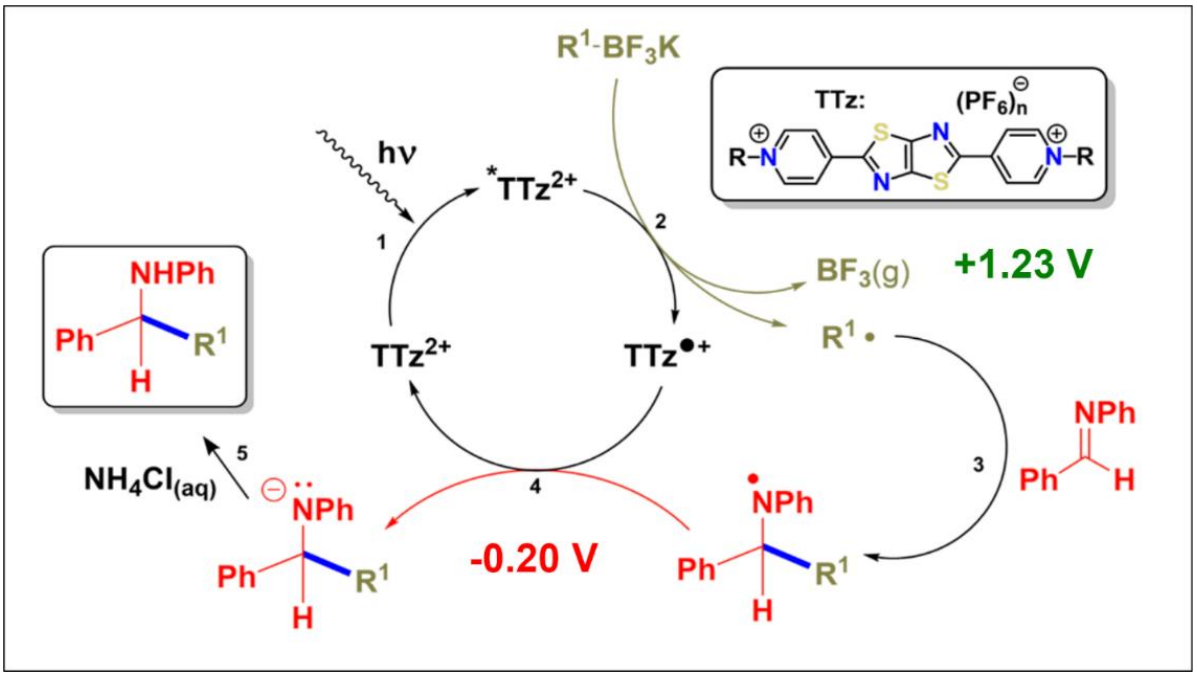

Figure 2.18: Catalytic Cycle

As the concentration of R-BF_3K increases within a reaction solution, the likelihood of TTz^{*2+} returning to the ground state through diffusion will increase as molecular collisions will occur more frequently. Therefore, as the concentration of R-BF_3K increases, the fluorescence quantum yield (as well as fluorescence intensity) is expected to decrease. This relationship can be used to create a Stern-Volmer plot which more clearly visualizes this relationship. The Stern-Volmer equation for dynamic quenching is given in Eq. 2.

Eq. 2.2 $$\frac{F_0}{F} = 1 + k_q\tau_0[Q] = 1 + K_D[Q] = \frac{\tau_0}{\tau}$$

The exact degree to which concentration effects quantum yield is expected to vary by R-BF_3K substrate. A substrate with a more readily oxidized carbon-boron bond is expected to have a greater slope on a Stern-Volmer plot. This analysis was conducted for the three R-BF_3K substrates analyzed in the initial studies, and the resulting plots are shown in Figure 2.19 and the resulting k_q value for each substrate are shown in Table 2.7.

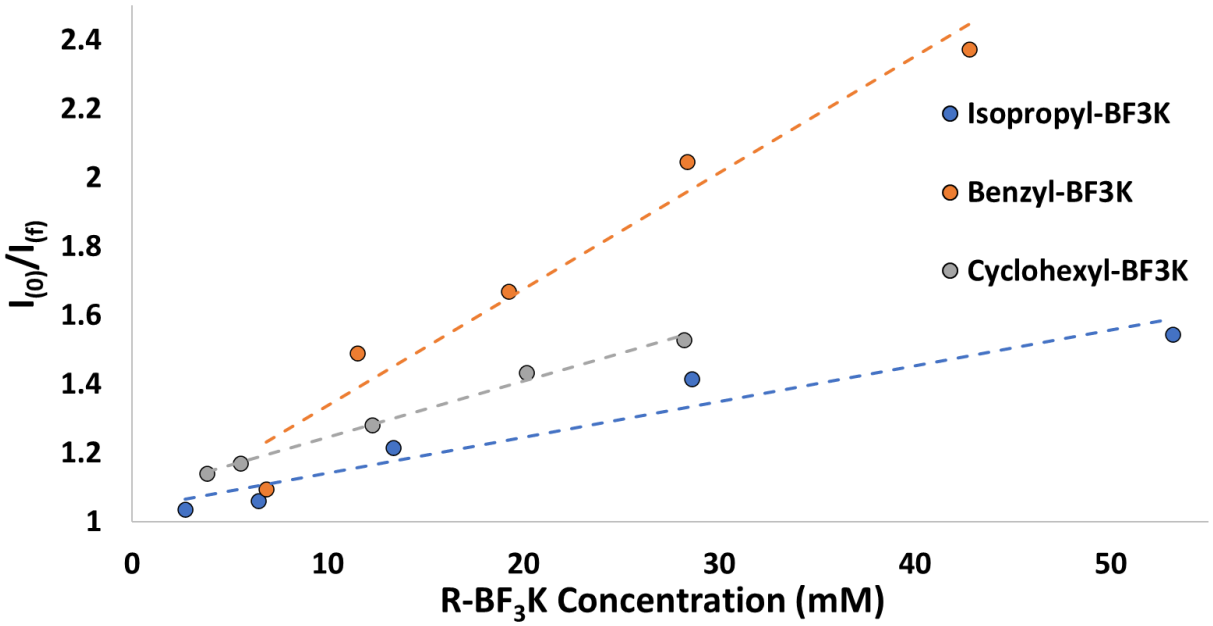

Figure 2.19: Stern-Volmer Plot and k_q Values

Table 2.7: k_q Values of R-BF_3K Substrates with $(MePy)_2TTz$ from Stern-Volmer Plot

Substrate	k_q ($L*mol^{-1}*s^{-1}$
Isopropyl-BF_3K	4188
Cyclohexyl-BF_3K	8709
Benzyl-BF_3K	16595

The results of this experiment demonstrate a significant relationship between substrate choice and k_q, implying an effect on the rate of step 2 in the catalytic cycle. Additionally, the trend between substrate and the value of k_q corresponds to the trend of expected organic radical stability. Following oxidation of the carbon-boron bond a carbon centered radical will be formed, the structures of which are shown in Figure 2.20.

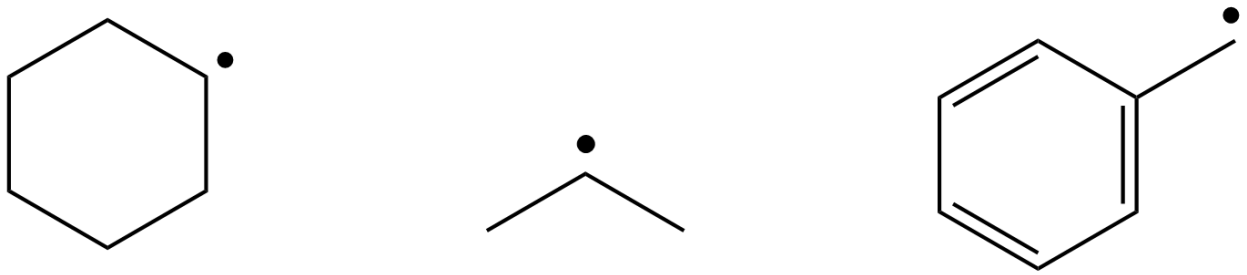

Figure 2.20: Carbon-centered radicals formed in photocatalytic cycle

A benzylic radical is expected to be more stable than a secondary radical, and between the two secondary radicals shown, the cyclohexyl radical is capable of additional stabilization relative to the isopropyl radical and has a greater expected stability.[35] Following this, Benzyl-BF_3K should be oxidized most readily, followed by the Cyclohexyl- Isopropyl- substrates. The greater stability of the benzylic radical may also explain why yields are lower with this substrate, as step 3 would be less favorable due to greater stability of the intermediate products. This is further supported by previous reaction screening using the iridium catalyst which suggested that species which form unstable carbon-centered radicals upon oxidation to not result in product formation.[26]

2.7 Probing the Color Changes

Multiple experiments were conducted to determine the relationship between the observed color changes in the reaction and product formation. Figure 14. shows that in the first 4 hours of the reaction, there is a distinct purple color that is observed. This was initially hypothesized to correspond to the singly reduced TTz species, as it appears purple when in other mediums. To probe this behavior, two samples were prepared - one containing the typical reaction mixture, and one without the imine substrate. Without the imine present in the mixture, the catalytic cycle cannot progress beyond step 2. It was expected that this would lead to an accumulation of the

singly reduced state that would linger for a longer period of time than in the typical reaction mixture. Shown in Figure 2.21 are the visual results of the experiment and shown in Figure 2.22 is the spectral analysis of a separate experimental run with the same conditions.

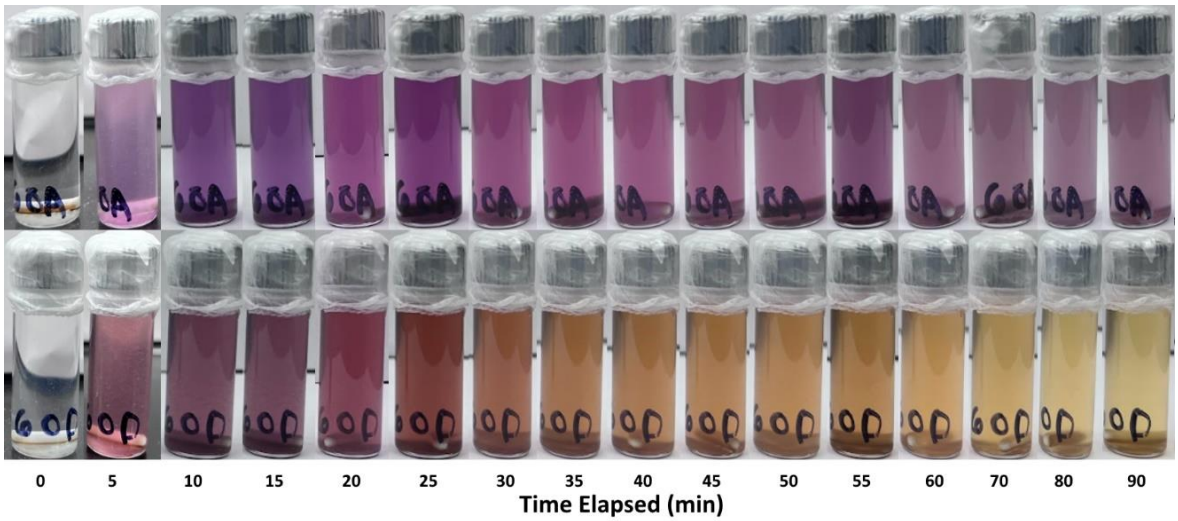

Figure 2.21: Visual Results of Color Tracking Experiments a) Standard Reaction b) No Imine Substrate

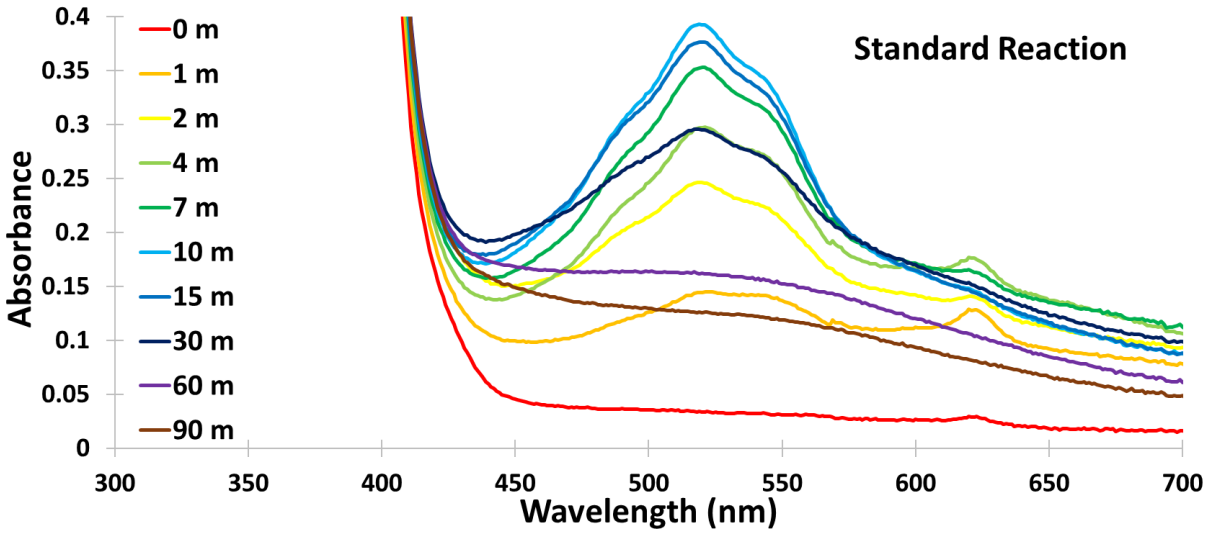

a)

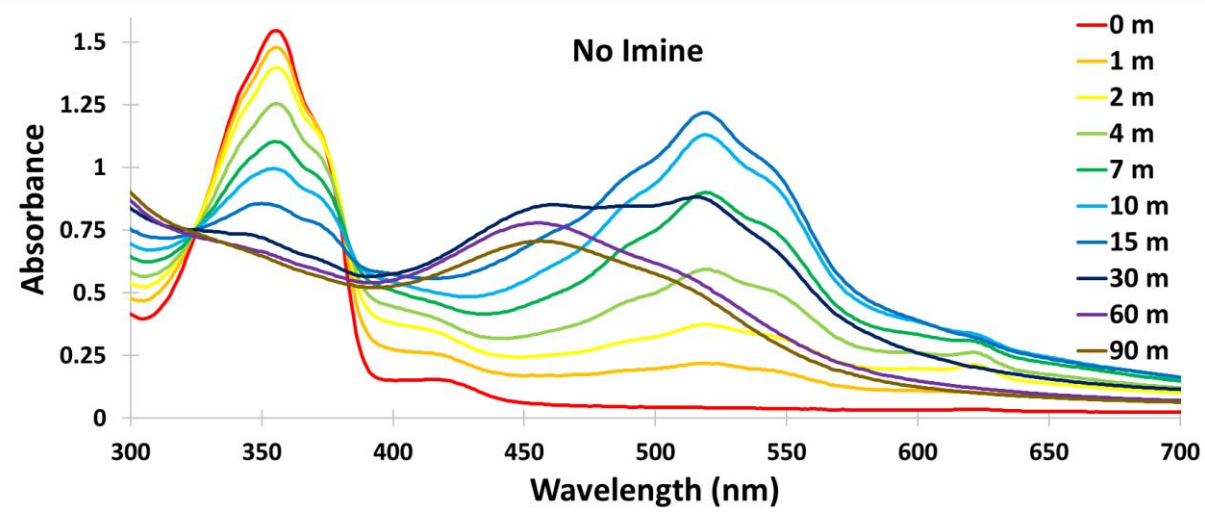

b)

Figure 2.22: – UV-Vis Spectra of Color Tracking Experiments a) Standard Reaction b) No Imine Substrate

This experiment produced surprising results relative to expectations. The purple-colored species seems more transient in the solution that does not contain any imine, appearing vividly for the first 5 minutes of the reaction, before quickly turning orange and fading into a colorless mixture. The standard reaction mixture remained purple for the first 4 hours as expected before changing to a continually darkening burnt-orange color until the 48-hour mark. In both

instances, the spectral measurements confirm a large increase of absorbance around 520 nm, and an initial small peak around 600 nm. The absorbance at 600 nm is hypothesized to be the singly reduced species, but there is no observed buildup of this state. Instead, the buildup is of another species that produces the orange color. This is speculated to be a variety of degraded catalyst species that have succumbed to photodegradation or photobleaching. Preliminary analysis via MALDI also suggests that this coloration could be from TTzs that have become alkylated via $R^{\bullet}$ present in the solution.

2.7.1 Catalyst Degradation Studies

A sample was prepared containing 50x more $[(MePy)_2TTz](PF_6)_2$ than would typically be used in a standard reaction mixture along with the standard mass of isopropyl-BF_3K. No imine was added to the solution. This sample was illuminated for 5 days with 2x 405 nm LED arrays. Following prolonged illumination, the reaction mixture was a dark brown color. H_1-NMR was conducted but provided no useful data. Analysis by MALDI was speculated to yield greater insight, thus MALDI analysis was conducted on a sample from the reaction mixture. The resulting MALDI data is shown in Figure 2.23.

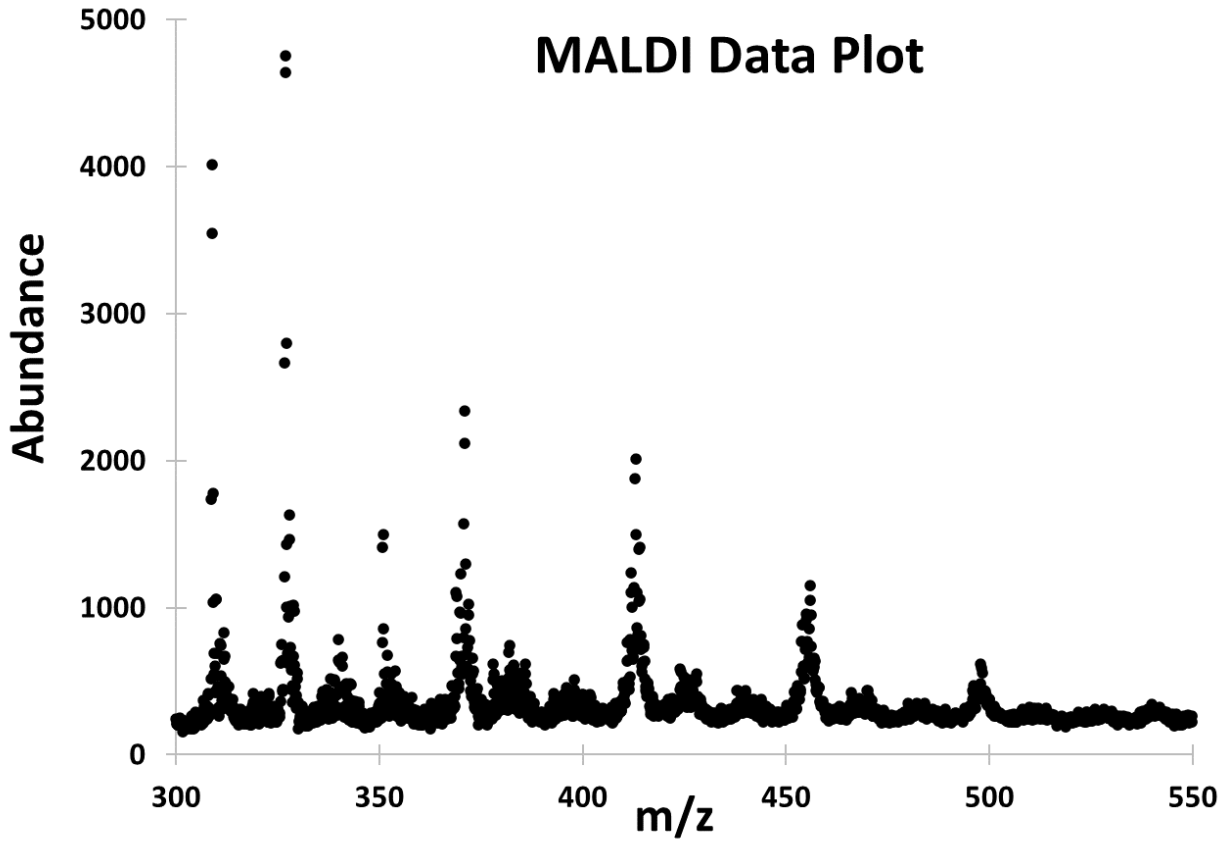

Figure 2.23: MALDI Data

Within the MALDI spectra there are several defined m/z peaks. The parent peak of $[(MePy)_2TTz](PF_6)_2$ is identified at m/z 327. Additionally, there were many other peaks at a seemingly repeating interval. Shown in Figure 2.24 are the normalized frequencies of the other notable peaks.

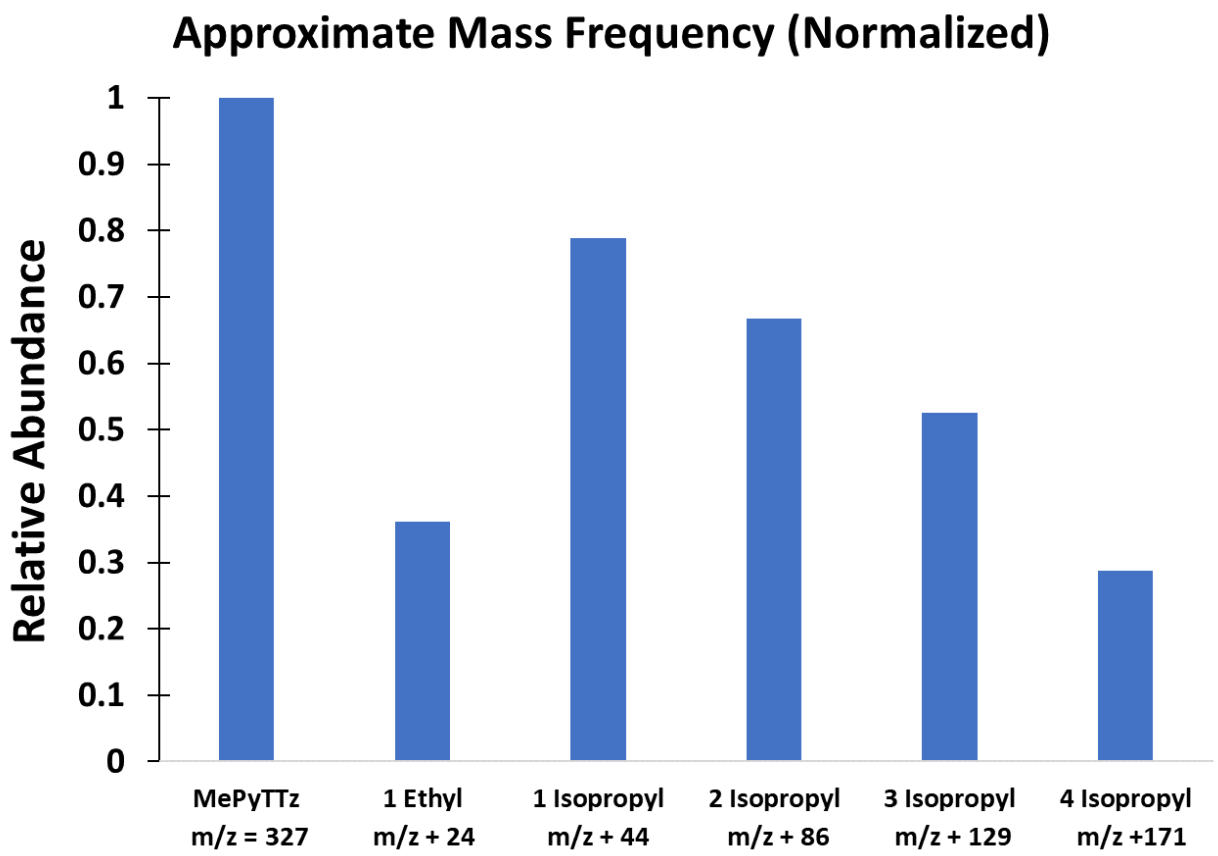

Figure 2.24: Relative Frequency of Peaks of Note from MALDI Data

As stated, the parent+ peaks seem to indicate the addition of mass equivalent to an isopropyl group (m/z +43), with an exception of a m/z +24 peak indicating the addition of 2 carbons (notated as ethyl). Interestingly, there were no discernible instances of the addition of an isopropyl group and the ethyl group, which would have been expected at m/z +67. Likely the addition of the ethyl group (or just 2 carbons) is another degradation pathway that discourages the addition of the isopropyl groups. Considering the decreasing relative abundance of the parent+ peaks, it is reasonable to believe that the addition of each subsequent isopropyl group is less favorable or at a slower rate than the last.

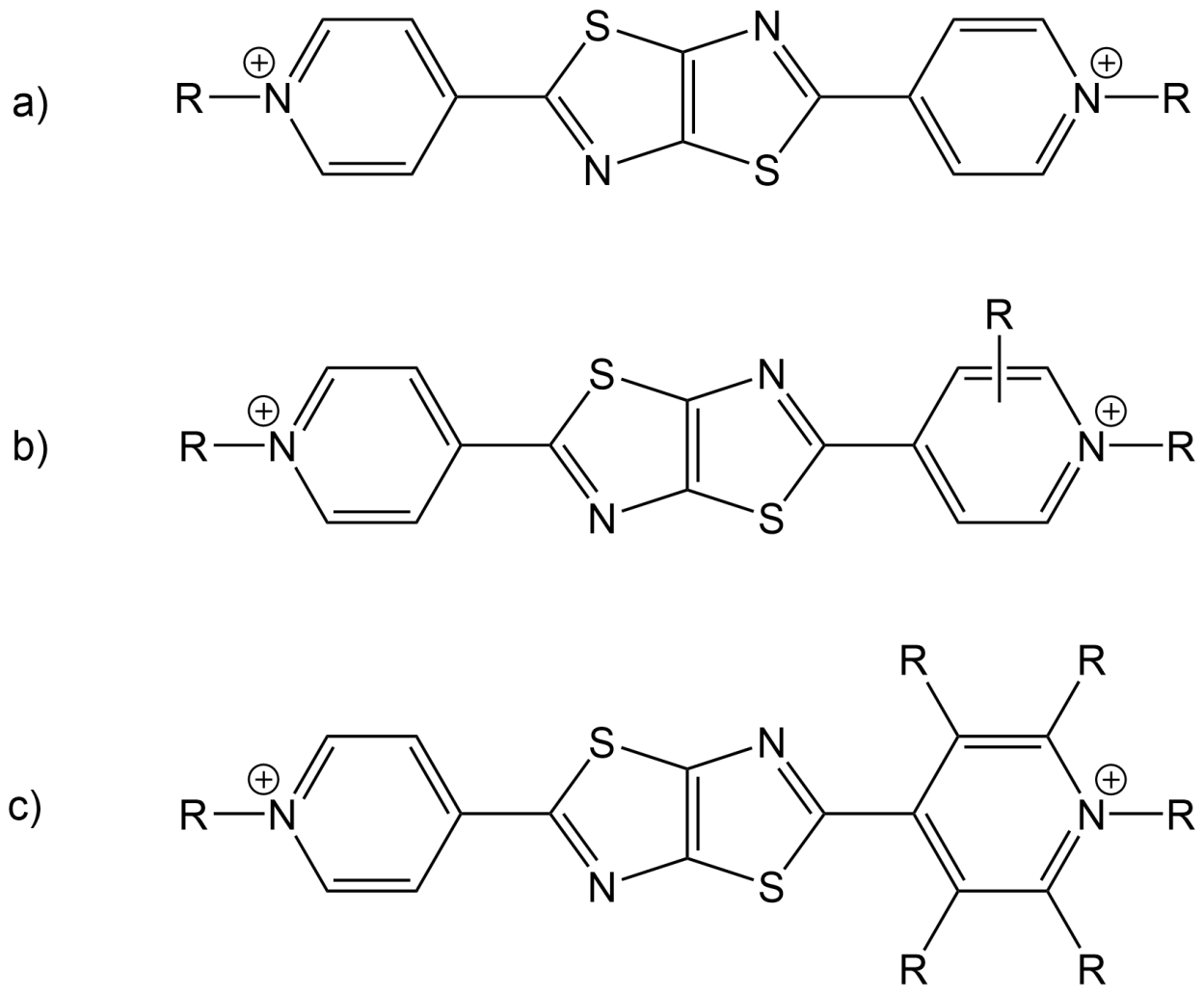

Figure 2.25: a) General initial structure of $(Py)_2TTz$ derivatives b) Initial addition of alkyl group through photodegradation c) Final product after 4 instances of alkyl addition to TTz

Considering the results of both the color tracking experiments and the MALDI data, we believe there is evidence that the orange color observed at the end of the photoreaction is not actually associated with product formation, but rather catalyst degradation.

2.8 Amine Oxidation Experiments

In addition to imine alkylation reactions, TTz photocatalysts have demonstrated their use as photocatalysts in other systems. The ability to drive amine oxidation has been demonstrated by $[(MePy)_2TTz](PF_6)_2$. Thus far, we have shown this with both DMAP and triethylamine, the structures of which are shown in Figure 2.26.

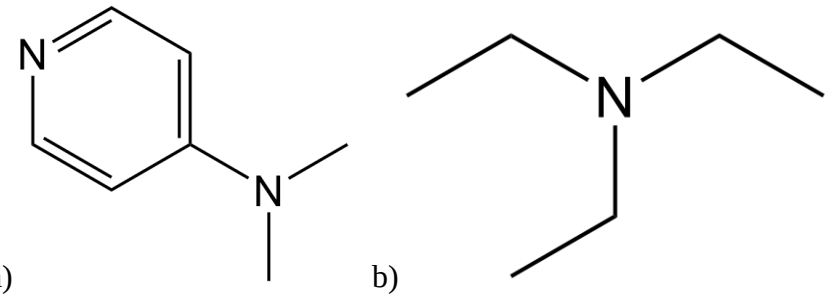

a) b)

Figure 2.26: Structure of a) DMAP and b) triethylamine

Both substrates are tertiary amines, which are currently the only type of amine that TTzs have been shown to oxidize in solution. The oxidation of these compounds is well studied in other systems and in the presence of oxygen will typically form amine oxides. In anerobic conditions, the structure of the oxidized product is more difficult to predict, especially as ^1H-NMR data has been inconclusive.

Shown in Figure 2.27 is the absorbance spectra of $[(MePy)_2TTz](PF_6)_2$ at various times in a reaction with DMAP accompanied by a picture of the vial at the associated times. This reaction was driven using a UV-Beast flashlight, which emits light centered at 395 nm.

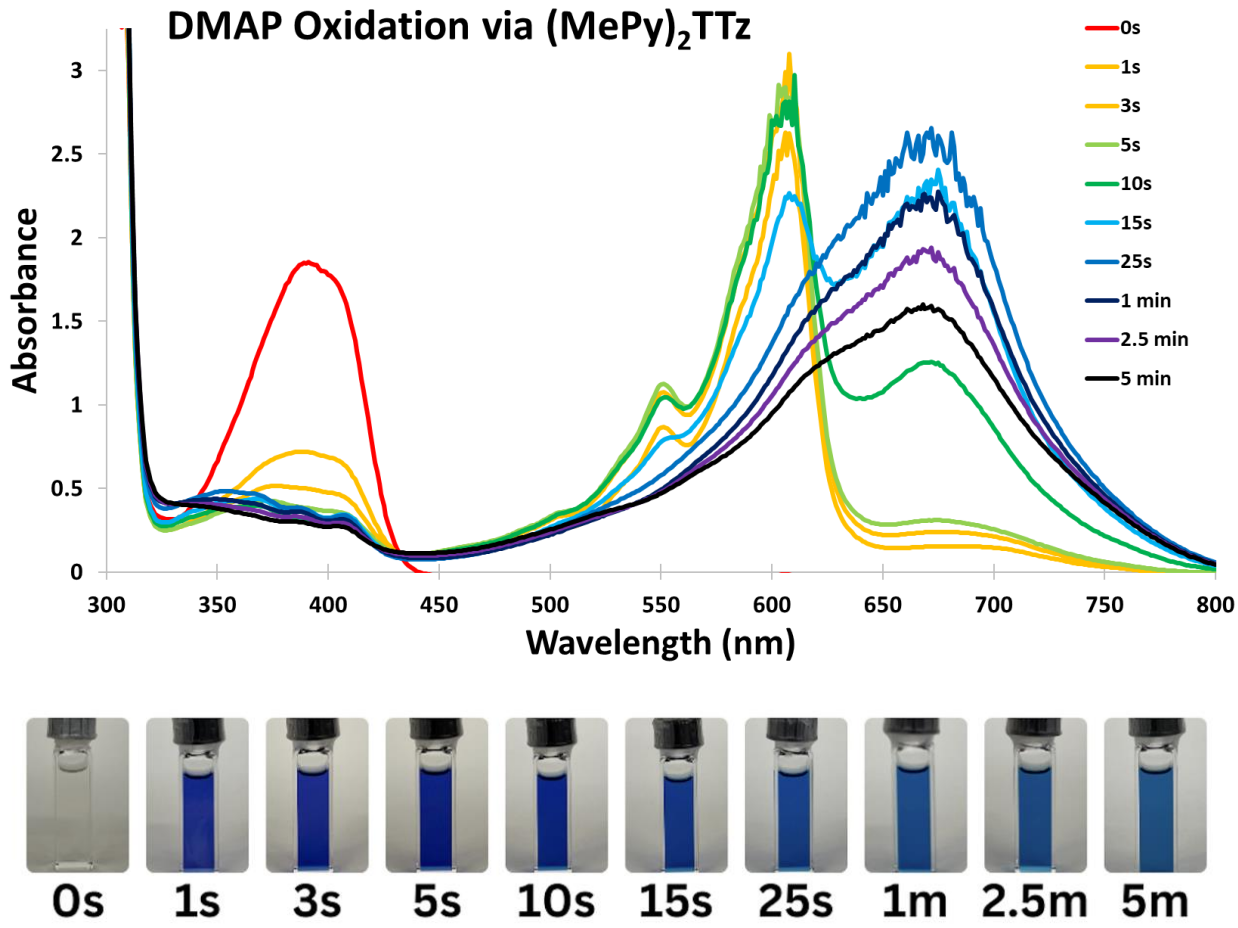

Figure 2.27: Absorbance Spectra and Vial Image of DMAP Oxidation with $[(MePy)_2TTz](PF_6)_2$

Figure 2.28 shows the redox energetics diagram for the oxidation of DMAP and triethylamine by $[(MePy)_2TTz](PF_6)_2$. This diagram visualizes the energetic favorability for the oxidation of these amines by the excited state of both the non-reduced and singly-reduced states.

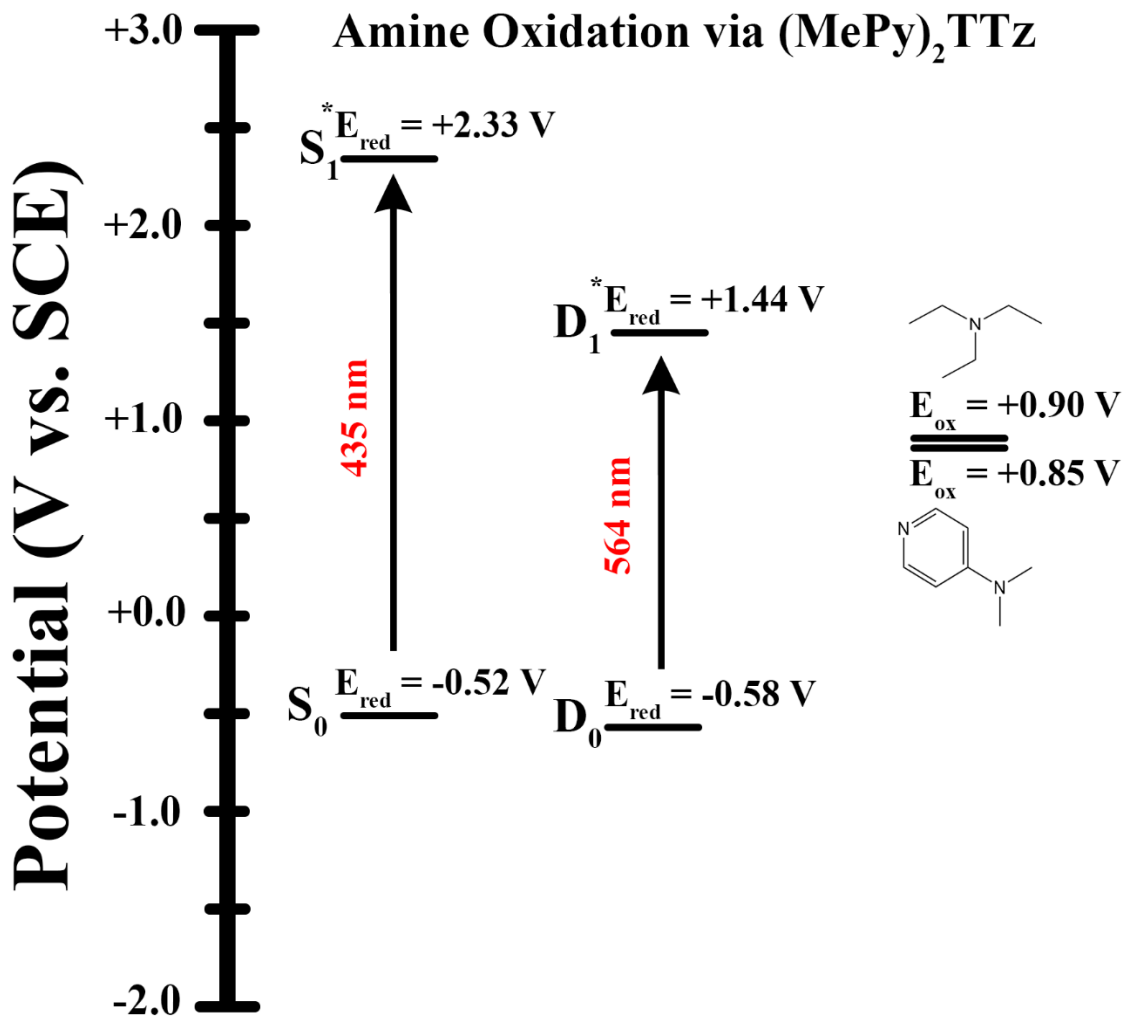

Figure 2.28: Redox Energetics of Amine Oxidation

The reaction begins nearly instantly, as the absorbance at 400 nm drops significantly after only one second of illumination. This decrease in absorbance at 400 nm is coupled with an increase in absorbance at 600 nm, which is believed to be due to formation of the singly-reduced TTz. This trend continues until 10 seconds of illumination, at which point the absorbance peak at 600 nm begins to decrease and a lower energy absorption band appears centered at 680 nm. This indicates the formation of the doubly-reduced TTz state. While this experiment further suggests the formation of the doubly-reduced TTz species the method of formation is not well understood.

Dual wavelength experimentation was conducted on the same reaction scheme to investigate the mechanistic possibilities. Two sets of two LEDs were used, with one set emitting at 405 nm and the other emitting at 595 nm. These were the LEDs that matched most closely with the maximum absorbance for TTz^{2+} and $TTz^{1+\bullet}$. As the previous experiment was conducted with a UV-Beast flashlight which has a higher intensity of emission, a control was performed using only the 405 nm LEDs. The control with only 405 nm LEDs demonstrated similar behavior to using only the UV beast, with an overall slower reaction rate. Seen in Figure 2.29. are the results of the dual wavelength experiment.

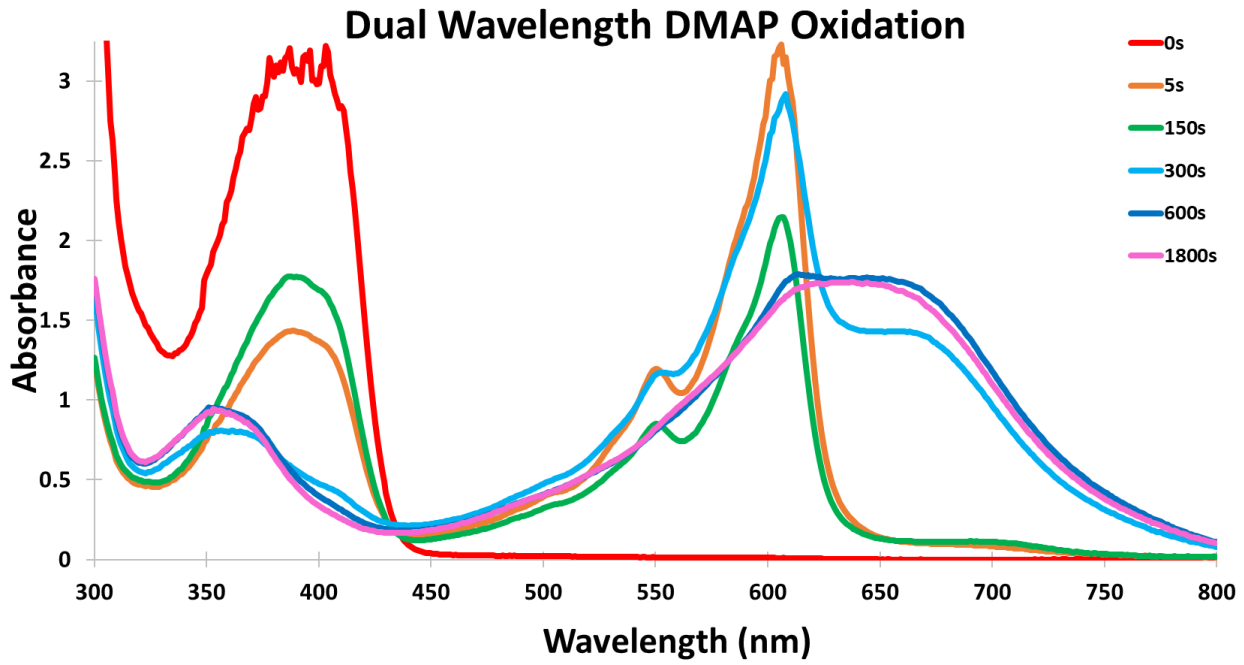

Figure 2.29: Dual Wavelength Amine Oxidation Experiment Results

The initial absorbance was obtained, which shows a single absorbance band centered on 400 nm. After 5 seconds of illumination with 405 nm LED arrays, this absorbance was greatly diminished, and as expected a strong absorbance peak was now present at 600 nm. Following this, only 595 nm lights were used until 150 seconds. While illuminated by this wavelength, there was very little change to the spectra. By 150 seconds, the spectrum indicated that $TTz^{1+\bullet}$

had begun to revert to TTz^{2+} as the intensity of the 400 nm absorbance increased with an accompanying decrease in absorption at 600 nm. There was an incredibly small amount of absorbance increase around 700 nm, so it is possible a small amount of doubly-reduced TTz formed in this time due to disproportionation. This generally suggests however, that the primary mechanism of conversion to the doubly-reduced state does not occur in the absence of light. After 150 seconds, the 405 nm lights were used again, which immediately caused an increase in the absorption at 600 nm and formed the doubly reduced peak at 650 nm. Illumination with the 405 nm LEDs was continued until 600 seconds, at which point the spectrum indicated near-total conversion to the doubly reduced species. For the next 20 minutes (total of 1800 seconds of reaction time) the 595 nm arrays were used again. During this time, the color seemed to be stable, with very little observed differences in the absorption. The results of this experiment indicate that 595 nm lights in isolation do not seem to be capable of converting the singly-reduced $TTz^{\bullet 1+}$ into the doubly-reduced TTz^{0} or enable it to oxidize and amine. While this could suggest that a different wavelength of light is required, or that the absorbance peak at ~600 nm is not caused by the singly-reduced species, it is more likely due to the short-lived excited state lifetimes of $TTz^{*\bullet 1+}$.

As stated before, the singly reduced TTz species, shown in Figure 26., while possessing favorable excited state redox potentials likely does not have a sufficiently long excited state lifetime to oxidize the amine.[30,31] While the lifetime of this species is not confirmed, this would align with the typical expectation for an excited radical doublet state. We therefore believe that while the formation of the doubly-reduced TTz^{0} occurs in this system, it is not through the oxidation of an amine substrate by $TTz^{*\bullet 1+}$. The results of this experiment provide additional

support and explanation for the lack of enhancement when using 595 nm light observed in the imine alkylation reactions.

2.9 Conclusion

TTzs were utilized as photoredox catalysts for driving imine alkylation reactions, which are of great synthetic importance. While this transformation has been demonstrated before with iridium catalysts, this work is a step towards finding more sustainable and economically viable photocatalysts for widespread adoption. Analysis with Stern-Volmer plots help to characterize the imine alkylation reaction as a whole and identify a link between reaction favorability and organic radical stability. Color tracking experiments with additional support from MALDI analysis also yielded key insights towards the reaction mechanism and catalyst degradation routes. Most importantly, the development of a photoreactor capable of probing the effects of wavelength on photocatalyst performance enabled a new type of experiment to be performed probing this characteristic. The results of this experiment found that $[(MePy)_2TTz](PF_6)_2$ does not seem to form additional product when exposed to multiple wavelengths of light. Additional studies with amine oxidation not only demonstrate another application of these catalysts, but dual-wavelength studies reinforce that lower energy wavelengths of light do not enable additional photocatalytic performance. While dual-wavelength studies may not have revealed new novel characteristics concerning TTz photocatalysis, this work has deepened the understanding of the catalyst series and gives key insights into future applications for these materials.

2.10 Appendix I: Supplementary Information

General Example of Yield Calculation

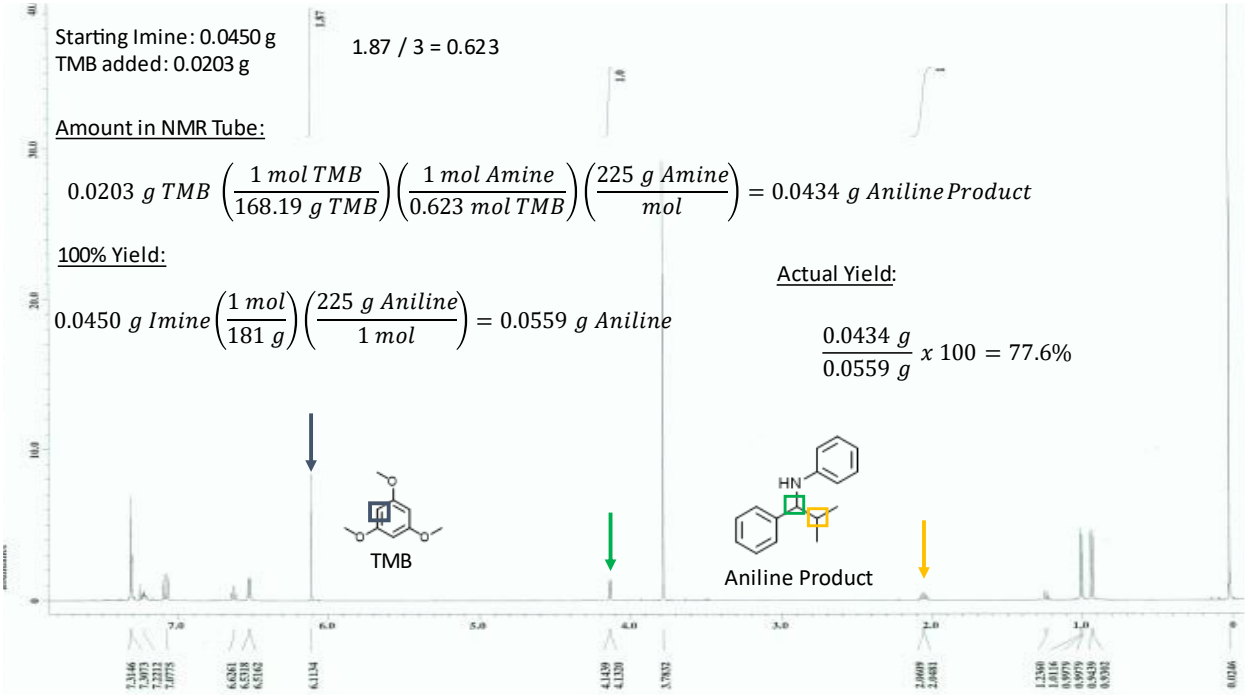

Supplementary Figure 1: Example calculation of ^{1}H-NMR yield determination using an internal standard.

Synthesis

Synthesis of 2,5-di(pyridin-4-yl)thiazolo[5,4-d]thiazole ***(Py$_2$TTz)***. Dithiooxamide (0.5020 g, 4.183 mmol) and 4-pyridinecarboxaldehyde (1.1802 g, 11.0 mmol) were refluxed in 25 mL of DMF at 140 ^{o}C for 6 h in an aerated environment. The reaction mixture was cooled to room temperature, and the obtained tan precipitate was filtered via vacuum. The solid was then washed with water and dried under vacuum to give a tan solid in 74.2% yield (0.9204 g). Molecular characterization data matched previously reported values.[36,37] **^{1}H-NMR** (300 MHz, $CDCl_3$): 8.78 (dd, J = 1.6, 4.6 Hz, 4H), 7.89 (dd, J = 1.6, 4.6 Hz, 4H) ppm.

Synthesis of N,N'-dimethyl 2,5-Bis(4-pyridinium)thiazolo[5,4-d]thiazole dihexafluorophosphate ***[(MePy)$_2$TTz^{2+}](PF$_6$)$_2$.*** Following the method of Roy et al.,[38] Py_2TTz (0.0552 g, 0.186 mmol), acetonitrile (5 mL), and iodomethane (2 mL) were refluxed at 50 ^oC for 6 h. The precipitate was collected, vacuum filtered, and rinsed with hexanes. The red solid was then dissolved in water (50 mL) and NH_4PF_6 (3 g) added. The suspension was then vacuum filtered and rinsed with water to give a white solid (0.0817 g, 71.2% yield). **^{1}H-NMR** (300 MHz, CD_3CN, TMS, δ): 8.75 (d, J = 6.87 Hz, 4H), 8.54 (d, J = 6.87 Hz, 4H), 4.34 (s, 6H).

Synthesis of N,N'-di(trimethylaminopropyl)-2,5-Bis(4-pyridinium)thiazolo[5,4-d]thiazole tetrahexafluorophosphate ***[(NPrPy)$_2$TTz^{+4}](PF$_6$)$_4$.*** Following the method of Luo et al.,[39] Py_2TTz (0.9104 g, 3.075 mmol) was refluxed with (3-bromopropyl) trimethylammonium bromide (2.0025 g, 7.672 mmol) in anhydrous DMF under nitrogen at 100 ^oC for 72 h. The precipitate obtained was vacuum filtered and rinsed with DMF and acetonitrile, then dried in the oven to give a yellow solid (2.5181 g, 95.2% yield). *[(NPrPy)$_2$TTz^{+4}]Br$_4$* (0.1474 g 0.180 mmol) was added to water (20 mL) and precipitated out with excess NH_4PF_6. The solution was then filtered and a pale-yellow solid collected (0.1539 g, 79.3% yield). **^{1}H-NMR** (ACN, 300 MHz): δ (ppm), 8.78 (d, 2H), 8.60 (d, 2H), 4.56 (t, 2H), 3.32 (t, 2H), 3.04 (s, 3H), 2.43 (m, 2H).

Synthesis of N,N'-dibenzyl 2,5-bis(4-pyridinium)thiazolo[5,4-d] thiazole dichloride ***[(BzPy)$_2$TTz^{+4}](PF$_6$)$_2$.*** $[(BzPy)_2TTz^{+4}](Br)_2$[40] (0.0974 g, 0.142 mmol) was added to water (100 mL) and NH_4PF_6 (4 g) added to precipitate out the product. The suspension was vacuum filtered and rinsed with water to give a white powder (0.0849 g, 78.1% yield). **^{1}H-NMR** (300 MHz, DMSO, TMS, δ): 8.91 (d, 2H), 8.50 (d, 2H), 7.48 (m, 5H), 5.73 (s, 2H).

Stern-Volmer Procedure

A stock solution of $[(MePy_2)TTz](PF_6)_2$ was prepared in anhydrous ACN with a concentration of ~10 uM inside of a nitrogen glovebox. A predetermined mass of R-BF_3K was measured and placed in a standard quartz cuvette with a 1 cm pathlength, which was brought into the glovebox after weighing. The cuvette was filled with 3 mL of the stock solution. The cuvette was sealed tightly and the lid wrapped in parafilm. After sealing, the cuvette was brought to the Horiba Fluoromax and the fluorescence lifetime was obtained.

Photophysical Properties

Fluorescence Lifetimes

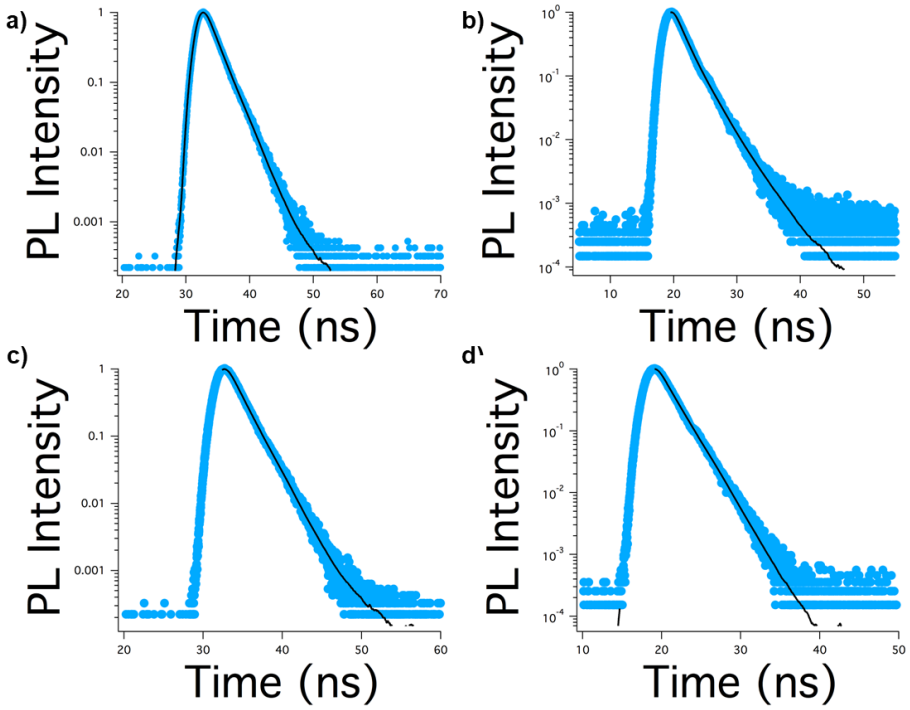

Supplementary Figure 2: Fluorescence lifetimes of TTz derivatives. All are in DCM except for NPr_2TTz in ACN. **a)** Bz_2TTz, **b)** $(F_5Bz)_2TTz$, **c)** Me_2TTz, and **d)** NPr_2TTz.

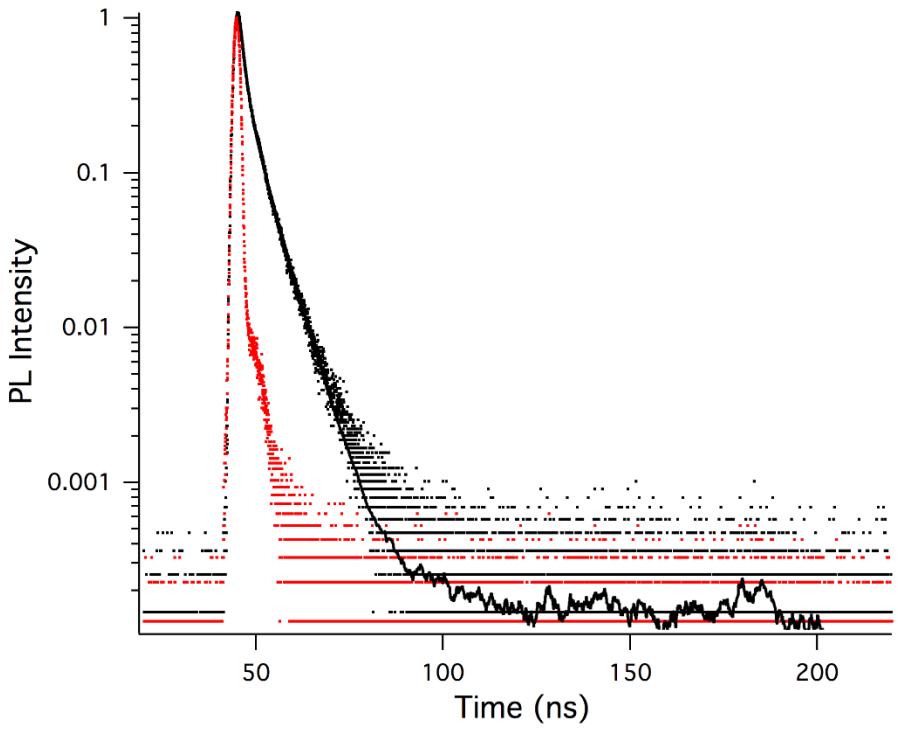

Supplementary Figure 3: Fluorescence lifetimes of singly reduced state ($TTz^{\bullet 1+}$) from Me_2TTz using 558 nm emission.The red dotted line is the prompt and the blank dotted line is the lifetime of $TTz^{\bullet 1+}$ with the fitted solid blank line.

Computation

For general vacuum optimizations, keywords: **# opt PBE1PBE/6-311+g(d,p) geom=save geom=connectivity** was used. Density functional theory (DFT) calculations were performed with Gaussian computational software using and PBE1PBE[41] density functionals and 6-311+G(d,p)[42] basis set.

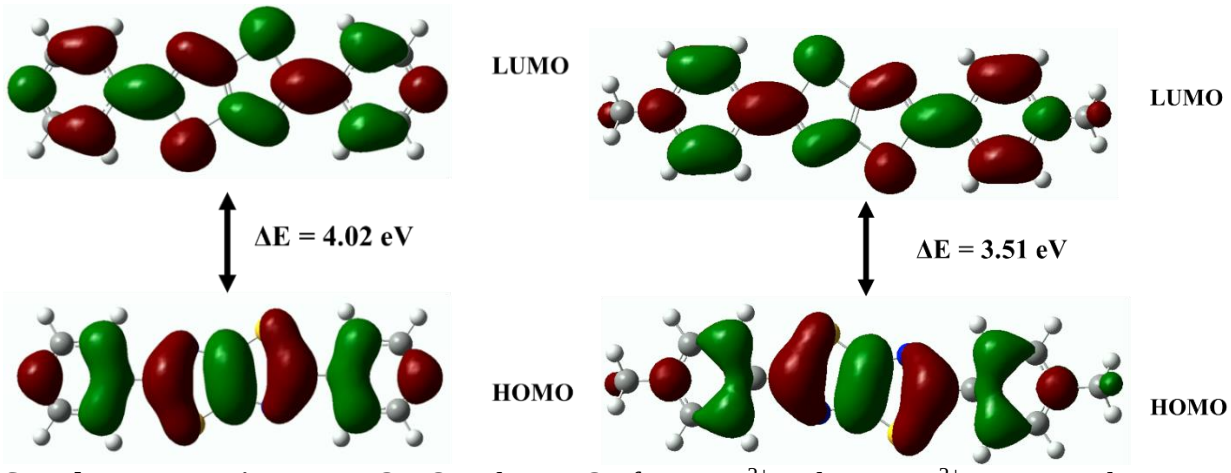

Supplementary Figure 4: HOMO and LUMO of Py_2TTz^{2+} and Me_2TTz^{2+}, respectively.

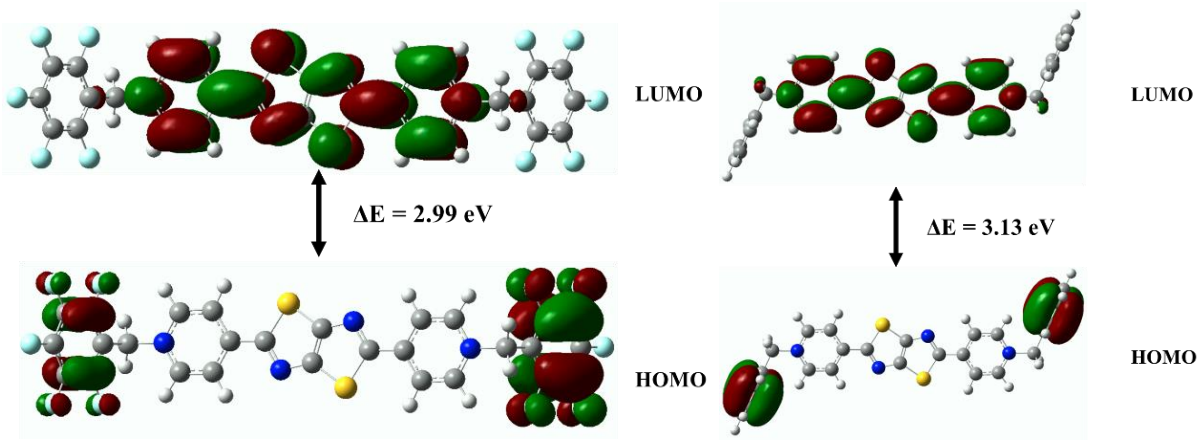

Supplementary Figure 5: HOMO and LUMO of $(F_5BzPy)_2TTz^{2+}$ and Bz_2TTz^{2+}, respectively.

Electrochemical Characterization

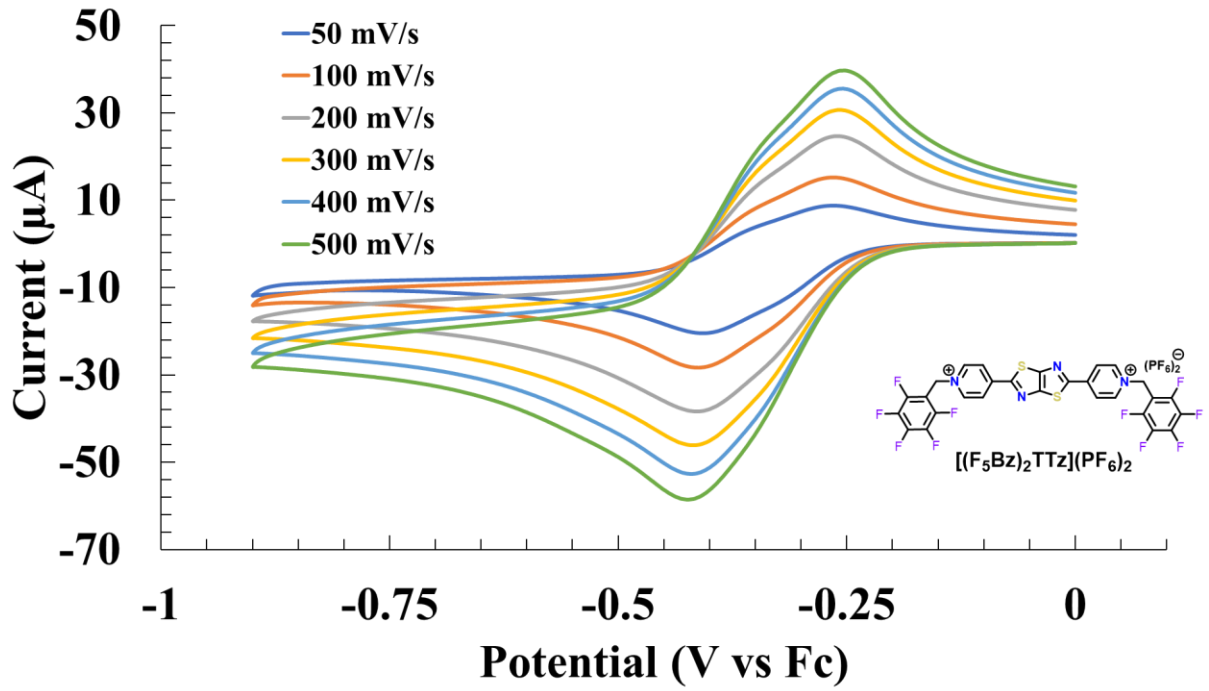

Supplementary Figure 6: Cyclic voltammetry of $(F_5BzPy)_2TTz^{2+}$ in conditions stated previously.

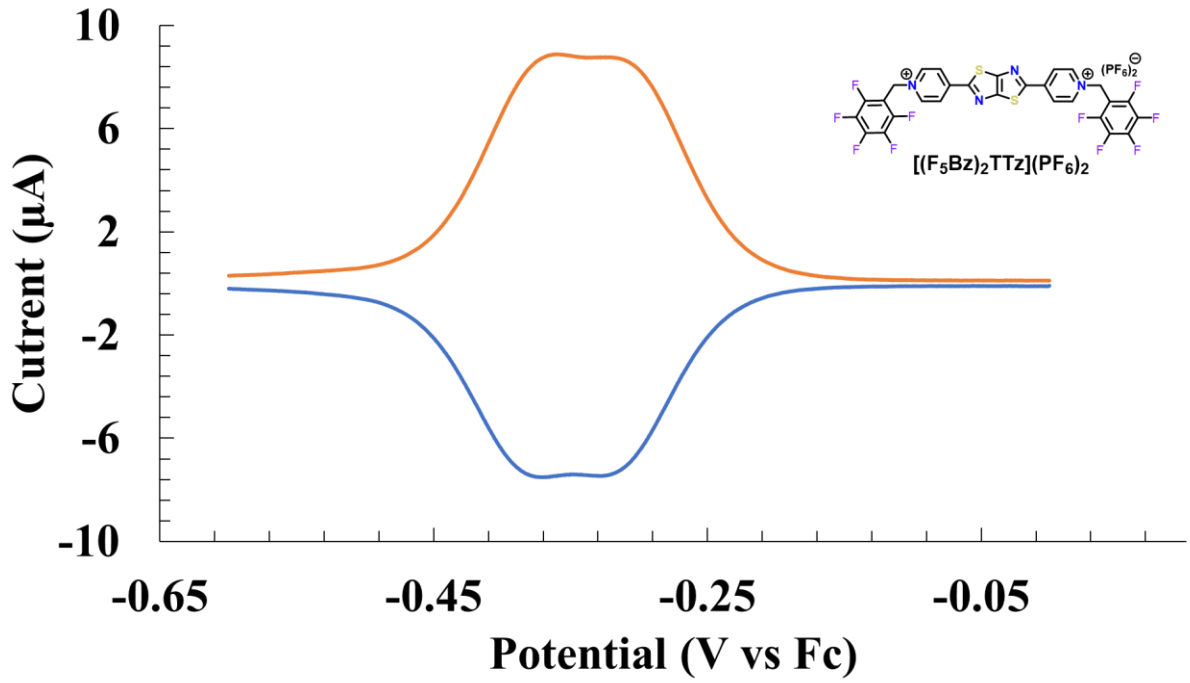

Supplementary Figure 7: Square wave voltammetry of $(F_5BzPy)_2TTz^{2+}$ in conditions stated previously.

^{1}H-NMR and GCMS

Aniline Products

N-(1-Isopropyl-1-phenylmethyl)aniline

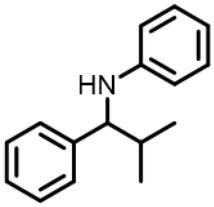

^{1}H NMR (400 MHz, $CDCl_3$): δ 0.91 (d, J = 6.79 Hz, 3H), 0.97 (d, J = 6.77 Hz, 3H), 1.98-2.06 (m, 1H), 4.10 (s, 1H), 4,12 (s, 1H), 6.49 (d, J = 7.88 Hz, 2H), 6.60 (t, J = 7.26 Hz, 1H), 7.03-7.07 (m, 2H), 7.17-7.22 (m, 1H), 7.26-7.29 (m, 4H) ppm. These data are in agreement with reported literature data.[43]

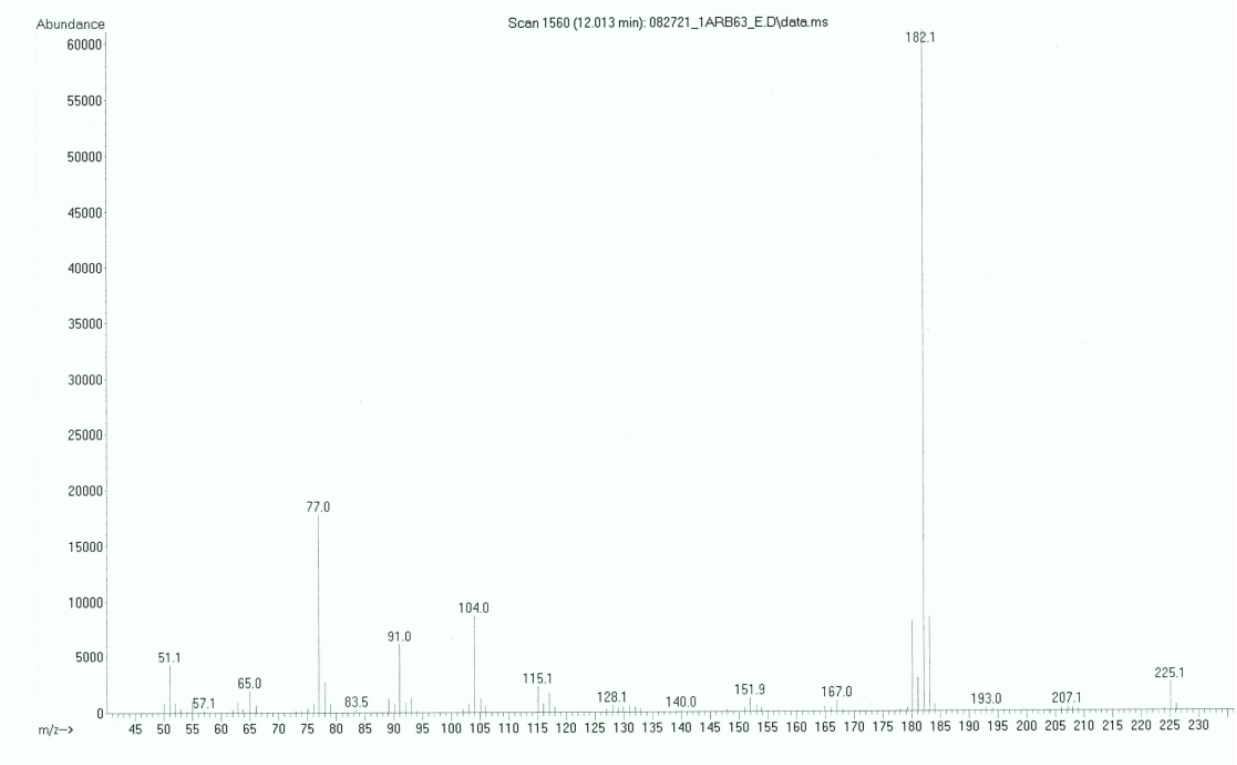

Supplementary Figure 8: MS of *N*-(1-Isopropyl-1-phenylmethyl)aniline.

<u>*N*-(1,2-Diphenylethyl)aniline</u>

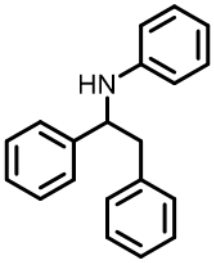

^{1}H-NMR ($CDCl_3$, 300 MHz): δ 7.38-7.19 (m, 8H), 7.18-7.11 (m, 2H),7.10-7.02 (m, 2H), 6.68-6.61 (m, 1H), 6.51-6.44 (m, 2H), 4.62-4.56 (m, 1H), 4.12 (br s, 1H), 3.20-2.97 (m, 2H). These data are in agreement with reported literature data.[44]

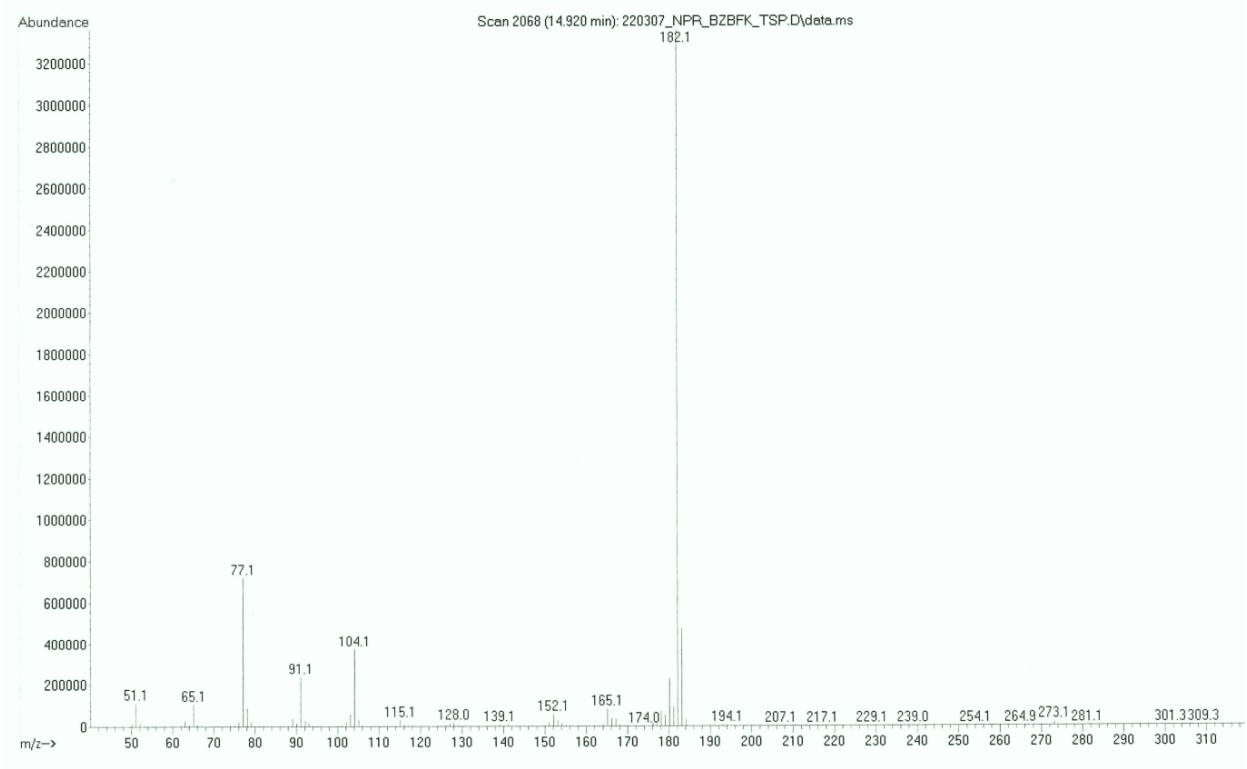

Supplementary Figure 9: MS of N-(1,2-Diphenylethyl)aniline.

N-(1-Cyclohexyl-1-phenylmethyl)aniline

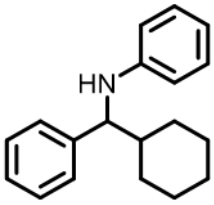

^{1}H-NMR ($CDCl_3$, 300 MHz): δ 7.31-7.16 (m, 5H), 7.10-7.01 (m, 2H), 6.64-6.56 (m, 1H), 6.52-6.45 (m, 2H), 5.86-5.68 (m, 1H), 4.15 (s, 1H), 4.11 (d, 1H), 4.18 (s, 1H), 1.94-1.44 (m, 6H), 1.30-0.94 (m, 5H). These data are in agreement with reported literature data.[45]

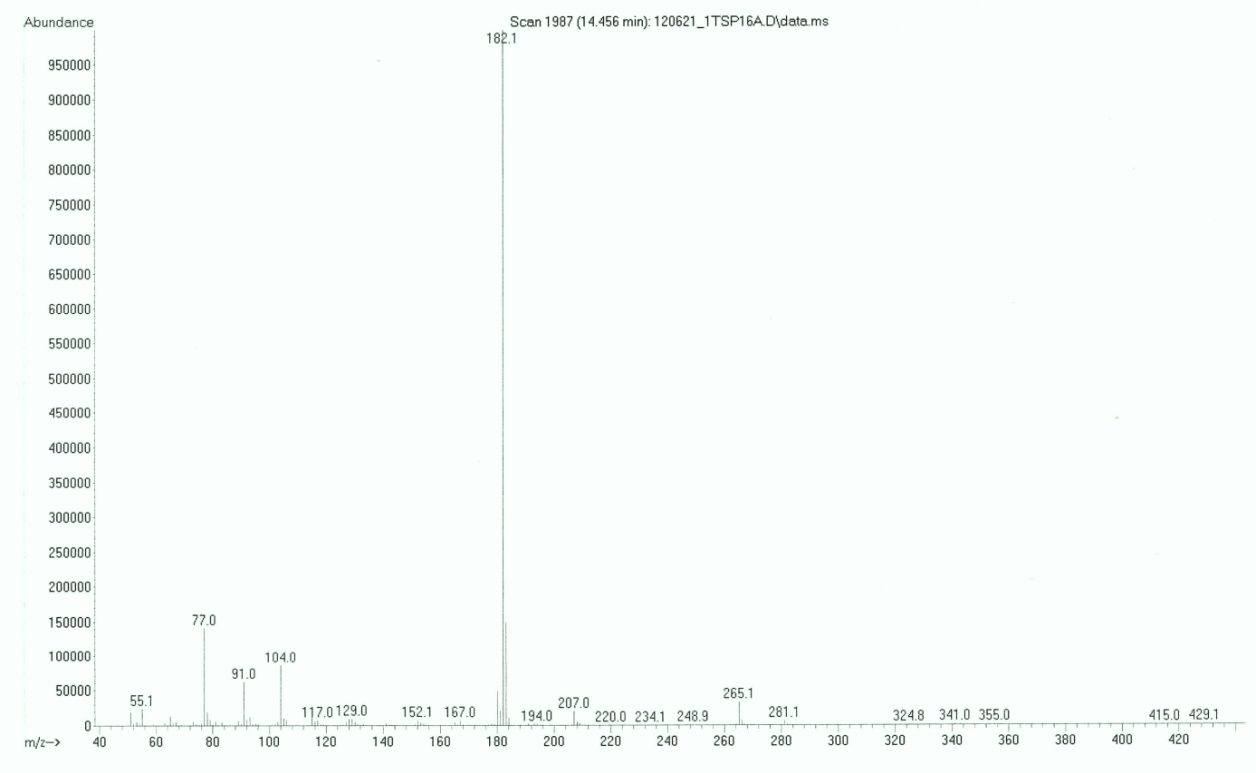

Supplementary Figure 10: MS of *N*-(1-Cyclohexyl-1-phenylmethyl)aniline.

New TTz Derivatives

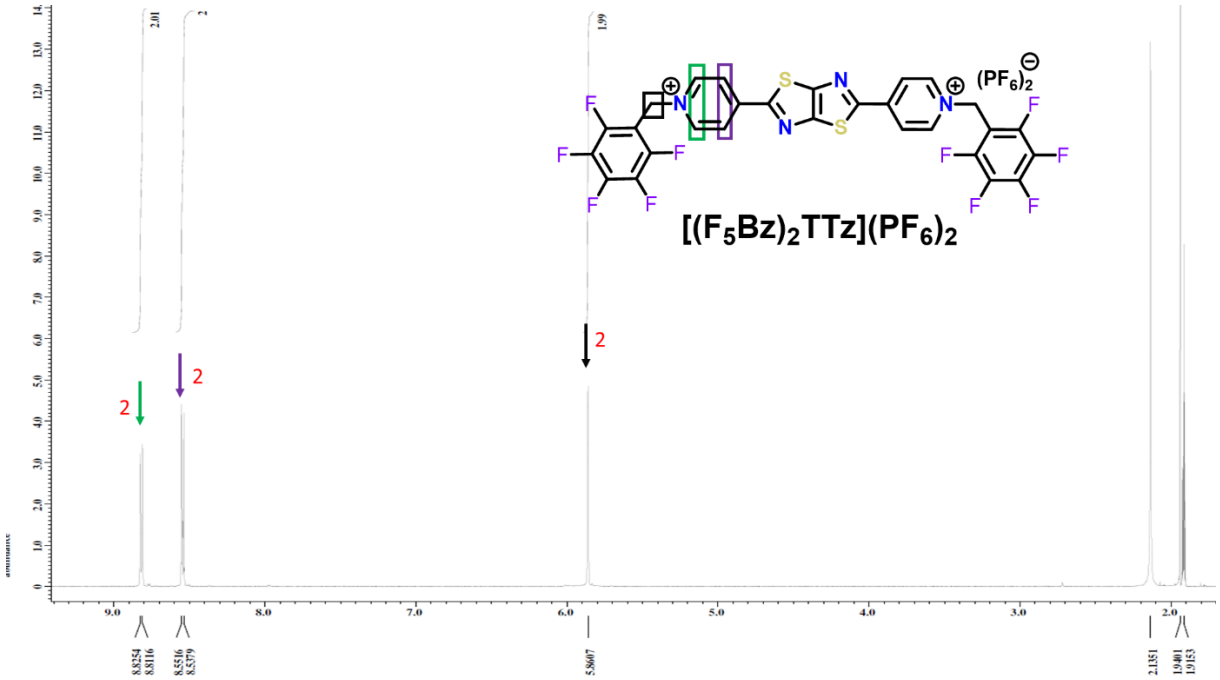

Supplementary Figure 11: ^{1}H-NMR of $[(F_5Bz)_2TTz](PF_6)_2$ in d-ACN.

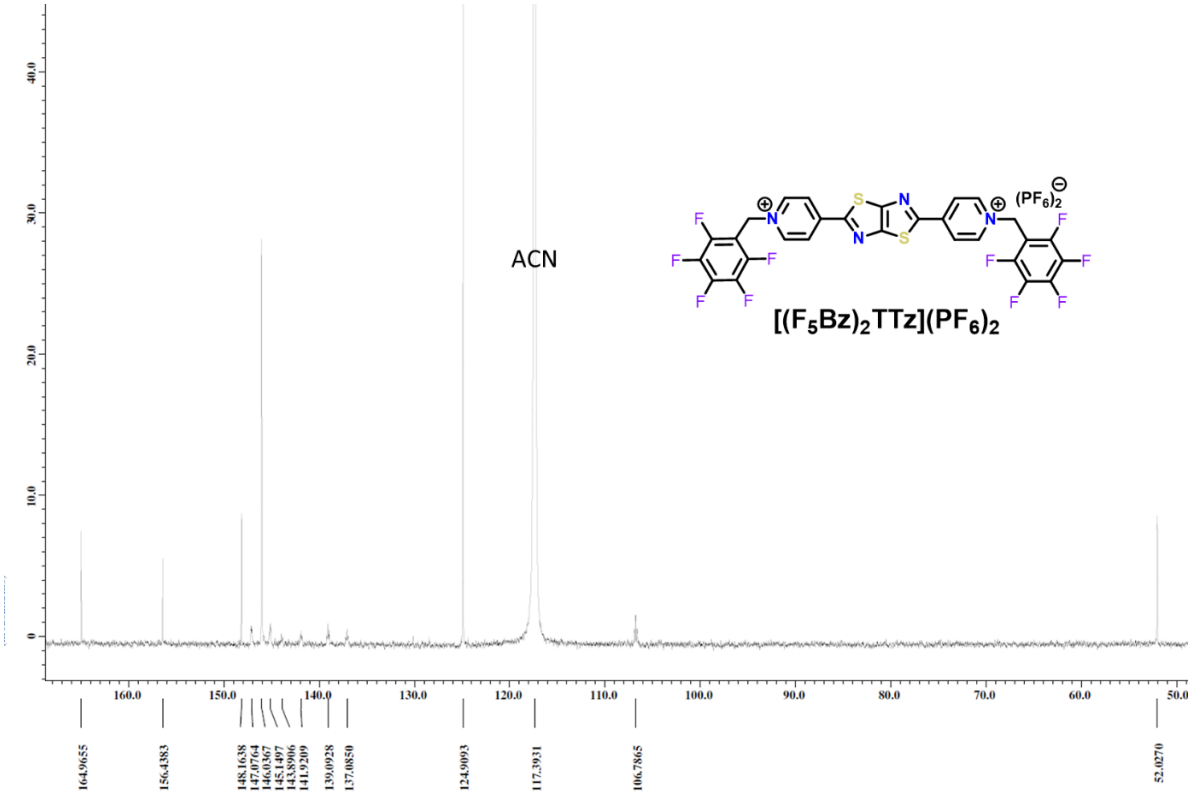

Supplementary Figure 12: ^{13}C-NMR of $[(F_5Bz)_2TTz](PF_6)_2$ in d-ACN.

MALDI

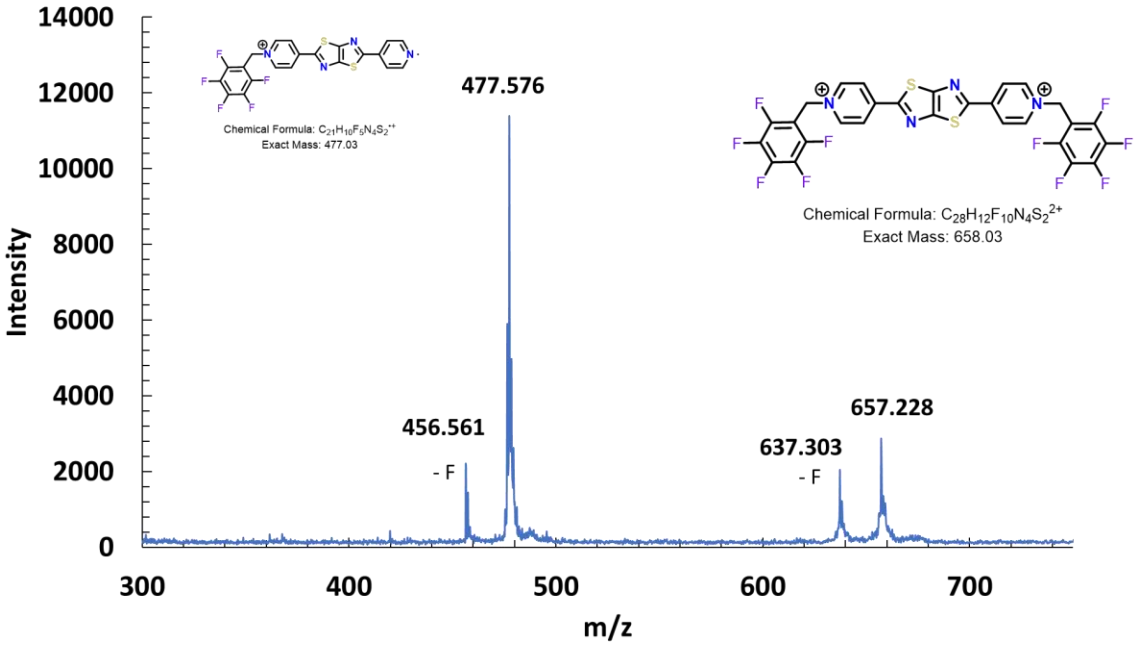

Supplementary Figure 13: MALDI-TOF of $[(F_5Bz)_2TTz](PF_6)_2$.

CHAPTER 3: NATURALLY DERIVED PERYLENEQUINONE PHOTOCATALYSTS

3.1 Introduction

Hypocrellins, which are a type perylenequinone (PQ) have recently demonstrated their use in photodynamic therapy. Hypocrellin B (HC-B) and *ent*-Shiraiachrome A (SH-A) are some of the most prominent members of this group of fungal metabolites. This portion of work was done largely in collaboration with a group from UNC-Greensboro, who have recently reported the isolation of additional types of PQ dyes from a fungus (*Shiraia*-like sp. strain MSX60519). These include HC-B, SH-A, and three hypomycins, hypomycin A (HM-A), hypomycin C (HM-C), and hypomycin E (HM-E). The hypomycin dyes are similar to hypocrellins on a structural level but feature an additional six-membered ring and a lesser degree of π-conjugation. The structure of the aforementioned PQ dyes are given in Figure 3.1.

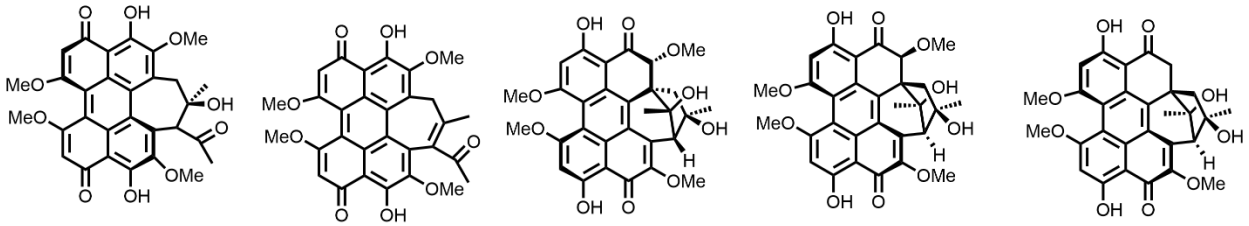

Figure 3.1: Chemical Structure of PQ Dye Series

The initial scope of this project was to simply characterize these dyes and report their photophysical properties. Due to the Walter Group's newly invigorated interest in photoredox catalysis, a decision was made on a whim to try these materials in the previously studied imine alkylation reaction. As data collection continued, it was found that these materials demonstrated curious behavior associated with the wavelengths used to illuminate the photoreactions. As these characteristics began to reveal themselves this project expanded in scope and now encompasses the remainder of this chapter.

3.1.1 Interest in PQ Photocatalysis

In the pursuit of more sophisticated organic photoredox catalysts, there have been new developments that have found organic photocatalysts with novel behaviors. These newly discovered materials can act as radical-photoreductants and closed shell super-photoreductants enabling opening new possibilities for photocatalysis.[33,34] Furthermore, perylene- and perylenequinone-like dyes, including hypocrellins, have previously been shown to function as efficient photocatalysts, capable of driving novel synthetic transformations.[19,46,47]

The organic transformation shown in Figure 3.2, was used in our previous works when characterizing TTz photocatalysts. As stated before, this transformation utilizes alkyl-trifluoroborates rather than organo-lithium compounds due to ease of synthesis, lower cost, and inert synthetic conditions.[28] In this work, we look to examine both the photophysical properties of the PQ dye series, while exploring their use as organic photocatalysts. The use of a transformation that has previously been studied by our lab will allow us to better understand the underlying mechanisms involved with the PQ photocatalysts.

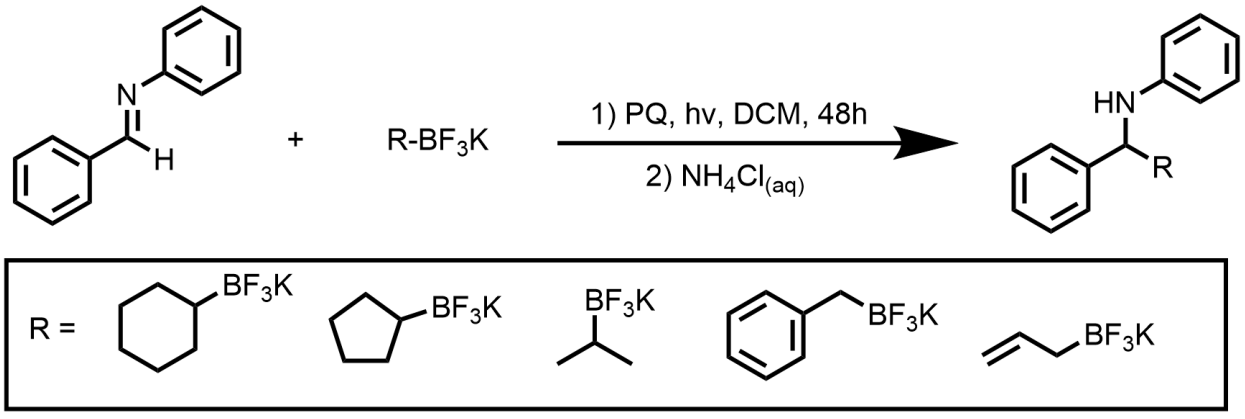

Figure 3.2: Photochemically driven R-BF_3K (R = alkyl, allyl, benzyl) coupling with an imine (N-Benzylaniline).

3.2 Results and Discussion

3.2.1 Photophysical Characterization of PQ Dyes

An investigation into the photophysical properties of the PQ dyes allows for better characterization of their behavior. Each PQ dye can undergo two reductions, and CV indicates a high degree of reversibility, with the singly reduced state of PQ dyes taking the form of a radical anion. Additionally, the PQ dyes demonstrate sufficient redox potentials, which is generally indicative of a compound's ability to perform as a photoredox catalyst. Both characteristics predict the ability of PQ dyes to drive redox chemistry and return to their original oxidation state. When PQ dyes enter an S_1 excited state by absorbing a photon, they are capable of functioning as an oxidizing agent. Each dye has a sufficiently high $^{*}E_{ox}$ (+1.25-1.50 V vs. SCE) to oxidize the carbon-boron bond of a secondary R-BF_3K substrate ($E_{ox} \approx +1.10$ V vs. SCE)

A comparison of the relative photophysical properties of the PQ dyes allows for a division into two sub-series, the Hypomycin series (HM-A, HM-C, and HM-E) and the Hypocrellin series (HC-B, and SH-A). Within each subseries, the dyes exhibit similar absorbance and emission spectra, with comparable redox potentials, quantum yields, and fluorescence lifetimes.

Each dye is characterized as a broad light absorber, with a high molar absorptivity.[48] Upon the absorption of a photon, these compounds demonstrate excited state lifetimes just above the diffusion limit (>1 ns), considered the lower limit of the excited state lifetimes capable of driving photochemistry.[2] These compounds also exhibit low fluorescence quantum yields (Φ_F = 0.11 – 0.16) indicating preference for non-radiative decay, such as the formation of a T_1 state. Triplet states are seen as favorable for the formation of singlet oxygen ($^1O_2$), which HC-B has been utilized in the formation of, and suggests that the presence of oxygen will be deleterious to product formation.[49] The spectral characteristics of the PQ dyes are reported in Table 3.1.

Table 3.1: Photophysical Properties for PQ Dyes in DCM

Compound	Absorbance (nm) λ_{max}	Emission (nm) λ_{max}	E^{*}_{red} (cat^{*}/cat^{-}), (V vs SCE) E_{red}^{α}	Fluorescence Quantum Yield[1] Φ_F	Fluorescence Lifetime[2] (ns)
Hypomycin A	413	545	1.29	0.11	2.55
Hypomycin C	414	547	1.29	0.12	2.95
Hypomycin E	414	551	1.24	0.12	3.58
Hypocrellin B	460	614	1.52	0.14	1.08
Ent-Shiraiachrome A	470	601	1.50	0.16	1.40

1. HM-A, HM-C, HM-E λ_{ex}=414, HC-B λ_{ex}=462 nm, SH-A λ_{ex}=470 nm 2. HM-A λ_{ex}= 405 nm, HM-C, HM-E, HC-B, SH-A λ_{ex}= 389 nm

Figure 3.3 displays the discrepancy between the TCSPC decay plots for HC-B (blue) and HM-C (red). This trend holds true across both dye sub-series, with the hypomycin series exhibiting longer lifetimes. Additional TCSPC plots for the other dyes, as well as isolated plots for HC-B and HM-C can be found in figures S14-S17.

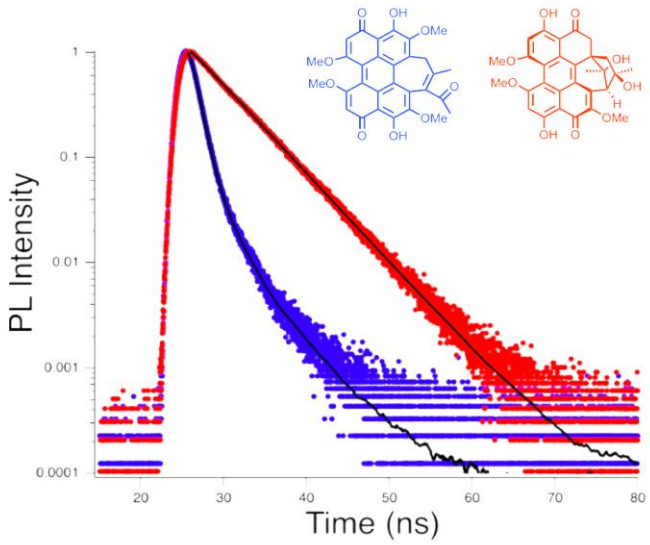

Figure 3.3: Comparison of fluorescent lifetime decay (τ_F) for HC-B (Blue) and HM-C (Red) PQ dyes (ex. 389 nm)

While the $^{*}E_{ox}$ of all PQ dyes is sufficient to favorably oxidize a secondary R-BF_3K substrate, the same cannot be said for each dye concerning favorability of the reduction of an N-centered radical species (~E_{red} = -0.78 V vs SCE).[50] Each of the hypomycin dyes possess reduction potentials deep enough to favorably reduce this species, however the hypocrellin dyes have reduction potentials that indicate unfavourability towards this reduction. Despite this unfavourability, product formation occurs when using both the hypomycin and hypocrellin dyes. Seen in Figure 3.4 is the spectroelectrochemistry for HC-B and HM-E with additional spectroelectrochemistry data found in figures S1-S5. From this data, the absorbance onset for the singly-reduced $PQ^{-\bullet}$ state, and the doubly-reduced PQ^{2-} state, can be utilized to characterize the redox potentials of the reduced states.

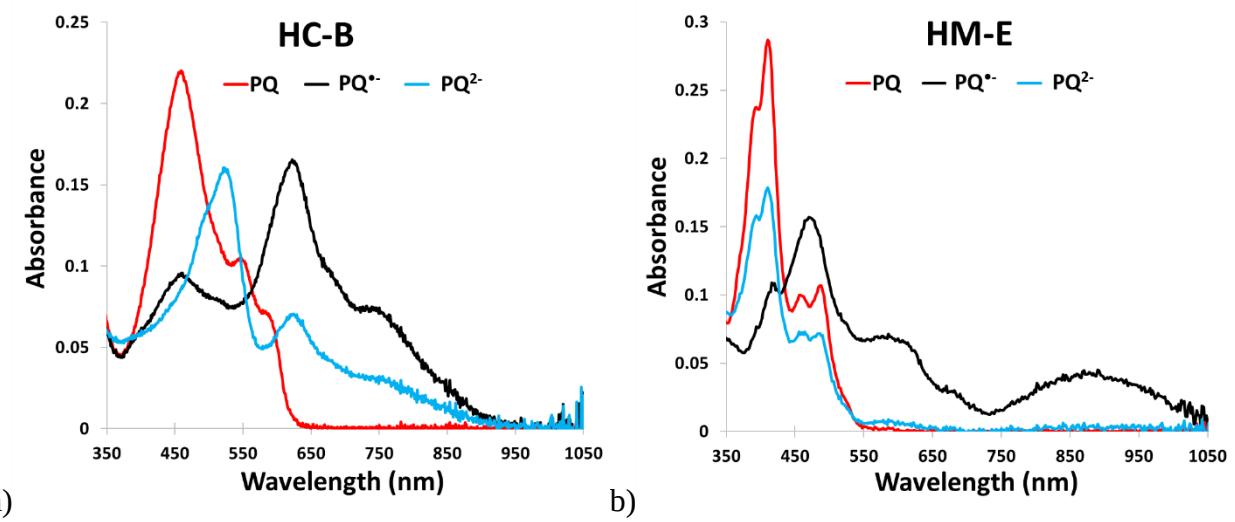

a) b)

Figure 3.4: Spectroelectrochemistry of a) HM-B and b) HM-E

3.2.2 PQ Photoredox Energetics

The excited state of the singly-reduced species is likely incapable of oxidizing an R-BF_3K substrate ($PQ^{*-\bullet}$, $^{*}E_{ox}$ = -0.27 - +0.59 V vs. SCE). The excited state of the singly-reduced dye has a lower $^{*}E_{ox}$ due to lower energy onset absorption and a greater reduction potential. Additionally, the typically short (<1 ns) lifetimes and relative instability of an excited doublet radical state make this process unlikely.[30,31,51] Considering that product formation occurs for each PQ dye despite the unfavourability for the reduction of an N-centered radical we believe an additional process is occurring within the system. More significantly, the effect of wavelength in relation to the generation of product lends evidence towards the existence of a super-reducing species of catalyst in the doubly reduced PQ^{2-} state similar to what has been reported in other systems.[34]

Other works have demonstrated that a radical doublet excited state, such as $PQ^{*-\bullet}$ could allow for such a process to occur. In those such systems, the occurrence of a novel behavior such as molecular twisting, enables anomalously long (>100 ps) excited radical doublet states.[33] While this possibility was considered, there is no current evidence that $PQ^{*-\bullet}$ exhibits such behavior.

We instead believe that evidence supports a process whereby the excited state of the doubly-reduced dye, PQ^{*2-} can act as a super-reducing species, capable of favorably reducing the N-centered radical. Shown in Figure 3.5 is a redox energy diagram showing the relative redox energy values for HM-A and HC-B and includes the energy levels for this proposed state. Redox diagrams for other dye species are found in figures S6-S8.

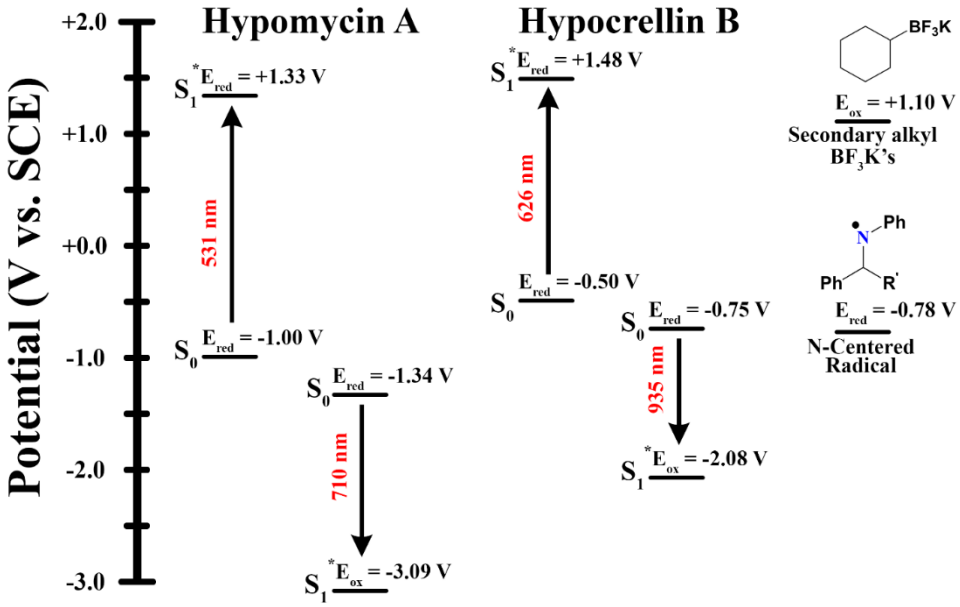

Figure 3.5: Redox Energetics Diagram for HM-A and HC-B Relative to Reactant Species

While both dyes can oxidize a secondary R-BF_3K, energetics suggest that the singly-reduced $PQ^{-\bullet}$ state for HM-B and SH-A cannot favorably reduce the N-centered radical. For both classes of dye, the proposed super-reducing state could reduce the N-centered radical with a high degree of favorability. The doubly-reduced PQ^{2-} state possesses different spectral characteristics than the non-reduced PQ state, and therefore experiences excitation with different wavelengths of light. Table 3.2 presents the redox potentials for each dye, and the energy of the proposed super-reducing species, PQ^{*2-}.

Table 3.2: Tabulated Redox Values for PQ Dye Series

Compound	PQ E_{red} (eV)	$^{*}PQ$ $^{*}E_{red}$ (eV)	$PQ^{\bullet-}$ E_{red} (eV)	$^{*}PQ^{2-}$ $^{*}E_{ox}$ (eV)
HM-A	-1.00	+1.33	-1.34	-3.09
HM-C	-1.04	+1.30	-1.33	-3.18
HM-E	-1.09	+1.25	-1.40	-3.16
HC-B	-0.50	+1.48	-0.75	-2.08
SH-A	-0.55	+1.50	-0.80	-2.13

3.2.3 PQ Photocatalyst Synthetic Trials

Table 3.3 presents the data obtained from a series of synthetic trials with each PQ dye using different sets of LED arrays. Additional results from synthetic trials can be found in Table S1. Each PQ dye was initially surveyed to determine the ideal catalyst loading concentration (given as mol%).

Table 3.3: Selected Single-Point, ^{1}H-NMR with Internal Standard, Determined Reaction Yields of amine product by PQ Dye and LED Array (Spectral characteristics given in figure S18)

LED Arrays	HM-A (0.1 mol%)	HM-C (0.2 mol%)	HM-E (0.1 mol%)	HC-B (0.2 mol%)	SH-A (0.2 mol%)
2x 405 nm[1]	82	71	79	58	60
2x 595 nm	1	15	18	14	20
2x 630 nm	0	7	15	23	30
2x 730 nm	0	0	0	0	0
2x 405 nm[1] + 2x 595 nm	80	79	78	64	62
2x 405 nm[1] + 2x 630 nm	78	87	80	80	72
2x 405 nm[1] + 2x 730 nm	69	72	85	67	80

1. 450 nm for HC-B

Initial trials were conducted using a single type of LED array to determine which generated the highest yield. For each PQ, except HC-B this wavelength was 405 nm, with HC-B preferring the 450 nm arrays. The hypomycin-class of dyes reported higher yields under optimal conditions (71-82%) compared to the hypocrellin-class (58-60%). This is believed to be due to the longer lifetimes of the hypomycins, and their deeper ground state reduction potentials. Additionally, it was noticed that the hypomycin dyes experienced a significant drop in yield when moving away from 405 nm (18-48% yield reduction) whereas the hypocrellin dyes experienced much smaller yield fluctuations (3-13% yield reduction).

Afterwords, a series of experiments were conducted using multiple wavelengths of light. These combined the arrays that produced the highest single wavelength yields with arrays emitting lower energy light. Dual-wavelength yields were greater in at least one combination for each PQ, excluding HM-A. Control experiments using only the lower energy LED arrays were conducted following this.

While the 595 and 630 nm arrays turned over a small amount yield for most of the PQs, the 730 nm arrays in isolation never resulted in detectable product formation when used alone. This enhancement was most significant for HC-B and SH-A, where the highest dual wavelength yield was comparable to the best single wavelength yields for HM-A and HM-E, while surpassing the best single wavelength yield for HM-C.

A visual representation of these yields relative to the absorbance of SH-A in the non-reduced and singly-reduced state is given in figure 3.6.

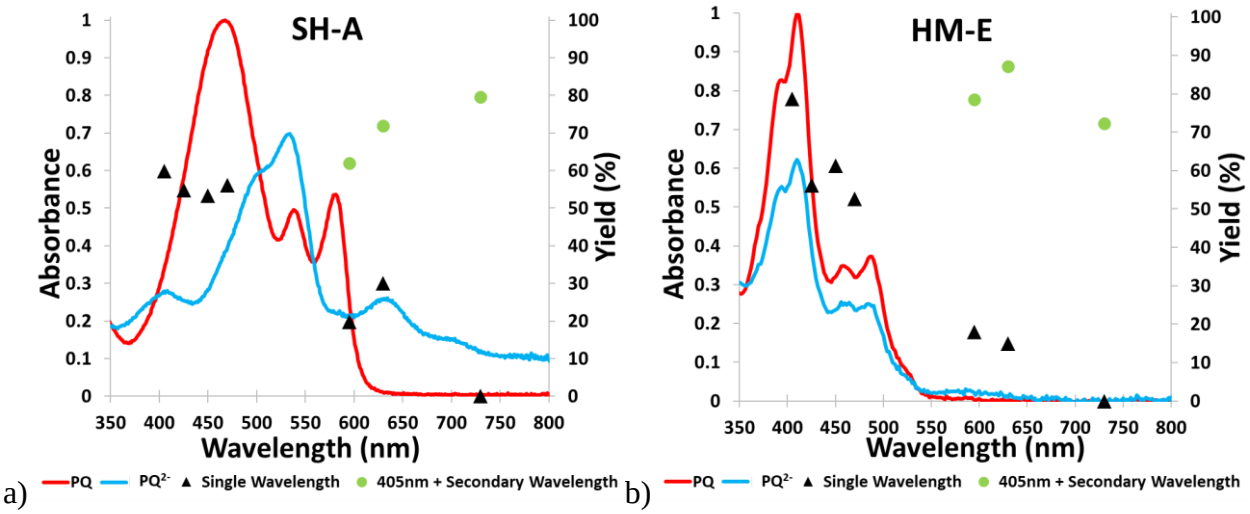

Figure 3.6: Spectroelectrochemistry with overlaid ^{1}H-NMR Yield for a) SH-A and b) HM-E

The visualization in figure 3.6 demonstrates that when using the blue and near-UV LED arrays there is greater yield variability for HM-E than SH-A. Additionally, for SH-A and HC-B there is higher yield generation when using the 630 nm arrays than the 595 nm arrays. While the 595 nm array is more strongly absorbed by the non-reduced state than the 630 nm array, the latter is more strongly absorbed by the doubly-reduced state and absorbed in only trace amounts by the non-reduced state. This characteristic supports the notion of a photoactive state other than PQ^{*} as both the singly- and doubly-reduced states absorb more strongly at 630 nm than 595 nm. Spectroelectrochemistry indicates a similar trend with the hypomycin dyes in this regime where the absorption trend is the same for both the PQ and PQ^{2-} states - exciting both strongly. The similar absorption trend partially explains why yield enhancement with two wavelengths of light is lessened (HM-C and HM-E) or non-existent (HM-A) for the hypomycin series. The poorer enhancement is also likely due to the favorability of reduction by the singly reduced $PQ^{-\bullet}$ state. Considering the yield data, spectroelectrochemistry, and redox values, we believe that there is compelling evidence for the existence of a super-reducing species for each of the PQ dyes, with

stronger evidence concerning the hypocrellin class. While there is a greater indication that PQ^{*2-} is the species responsible for this behavior, the role of $PQ^{-\bullet}$ in this process cannot be excluded. Figure 3.7 shows the proposed catalytic cycle and includes the possibility of either a $PQ^{*-\bullet}$ or PQ^{*2-} super-reducing species.

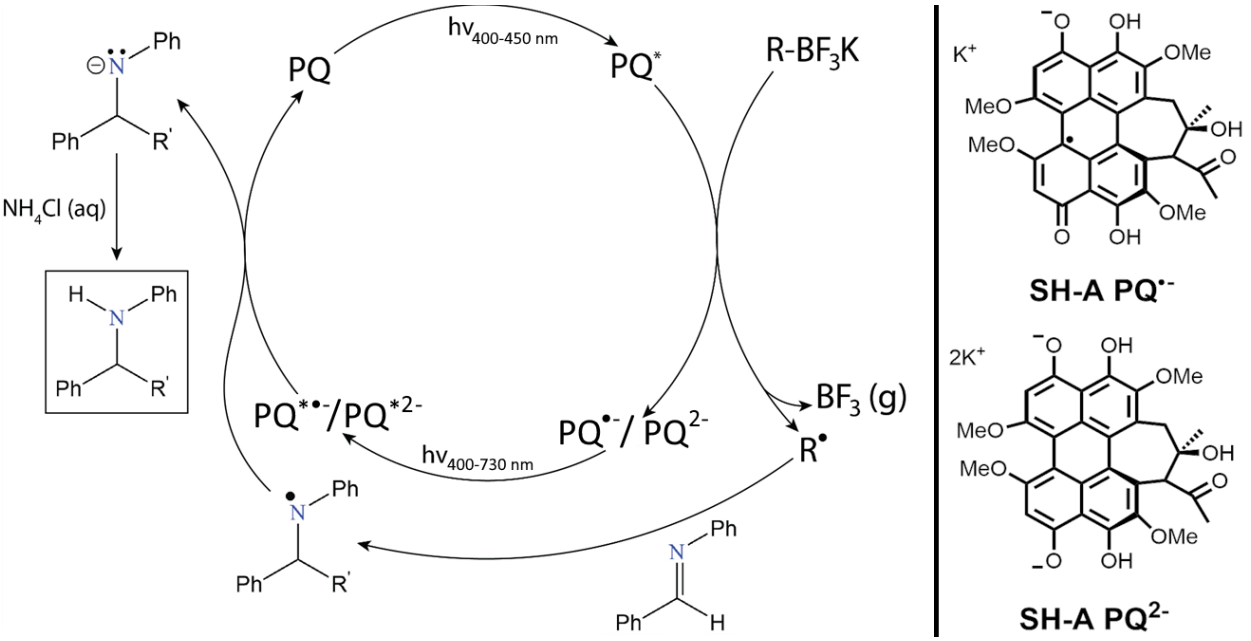

Figure 3.7: a) Proposed Catalytic Cycle with reducing PQ / PQ^{2-} species and b) Proposed structures of singly- and doubly-reduced SH-A PQ dyes

The enhancement of product yield with multiple wavelengths of light that corresponds to the spectroelectrochemical data for the PQ dyes indicates the presence of an additional photoactive PQ species. While the exact mechanism is difficult to elucidate for the PQ dye series, the increase in product yield suggests that the excited state lifetime of either $PQ^{*-\bullet}$ or PQ^{*2-} is lengthy enough to drive chemical reduction.

3.3 Conclusion

Naturally derived perylenequinone-like compounds possess a variety of intriguing properties that make them capable of functioning as photoredox catalysts. Due to their broad and intense absorption of light, coupled with sufficiently high redox potentials, and long enough excited state lifetimes, each PQ dye in this series demonstrates this fact. Additionally, due to the link between an increase in product formation and multi-wavelength light exposure, there is a likely secondary process that these PQ dyes undergo which allows for a deepening of reduction potentials. This process further enhances their performance and versatility as organic photoredox catalysts. These findings stress the importance of examining wavelength dependent behavior of photocatalysts. Their capabilities and novel behavior present an exciting possibility to obtain a deeper understanding of photocatalytic processes and their natural origin represents a move towards a greater degree of sustainability within the field of photocatalysis.

3.4 Appendix II: Supplementary Information

Supplementary Table 1: Complete Single-Point, ^{1}H-NMR with Internal Standard, Determined Reaction Yields by PQ Dye and Lighting Configuration

Lighting Configuration	Hypomycin A (0.1 mol%)	Hypomycin C (0.2 mol%)	Hypomycin E (0.1 mol%)	Hypocrellin B (0.2 mol%)	Ent-Shiraiachrome A (0.2 mol%)
2x 405 nm	82	71	79	55	60
2x 425 nm	43	47	56	52	55
2x 450 nm	-	50	61	58	53
2x 470 nm	34	43	53	45	56
2x 595 nm	1	15	18	14	20
2x 630 nm	0	7	15	23	30
2x 730 nm	0	0	0	0	0
2x 405 nm[1] + 2x 595 nm	80	79	78	64	62
2x 405* nm[1] + 2x 630 nm	78	87	80	80	72
2x 405* nm[1] + 2x 730 nm	69	72	85	67	80

1. 405 nm lights were replaced with 450 nm lights for Hypocrellin B

Spectroelectrochemistry

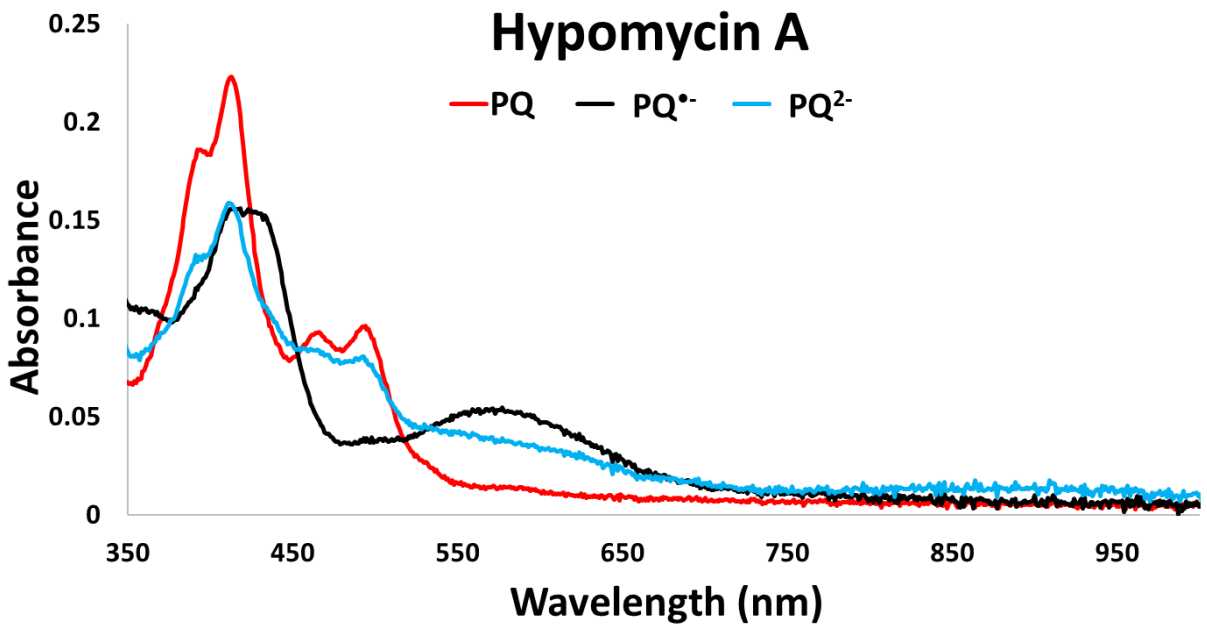

Supplementary Figure 1: Spectroelectrochemistry of Hypomycin A

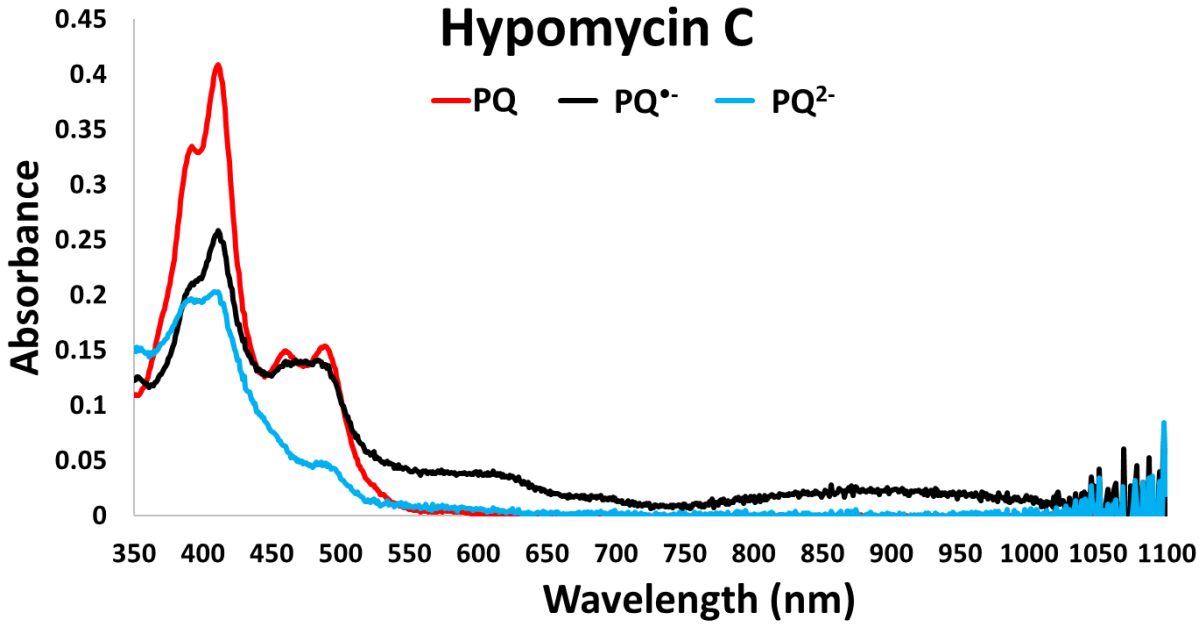

Supplementary Figure 2: Spectroelectrochemistry of Hypomycin C

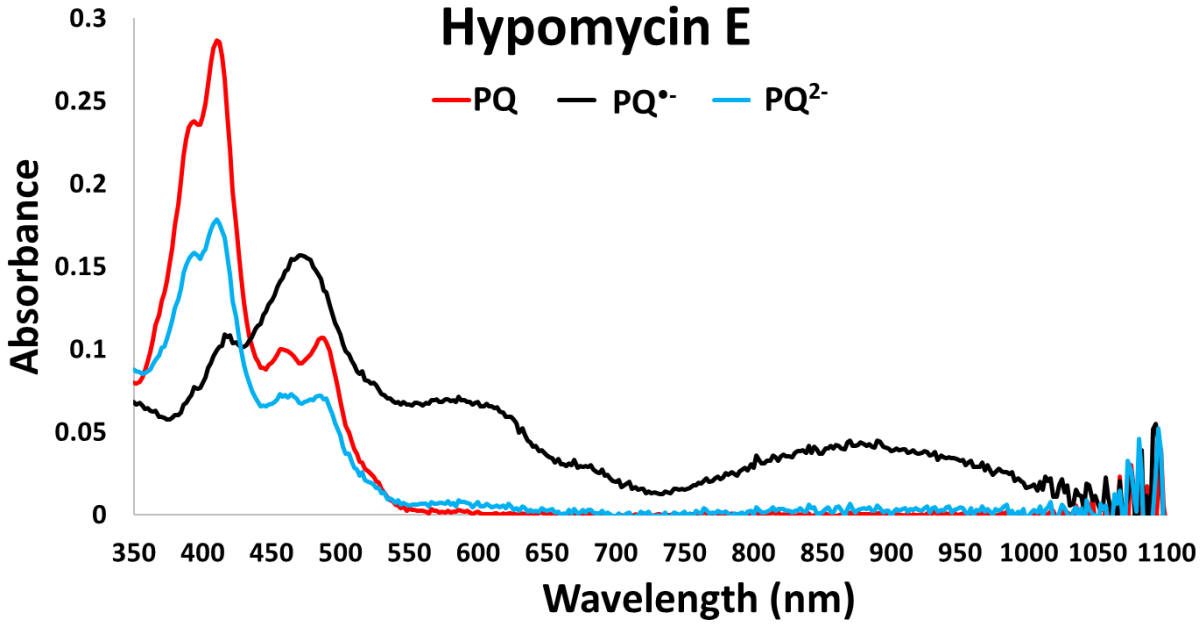

Supplementary Figure 3: Spectroelectrochemistry of Hypomycin E

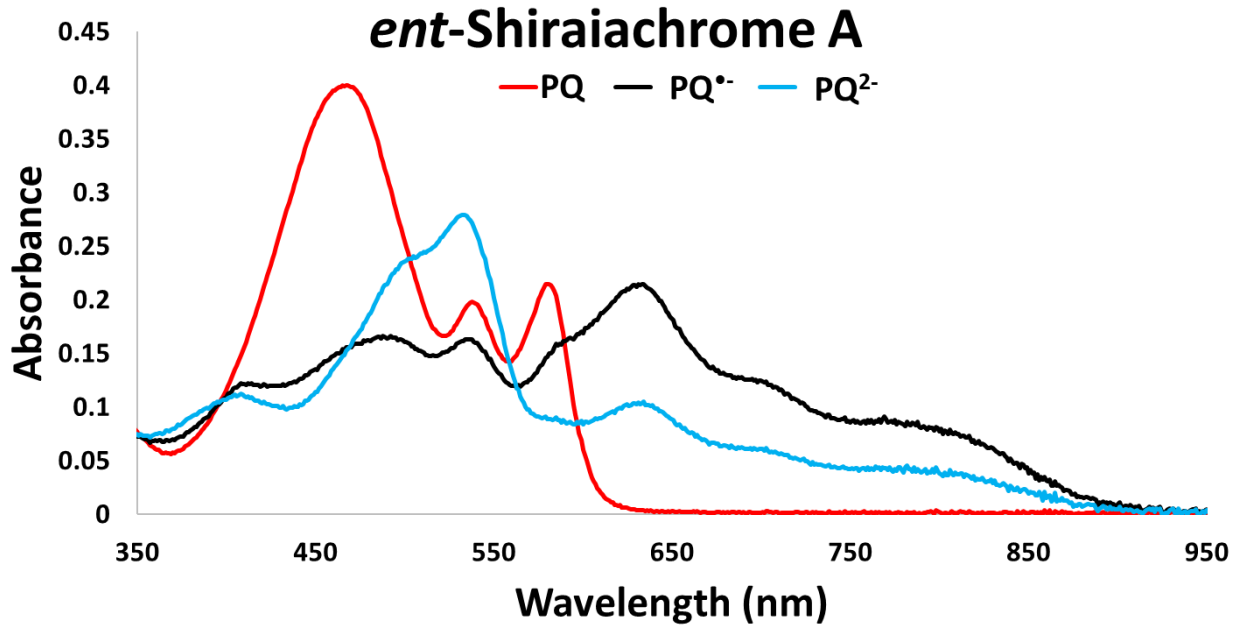

Supplementary Figure 4: Spectroelectrochemistry of *ent*-Shiraiachrome A

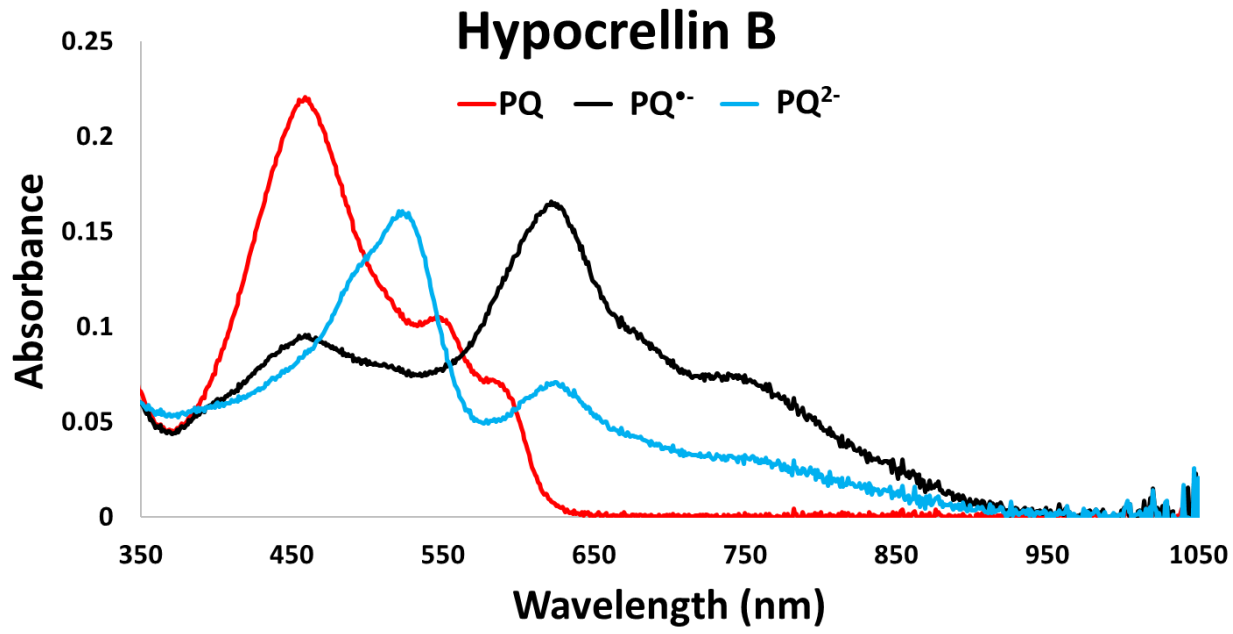

Supplementary Figure 5: Spectroelectrochemistry of Hypocrellin B

Redox Energy Diagrams

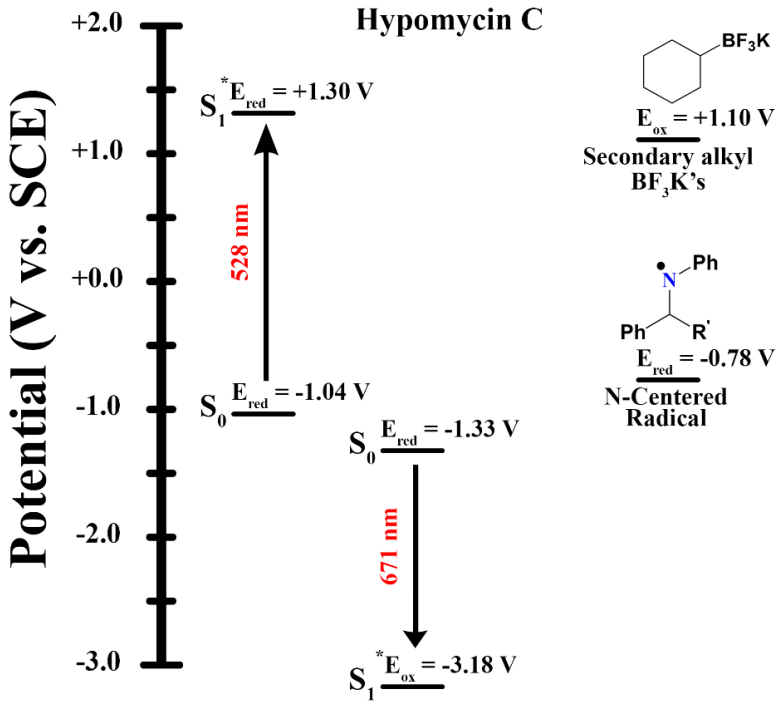

Supplementary Figure 6: Redox Energy Diagram of Hypomycin C

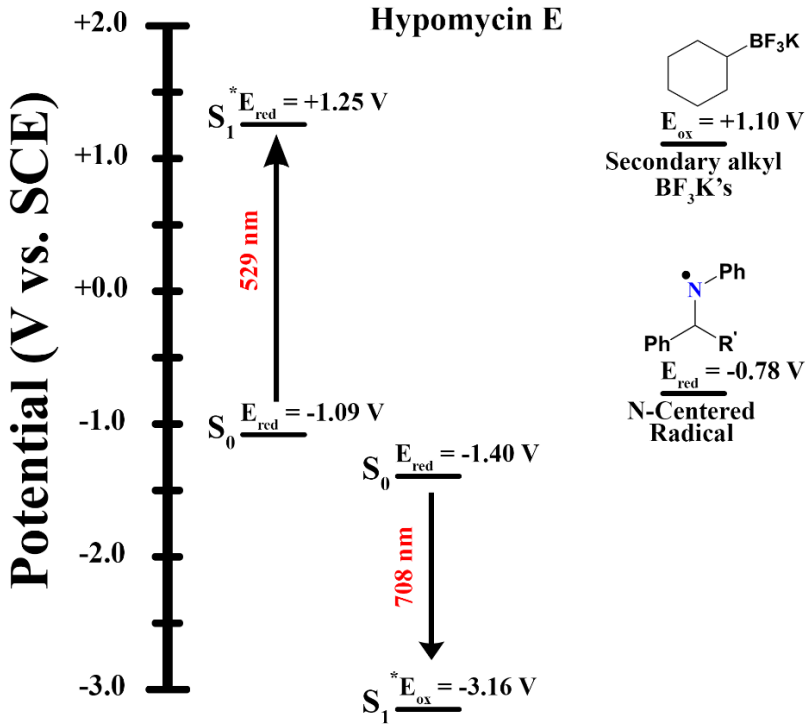

Supplementary Figure 7: Redox Energy Diagram of Hypomycin E

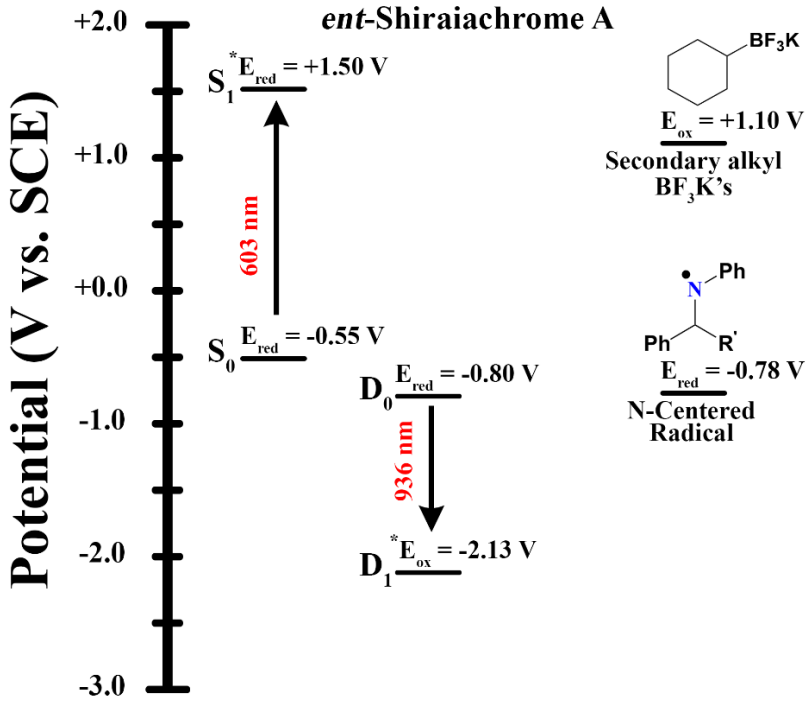

Supplementary Figure 8: Redox Energy Diagram of *ent*-Shiraiachrome A

Spectroelectrochemistry and Yield Combined Graphs

Collected and plotted by Marcos Tapia (UNCG)

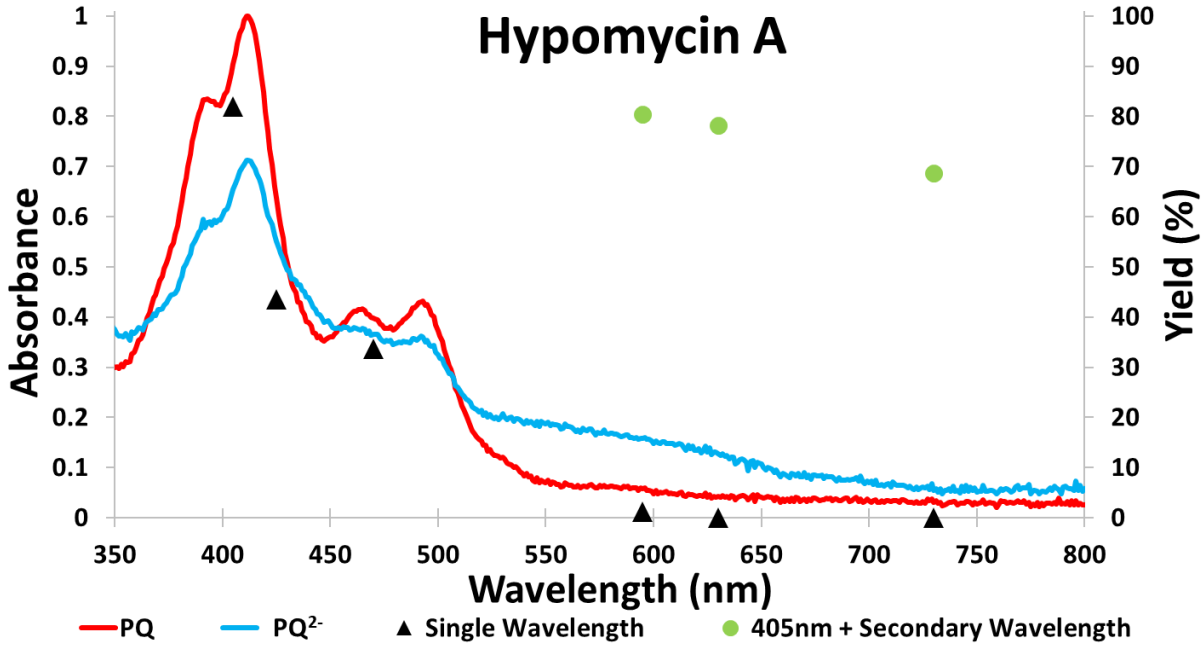

Supplementary Figure 9:Spectroelectrochemistry of Hypomycin A with overlaid ^{1}H-NMR Yield

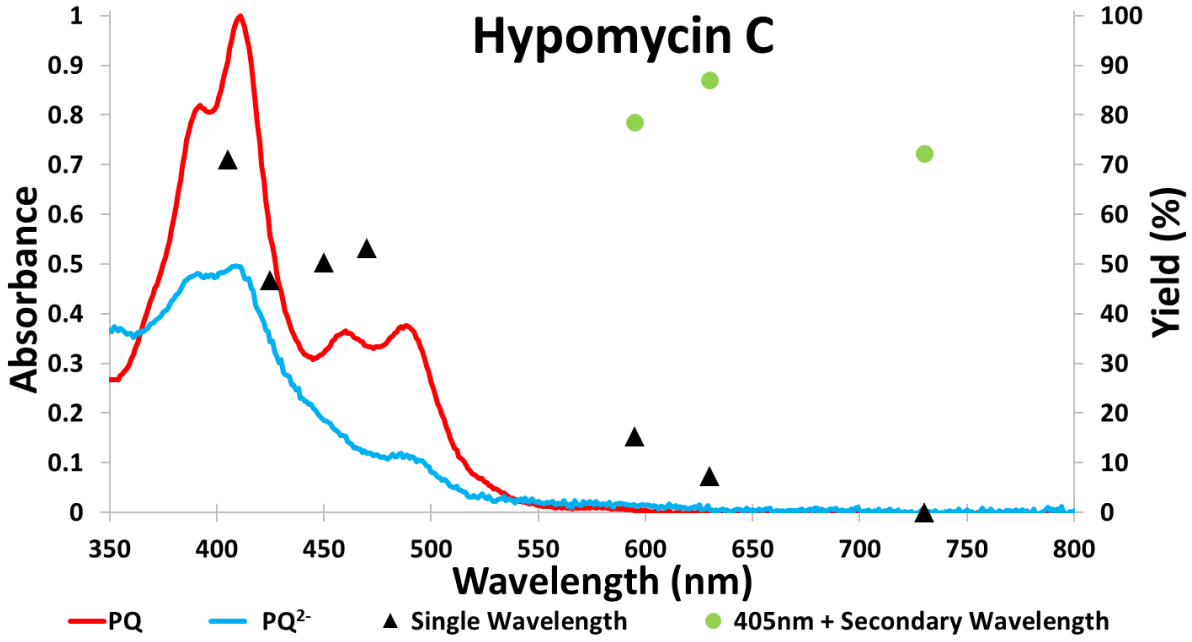

Supplementary Figure 10: Spectroelectrochemistry of Hypomycin C with overlaid ^{1}H-NMR Yield

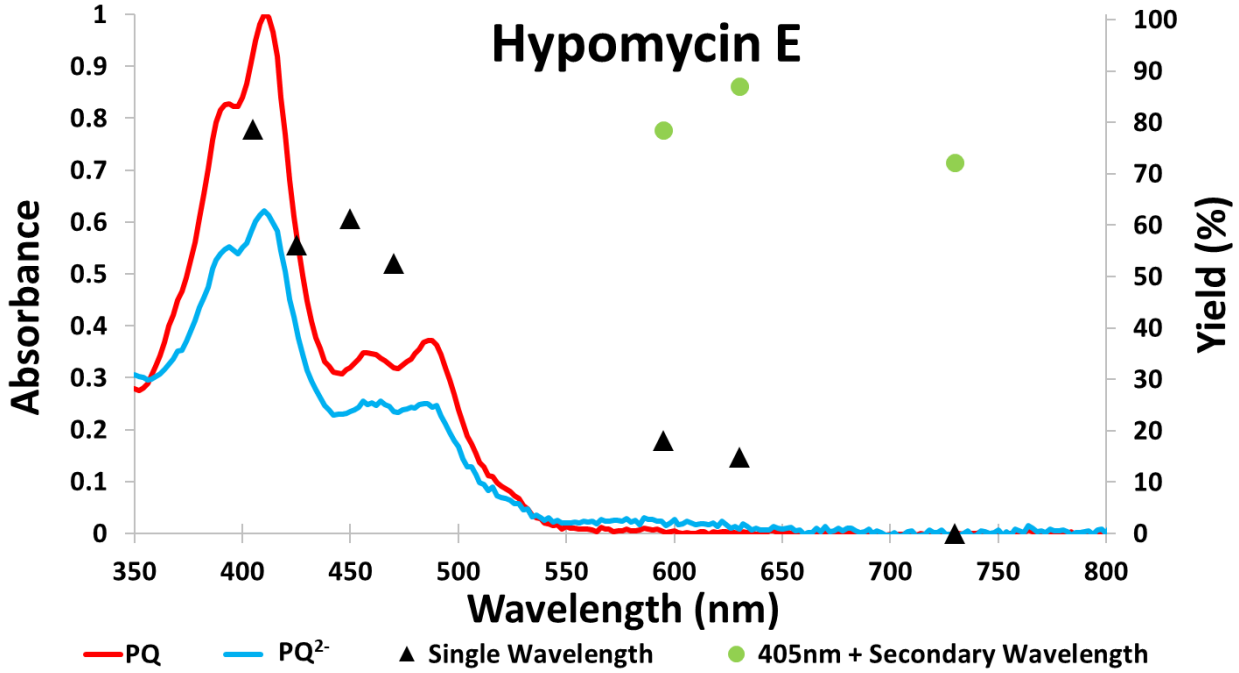

Supplementary Figure 11: Spectroelectrochemistry of Hypomycin E with overlaid ^{1}H-NMR Yield

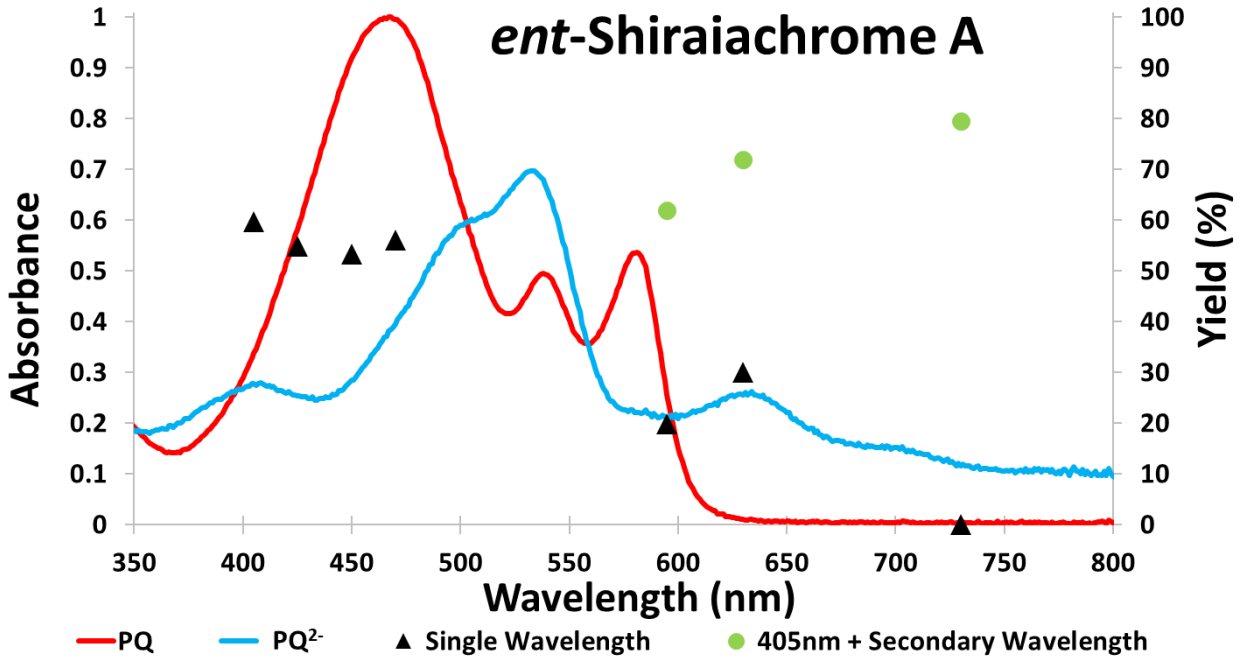

Supplementary Figure 12: Spectroelectrochemistry of *ent*-Shiraiachrome A with overlaid ^{1}H-NMR Yield

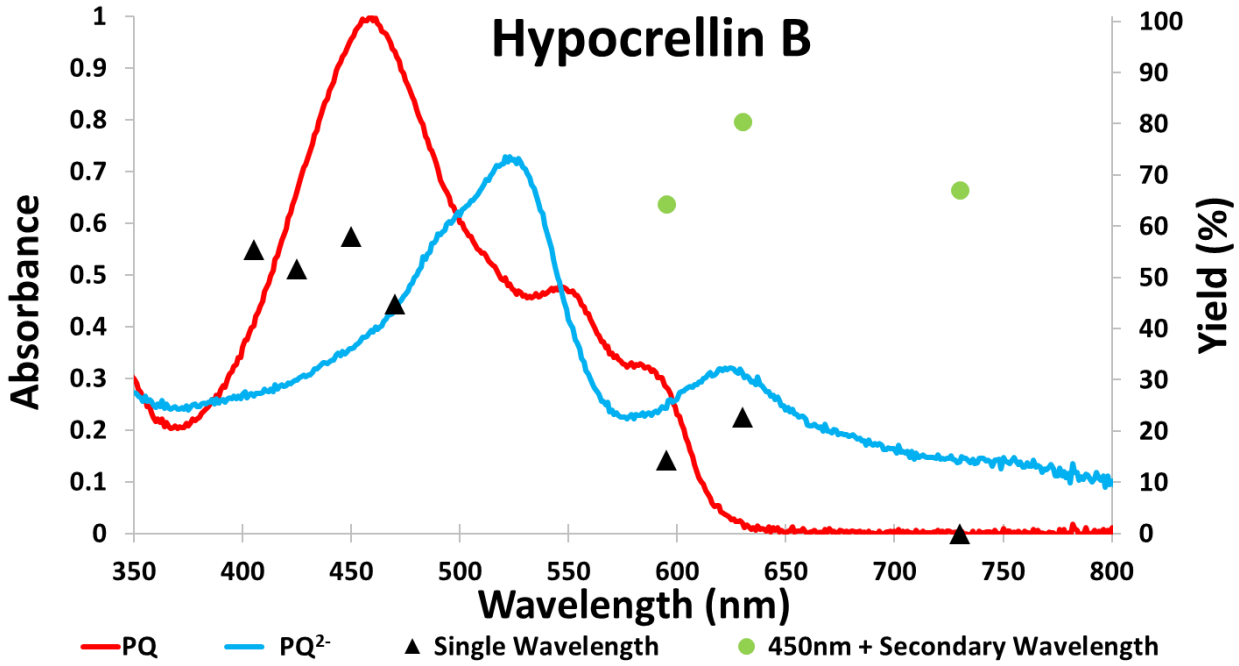

Supplementary Figure 13: Spectroelectrochemistry of Hypocrellin B with overlaid ^{1}H-NMR Yield

Spectral Data Acquisition

Absorbance data was collected using a Cary 300 UV-Vis dual-beam spectrophotometer. Emission data was collected using a Horiba FluoroMax+ SpectroFluorometer. 1 cm pathlength quartz cuvettes were used to hold the dissolved sample solution.

Fluorescence Lifetime and Quantum Yield

Fluorescence lifetime and quantum yield data was obtained using a Horiba FluoroMax+ SpectroFluorometer. Quantum yield measurements were determined using an integrating sphere module attached to the instrument.

CHAPTER 4: CONCLUSION

This work has examined the applications and properties of two types of photoredox catalysts, with four TTz dyes and five PQ dyes fully characterized. Thus far, the scope of synthetic applications has been limited to imine alkylation reactions and amine oxidation reactions, which are useful tools for the production of many pharmaceutically significant organic compounds. Both dye series have many traits in common, such as multiple electrochemical reductions, short (~1-5 ns) excited state lifetimes, and sufficiently high redox potentials. Despite the similarities shared between the two types of dyes, each seems to exhibit different photochemical responses to multiple wavelengths of light.

Multi-wavelength experimentation was carried out for both dye series with different results. For TTzs the results indicate that currently, there is no strong evidence for a photoactive species besides TTz^{*2+}. The results from both the imine alkylation reactions and amine oxidation reactions found no compelling evidence that lower energy wavelengths of light (eg. 595 nm) were capable of driving photochemistry with TTz dye derivatives. On the other hand, there is compelling evidence that lower energy wavelengths enhance catalyst performance for at least some of the PQ dyes.

The mechanism for this enhancement is still difficult to determine with certainty, but likely involves the photoexcitation of the doubly-reduced state for the PQ dyes. Alternatively, there could be a process which allows the singly-reduced PQ state to become excited into a surprisingly stable doublet excited state whereby it is capable of driving photochemistry due to an excited state lifetime which exceeds the diffusion limit. This discovery emphasizes the importance of studying the effects of wavelength on catalyst performance. Additionally, the hypothesized mechanism for this process involves a catalyst with multiple reductions which can

function as a photooxidizer and photoreductant depending on the oxidation state. Future investigations should be conducted on materials with multiple reductions to determine if this is a trait which is more common than previously theorized.

Overall, this work demonstrates that two new types of materials can function as viable photoredox catalysts. These materials represent a move towards cost effective, and sustainable means of driving chemical synthesis though photoredox catalysis. New mechanisms and characteristics of these dyes represent powerful new tools for designing and studying photoredox catalysts.

REFERENCES

1 International Union of, P. & Applied, C.

2 Romero, N. A. & Nicewicz, D. A. Organic Photoredox Catalysis. *Chemical Reviews* **116**, 10075-10166 (2016). https://doi.org:10.1021/acs.chemrev.6b00057

3 Baniyounes, A. M., Ghadi, Y. Y., Rasul, M. G. & Khan, M. M. K. An overview of solar assisted air conditioning in Queensland's subtropical regions, Australia. *Renewable and Sustainable Energy Reviews* **26**, 781-804 (2013). https://doi.org:https://doi.org/10.1016/j.rser.2013.05.053

4 Solangi, K. H., Islam, M. R., Saidur, R., Rahim, N. A. & Fayaz, H. A review on global solar energy policy. *Renewable and Sustainable Energy Reviews* **15**, 2149-2163 (2011). https://doi.org:https://doi.org/10.1016/j.rser.2011.01.007

5 Bobo, M. V., Kuchta, J. J. & Vannucci, A. K. Recent advancements in the development of molecular organic photocatalysts. *Organic & Biomolecular Chemistry* **19**, 4816-4834 (2021). https://doi.org:10.1039/D1OB00396H

6 Buglioni, L., Raymenants, F., Slattery, A., Zondag, S. D. A. & Noël, T. Technological Innovations in Photochemistry for Organic Synthesis: Flow Chemistry, High-Throughput Experimentation, Scale-up, and Photoelectrochemistry. *Chemical Reviews* **122**, 2752-2906 (2022). https://doi.org:10.1021/acs.chemrev.1c00332

7 Du, Y. *et al.* Strongly Reducing, Visible-Light Organic Photoredox Catalysts as Sustainable Alternatives to Precious Metals. *Chemistry – A European Journal* **23**, 10962-10968 (2017). https://doi.org:https://doi.org/10.1002/chem.201702926

8 Azzaroni, O. Polymer brushes here, there, and everywhere: Recent advances in their practical applications and emerging opportunities in multiple research fields. *Journal of Polymer Science Part A: Polymer Chemistry* **50**, 3225-3258 (2012). https://doi.org:https://doi.org/10.1002/pola.26119

9 Teegardin, K., Day, J. I., Chan, J. & Weaver, J. Advances in Photocatalysis: A Microreview of Visible Light Mediated Ruthenium and Iridium Catalyzed Organic Transformations. *Organic Process Research & Development* **20**, 1156-1163 (2016). https://doi.org:10.1021/acs.oprd.6b00101

10 Shaw, M. H., Twilton, J. & MacMillan, D. W. C. Photoredox Catalysis in Organic Chemistry. *The Journal of Organic Chemistry* **81**, 6898-6926 (2016). https://doi.org:10.1021/acs.joc.6b01449

11 Clapp, M., Zalitis, C. M. & Ryan, M. Perspectives on current and future iridium demand and iridium oxide catalysts for PEM water electrolysis. *Catalysis Today* **420**, 114140 (2023). https://doi.org:https://doi.org/10.1016/j.cattod.2023.114140

12 Buzzetti, L., Crisenza, G. E. M. & Melchiorre, P. Mechanistic Studies in Photocatalysis. *Angewandte Chemie International Edition* **58**, 3730-3747 (2019). https://doi.org:https://doi.org/10.1002/anie.201809984

13 Nicewicz, D. A. & MacMillan, D. W. C. Merging Photoredox Catalysis with Organocatalysis: The Direct Asymmetric Alkylation of Aldehydes. *Science* **322**, 77-80 (2008). https://doi.org:10.1126/science.1161976

14 Martin, S. F. Recent applications of imines as key intermediates in the synthesis of alkaloids and novel nitrogen heterocycles. **81**, 195-204 (2009). https://doi.org:doi:10.1351/PAC-CON-08-07-03

15 Patel, N. R., Kelly, C. B., Siegenfeld, A. P. & Molander, G. A. Mild, Redox-Neutral Alkylation of Imines Enabled by an Organic Photocatalyst. *ACS Catalysis* **7**, 1766-1770 (2017). https://doi.org:10.1021/acscatal.6b03665

16 Miyabe, H., Ueda, M. & Naito, T. -Sulfonylimines as an excellent acceptor for intermolecular radical reactions. *Chemical Communications*, 2059-2060 (2000). https://doi.org:10.1039/B006574I

17 Fernández-Salas, J. A., Rodríguez-Fernández, M. M., Maestro, M. C. & García-Ruano, J. L. Synthesis of Enantiomerically Pure (α-Phenylalkyl)amines with Substituents at the ortho Position through Diastereoselective Radical Alkylation Reaction of Sulfinimines. *European Journal of Organic Chemistry* **2014**, 5265-5272 (2014). https://doi.org:https://doi.org/10.1002/ejoc.201402355

18 Yang, C. *et al.* Heterogeneous photoredox flow chemistry for the scalable organosynthesis of fine chemicals. *Nature Communications* **11**, 1239 (2020). https://doi.org:10.1038/s41467-020-14983-w

19 Zeng, L., Huang, L., Lin, W., Jiang, L.-H. & Han, G. Red light-driven electron sacrificial agents-free photoreduction of inert aryl halides via triplet-triplet annihilation. *Nature Communications* **14**, 1102 (2023). https://doi.org:10.1038/s41467-023-36679-7

20 Zhong, M. & Sun, Y. Recent advancements in the molecular design of deep-red to near-infrared light-absorbing photocatalysts. *Chem Catalysis*, 100973 (2024). https://doi.org:https://doi.org/10.1016/j.checat.2024.100973

21 Fagnoni, M. Modern Molecular Photochemistry of Organic Molecules. By Nicholas J. Turro, V. Ramamurthy and Juan C. Scaiano. *Angewandte Chemie International Edition* **49**, 6709-6710 (2010). https://doi.org:https://doi.org/10.1002/anie.201003826
22 Woodward, A. N. *et al.* Thiazolothiazole Fluorophores Exhibiting Strong Fluorescence and Viologen-Like Reversible Electrochromism. *Journal of the American Chemical Society* **139**, 8467-8473 (2017). https://doi.org:10.1021/jacs.7b01005
23 Sayresmith, N. A. *et al.* Photostable Voltage-Sensitive Dyes Based on Simple, Solvatofluorochromic, Asymmetric Thiazolothiazoles. *Journal of the American Chemical Society* **141**, 18780-18790 (2019). https://doi.org:10.1021/jacs.9b08959
24 Adams, T. J. *et al.* Obtaining Reversible, High Contrast Electrochromism, Electrofluorochromism, and Photochromism in an Aqueous Hydrogel Device Using Chromogenic Thiazolothiazoles. *Advanced Functional Materials* **31**, 2103408 (2021). https://doi.org:https://doi.org/10.1002/adfm.202103408
25 Lowry, M. S. *et al.* Single-Layer Electroluminescent Devices and Photoinduced Hydrogen Production from an Ionic Iridium(III) Complex. *Chemistry of Materials* **17**, 5712-5719 (2005). https://doi.org:10.1021/cm051312+
26 Plasko, D. P., Jordan, C. J., Ciesa, B. E., Merrill, M. A. & Hanna, J. M. Visible light-promoted alkylation of imines using potassium organotrifluoroborates. *Photochem. & Photobiol. Sci.* **17**, 534-538 (2018). https://doi.org:10.1039/C8PP00061A
27 Chenneberg, L. *et al.* Single-Electron-Transfer Oxidation of Trifluoroborates and Silicates with Organic Reagents: A Comparative Study. *Synlett* **27**, 731-735 (2016). https://doi.org:10.1055/s-0035-1561337
28 Dilauro, G., Dell'Aera, M., Vitale, P., Capriati, V. & Perna, F. M. Unprecedented Nucleophilic Additions of Highly Polar Organometallic Compounds to Imines and Nitriles Using Water as a Non-Innocent Reaction Medium. *Angewandte Chemie International Edition* **56**, 10200-10203 (2017). https://doi.org:https://doi.org/10.1002/anie.201705412
29 Cismesia, M. A. & Yoon, T. P. Characterizing chain processes in visible light photoredox catalysis. *Chemical Science* **6**, 5426-5434 (2015). https://doi.org:10.1039/C5SC02185E
30 Johnston, L. J. Photochemistry of radicals and biradicals. *Chemical Reviews* **93**, 251-266 (1993). https://doi.org:10.1021/cr00017a012
31 Samanta, A. *et al.* Quenching of excited doublet states of organic radicals by stable radicals. *The Journal of Physical Chemistry* **93**, 3651-3656 (1989). https://doi.org:10.1021/j100346a055
32 Le, C. C. *et al.* A General Small-Scale Reactor To Enable Standardization and Acceleration of Photocatalytic Reactions. *ACS Central Science* **3**, 647-653 (2017). https://doi.org:10.1021/acscentsci.7b00159
33 MacKenzie, I. A. *et al.* Discovery and characterization of an acridine radical photoreductant. *Nature* **580**, 76-80 (2020). https://doi.org:10.1038/s41586-020-2131-1
34 Sau, A. *et al.* Mechanistic Investigation of a Photocatalyst Model Reveals Function by Perylene-Like Closed Shell Super-Photoreductant Capable of Reducing Unactivated Arenes. *ACS Catalysis* **14**, 2252-2263 (2024). https://doi.org:10.1021/acscatal.3c05386
35 Griller, D. & Ingold, K. U. Persistent carbon-centered radicals. *Accounts of Chemical Research* **9**, 13-19 (1976). https://doi.org:10.1021/ar50097a003
36 Luo, J., Hu, B., Debruler, C. & Liu, T. L. A π-Conjugation Extended Viologen as a Two-Electron Storage Anolyte for Total Organic Aqueous Redox Flow Batteries. *Angewandte Chemie International Edition* **57**, 231-235 (2018). https://doi.org:10.1002/anie.201710517
37 Woodward, A. N. *et al.* Thiazolothiazole Fluorophores Exhibiting Strong Fluorescence and Viologen-Like Reversible Electrochromism. *J. Am. Chem. Soc.* **139**, 8467-8473 (2017). https://doi.org:10.1021/jacs.7b01005
38 Roy, I. *et al.* ExTzBox: A Glowing Cyclophane for Live-Cell Imaging. *J. Am. Chem. Soc.* **140**, 7206-7212 (2018). https://doi.org:10.1021/jacs.8b03066
39 Luo, J., Hu, B., Debruler, C. & Liu, T. L. A pi-Conjugation Extended Viologen as a Two-Electron Storage Anolyte for Total Organic Aqueous Redox Flow Batteries. *Angewandte Chemie-International Edition* **57**, 231-235 (2018). https://doi.org:10.1002/anie.201710517
40 Adams, T. J. *et al.* Obtaining Reversible, High Contrast Electrochromism, Electrofluorochromism, and Photochromism in an Aqueous Hydrogel Device Using Chromogenic Thiazolothiazoles. *Advanced Functional Materials* **31** (2021). https://doi.org:10.1002/adfm.202103408
41 Adamo, C. & Barone, V. Toward reliable density functional methods without adjustable parameters: The PBE0 model. *Journal of Chemical Physics* **110**, 6158-6170 (1999). https://doi.org:10.1063/1.478522

42 Ditchfield, R., Hehre, W. J. & Pople, J. A. SELF-CONSISTENT MOLECULAR-ORBITAL METHODS .9. EXTENDED GAUSSIAN-TYPE BASIS FOR MOLECULAR-ORBITAL STUDIES OF ORGANIC MOLECULES. *J. Chem. Phys.* **54**, 724-+ (1971). https://doi.org:10.1063/1.1674902
43 Shen, Z. L. & Loh, T. P. Indium-copper-mediated barbier-grignard-type alkylation reaction of Imines in aqueous media. *Organic Letters* **9**, 5413-5416 (2007). https://doi.org:10.1021/ol702263b
44 Zhang, Y. M., Yan, T. L., Cheng, W., Zuo, J. M. & Zhao, W. J. Solvent-free allylation and benzylation of aldimines mediated by zinc powder. *Tetrahedron Letters* **50**, 2925-2928 (2009). https://doi.org:10.1016/j.tetlet.2009.03.184
45 Shen, Z. L. *et al.* Synthesis of Water-Tolerant Indium Homoenolate in Aqueous Media and Its Application in the Synthesis of 1,4-Dicarbonyl Compounds via Palladium-Catalyzed Coupling with Acid Chloride. *Journal of the American Chemical Society* **132**, 15852-15855 (2010). https://doi.org:10.1021/ja106925f
46 Miyake, G. M. & Theriot, J. C. Perylene as an Organic Photocatalyst for the Radical Polymerization of Functionalized Vinyl Monomers through Oxidative Quenching with Alkyl Bromides and Visible Light. *Macromolecules* **47**, 8255-8261 (2014). https://doi.org:10.1021/ma502044f
47 Huang, Z. *et al.* Rapid Degradation of Rhodamine B through Visible-Photocatalytic Advanced Oxidation Using Self-Degradable Natural Perylene Quinone Derivatives—Hypocrellins. *Bioengineering* **9**, 307 (2022). https://doi.org:10.3390/bioengineering9070307
48 Al Subeh, Z. Y. *et al.* Structural Diversity of Perylenequinones Is Driven by Their Redox Behavior. *The Journal of Organic Chemistry* **87**, 2697-2710 (2022). https://doi.org:10.1021/acs.joc.1c02639
49 Zhou, Z. *et al.* Photocytotoxicity of Hypocrellin B (HB) was Enhanced by Liposomalization in Vitro. *International Journal of Toxicology* **30**, 174-180 (2011). https://doi.org:10.1177/1091581810394548
50 Jonsson, M., Wayner, D. D. M. & Lusztyk, J. Redox and Acidity Properties of Alkyl- and Arylamine Radical Cations and the Corresponding Aminyl Radicals. *The Journal of Physical Chemistry* **100**, 17539-17543 (1996). https://doi.org:10.1021/jp961286q
51 Weir, D. & Scaiano, J. C. Substituent effects on the lifetime and fluorescence of excited diphenylmethyl radicals in solution. *Chemical Physics Letters* **128**, 156-159 (1986). https://doi.org:https://doi.org/10.1016/0009-2614(86)80316-5